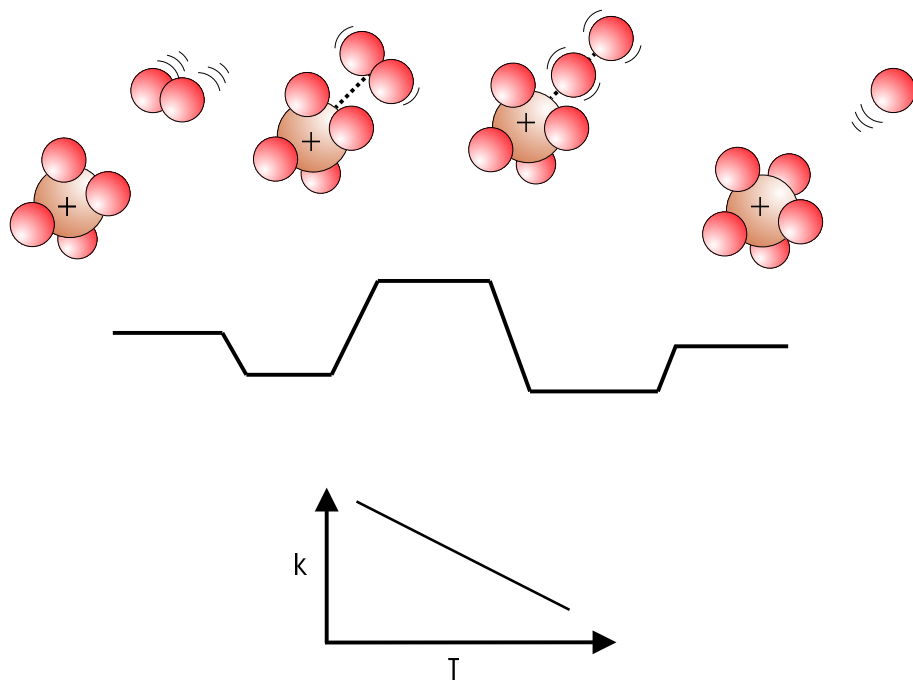# Experiments with Ions and Clusters in a variable temperature 22-pole ion trap

Oskar Asvany

Experiments with Ions and Clusters in a variable temperature 22-pole ion trap

Bibliographische Beschreibung

Experiments with Ions and Clusters in a variable temperature 22-pole ion trap

Dissertation an der Fakultät für Naturwissenschaften der
Technischen Universität Chemnitz, Institut für Physik,
von Oskar Asvany
Chemnitz, 2003

- 110 Seiten inkl. 3 Publikationen

- in englischer Sprache mit 9 Tabellen und 44 Abbildungen

Referat

Im Rahmen dieser Arbeit wurden zwei Apparaturen mit 22-Pol-Ionenfallen benutzt, um protonierte Wassercluster $H^+(H_2O)_n$ (n=4..10) und kleine ionische Kohlenwasserstoffe CH_n^+ (n=2..5) bei tiefen Temperaturen zu untersuchen.
Die in einer Koronaentladungsquelle erzeugten Cluster $H^+(H_2O)_n$ wurden kinetisch und spektroskopisch untersucht. Dazu wurden sie in einem 22-Pol-Speicher mithilfe eines He-Puffergases auf einer Temperatur zwischen 80K und 350K thermalisiert. Die Bestimmung der Bindungsenergien für Cluster der Größe n=4..10 wird ermöglicht durch die Messung der temperaturabhängigen Dissoziationsraten und durch die Ermittlung der inneren Energien mittels berechneter Schwingungsfrequenzen. Temperaturabhängige IR-Spektren im Bereich der freien OH-Streckschwingung wurden aufgenommen.
Die Austausch- und Abstreifreaktionen von ionischen Kohlenwasserstoffen CH_n^+ (n=2..5) mit H_2, HD und D_2 und die darauffolgenden Assoziationsprozesse wurden im Temperaturbereich 15K bis 300K untersucht. Es stellt sich z.B. heraus, dass der H-D-Austauschprozess zwischen CH_5^+ und HD bei 15K langsamer als 5×10^{-18} cm^{3}s^{-1} ist, wogegen CH_3^+ mit jeder Kollision einen Austausch ausführt. In der Abstreifreaktion von CH_4^+ mit Wasserstoffmolekülen beobachtet man eine inverse Temperaturabhängigkeit (siehe Deckblatt-Illustration). Dies wird vorläufig mit einer längeren Komplexlebensdauer bei tiefen Temperaturen erklärt. Tunneln durch eine Barriere bei tiefen Temperaturen spielt bei diesem System eine untergeordnete Rolle.

Schlagwörter

Ionenspeicher, Ionen-Molekül-Reaktion, Deuterierung, Austauschreaktion, Abstreifreaktion, Assoziationsreaktion, Cluster, protonierte Wassercluster $H^+(H_2O)_n$, Deuterium Hydrid HD, ionische Kohlenwasserstoffe CH_n^+, interstellares Medium

Contents

Chapter 1

Introduction

1.1 The interstellar medium

1.1.1 Physical conditions in the interstellar medium

Since the Big Bang and the following nuclear fusion processes in the stars, forming heavier species than the initially available hydrogen, deuterium, helium and lithium nuclei, the formed nuclear species have gathered in the vast space between the stars, the so-called interstellar medium (ISM), giving possibly rise to new formation of stars. But once the nuclear processes stopped, and the nuclei recombined with electrons to form atoms, chemical processes could take over and there is a rich chemistry going on in these interstellar clouds since millions of years. This chemistry is governed by the temperature and density conditions, ranging from about T=10K and [H_2]=10^6 cm^{-3} for dense clouds to roughly T=100K and [H_2]=10^3 cm^{-3} for diffuse clouds, enabling just certain chemical pathways to proceed. For example, endothermic reactions, exothermic reactions with a barrier or three-body processes are strongly inhibited by the mentioned conditions. Up to date, more than 120 species have been identified in the ISM (for a list see [dis99] or [kai02]), mostly by microwave spectroscopy, ranging from the most simple molecule H_2 to more complex substances like $HC_{11}N$ or C_6H_6. Of course, H_2 is the most abundant molecular species with number densities as given above. The other species are much less abundant with number densities detected down to 10^{-11} with respect to H_2. The chemical reactions driving the evolution of such interstellar clouds are to a great part ion-molecule reactions ([smi92], [ger93]) owing to the long-range attraction between ions and molecules, but also gas-grain interactions (confer [dis99] or [ber03]) and neutral-neutral processes [kai02] play a very important role, especially when ion-molecule processes are slow. There is for example still an intense research interest about how exactly H_2 forms on ice-covered grains in the ISM (Pirronello et al. [pir97, ros02]).

Our present understanding of the aforementioned processes is based on an interdisciplinary work of observational astronomers, chemical theoreticians, modelers of the ISM-chemistry and experimentalists measuring the above mentioned processes in the laboratory. The work presented in this thesis belongs to the last category, investigating clusters and ion-molecule interactions at temperatures prevailing in the ISM. This was done in the framework of the Forschergruppe Laboratory Astrophysics (FGLA) funded by the Deutsche Forschungsgemeinschaft (DFG).

1.1.2 Deuterium fractionation

A very sensitive probe for the conditions in the ISM are molecules containing deuterium atoms. These can be easily distinguished from their hydrogen containing counterparts by their different spectral fingerprints and in the last decades about 20 singly, some doubly (NHD_2, D_2CO and CHD_2OH, see Table 1 in [mil02]) and even triply deuterated molecules (ND_3 [lis02], CD_3OH [par04]) have been detected in cold interstellar clouds. Surprisingly, the measured abundance ratios of the singly deuterated molecules to their undeuterated counterparts tend to be a factor of up to 10^4 greater than expected from the D/H elemental (cosmic) ratio of roughly 1.5×10^{-5}. It is now understood, mostly as a result of detailed low-temperature studies of ion-molecule reactions, that this enrichment is largely due to the phenomenon of 'isotope fractionation'. As the deuterium in molecular clouds is mostly contained in the form of HD, it is assumed that the deuterium fractionation is initiated by ion-molecule D-atom exchange reactions involving HD as the neutral reactant. As these deuterium exchange reactions are often without significant barriers on their reaction pathway and exothermic due to zero point vibrational energy differences, they 'shovel' the deuterium one-way to more complex molecules. Up to date only three of these primary deuteration reactions are known to be fast, these are the reactions of H_3^+, CH_3^+ and $C_2H_2^+$ with HD [mil02, ger02a, ger02b].

1.2 Ion-molecule reactions

As described in the preceeding subsections, ion-molecule reactions, i.e. reactions of the type

$$A^+ + B \quad \longrightarrow \quad C^+ + D \ , \tag{1.1}$$

and especially their behavior at cryogenic temperatures, are of uttermost importance for explaining the chemical evolution of the ISM. A scheme showing the basic initial processes in dense and diffuse clouds is presented in figure 1.1, including the hydrocarbon ions CH_n^+ (n=2..5) treated in this thesis. Except the reactions of ions with molecules (mostly with H_2), there are also reactions with H-atoms, association reactions and ion-electron dissociative recombinations driving the ISM-chemistry. The significance of the ion-molecule interaction derives from the large cross section between ions and polarizable molecules with rate coefficients up to $\sim 10^{-9}$ cm^3s^{-1}, and the cross section is even larger for molecules with a permanent dipole moment (for instance H_2O). In contrast, neutral-neutral reactions generally tend to have rate coefficients about 2 orders of magnitude lower.

But it is necessary to stress here that the investigations of ion-molecule reactions not only serve to fill some astrophysical databases. Also here on earth these data are necessary to explain the rich ion-molecule chemistry in the upper atmosphere initiated by ionizing UV-photons and cosmic radiation, and also to elucidate the processes in plasmas and high-temperature flames. Finally, these investigations are also fundamental research which in the last century opened the door to a more microscopic, physical view of how a reaction is proceeding in detail. By applying laser schemes, chemical or physical quenching, temperature dependent measurements, or other suitable methods, detailed state-specific rate coefficients, for example for low lying fine structure or rotational states, as well as
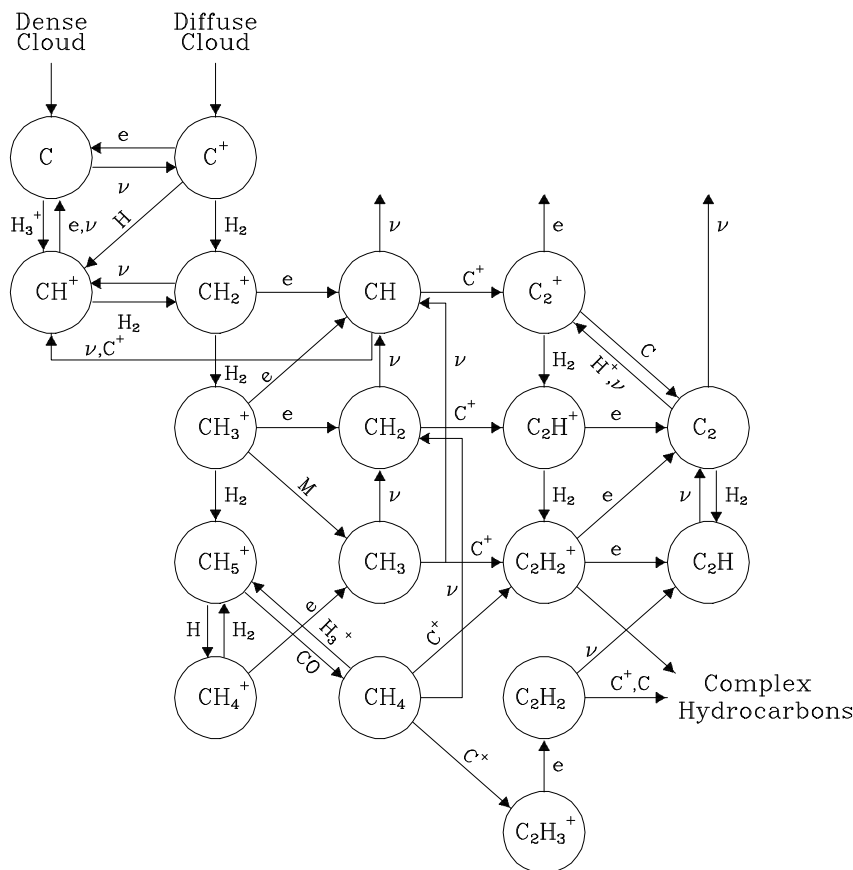
Figure 1.1: Initial steps in the gas-phase carbon chemistry in diffuse and dense clouds. Dominant processes are dissociative recombination (e), photodissociation (ν), abstraction reaction or radiative association with H_2 or carbon insertion (C^+). Figure taken from [dis99].

small differences in zero point energies caused by isotopic substitution can be investigated. Furthermore, the mentioned methods allow to explore the governing reaction dynamics, giving clues about possible intermediates, transition states and molecular structure. The obtained findings have of course to be corroborated by theoretical *ab initio* calculations or other types of experiments.

1.3   Experimental techniques

To study the ion-molecule processes, many experimental techniques have been devised beginning with simple Mass Spectrometric (MS) investigations in the first half of the 20th century. In these experiments the basic ionic processes could be observed by ionizing a gas or a gas mixture and detecting the mass spectrum of the extracted ions. These measurements gave the first insights into this interesting field, although they were hampered by the fact that mostly only the results of subsequent or parallel reaction sequences could be observed and furthermore that the internal energy of the electron-impact generated

ions was difficult to control.

First advances in this field came with the advent of **swarm techniques**, for example the Flowing Afterglow (FA) pioneered by Fergusson, Fehsenfeld and Schmeltekopf and later the Selected Ion Flow Tube (SIFT) developed by Smith and Adams (for a review of both see [smi79]). In the latter technique, mass-selected reactant ions are injected into a tube with a uniform flow of a carrier gas, usually helium. In this flow, the ions are internally relaxed by collisions, and then more downstream, a neutral reactant gas can be added. The produced ions are finally monitored at different positions of the flow, i.e. at different reaction times. To this category of techniques belongs also the CRESU (Cinétique de Réaction en Encoulement Supersonique Uniforme) method which uses a Laval nozzle to produce a uniform supersonic flow of neutral precursors (Rowe et al. [row84]). Electron bombardment or laser methods can then be used to generate ions or radicals whose collision processes can be investigated in the flow.

Another approach in the investigation of ion-molecule interactions is the use of **ion trap techniques**. An example for such a method is Ion Cyclotron Resonance (ICR) mass spectrometry (for a review see [mar98]) which is similar in operation principle to the Penning trap. Static electric and magnetic fields confine the ions on circular trajectories. The evolution of the ion masses in a bath of neutral reactants can then be observed in-situ by exciting the cyclotron motion of the ions by a suitable RF-signal and detecting the image currents of the resonant masses. A trap similar to the Penning trap is the Paul trap [pau90] which uses an alternating electric quadrupole field for ion confinement. After the invention of the Paul trap and the linear quadrupole, also higher order multipole radio-frequency traps and guides (octupoles, hexadecapoles etc.) emerged. In the 1990s, a radio-frequency ion trap consisting of 22 small RF-electrodes (called in the following 22-pole ion trap) was developed by Gerlich and coworkers [ger92] and opened the way to sensitive low-temperature investigations of ions.

Most of the results with the techniques mentioned above have been obtained at room temperature and in the early experiments, especially in the MS results, the internal energy of the ions is difficult to specify. If ion-molecule reactions at low temperatures are to be investigated at defined thermal conditions, as needed for astrochemistry, just some of the mentioned techniques can be applied. The SIFT-apparatus has been modified to obtain rate coefficients down to 80K by cooling the He flow by liquid nitrogen, and the Penning trap technique has been extended to temperatures as low as 13K by using liquid He cooling [lui85]. The CRESU technique doesn't need any external cooling because internal temperatures down to about 20K are obtained in the supersonic expansion. The 22-pole trap has the unique capability of operating at low temperatures and low neutral densities.

1.4 Overview

The experimental results presented in this thesis were taken with 22-pole machines in the laboratory of Prof. Dr. Huan Chen Chang at the Institute of Atomic and Molecular Sciences in Taipei (Taiwan) and in the group of Prof. Dr. Dieter Gerlich in Chemnitz (Germany). The operational principles of these machines are identical and are explained in section 2.1. More details about the Chemnitz 22-pole machine setup are given in the rest of chapter 2.

The experimental results are summarized in the form of published or submitted papers in the appendix. In Taipei, experiments were conducted predominantly with protonated water clusters $H^+(H_2O)_n$ (n=4..10) investigating their infrared spectra in the free OH-stretching region and the dissociation in a bath of He at low temperatures. The corresponding paper can be found in appendix A, and some more supplementary details are collected in chapter 3.

In Chemnitz, we investigated the low-temperature ion-molecule reactions of small ionic hydrocarbons CH_n^+ (n=2..5) with HD, H_2 and D_2. The governing chemistry revealed a wealth of information about the ongoing exchange-, abstraction- and association-processes, covering a range of more than 6 orders of magnitude in reaction velocities from about 10^{-9} cm^{3}s^{-1} for fast abstraction reactions to about 10^{-16} cm^{3}s^{-1} for slow radiative association processes. The results are split up into 2 publications in the appendix, treating the temperature dependence and the dynamics of the reactions with CH_4^+ (appendix B) and the reactions of CH_n^+ (n=3..5) with HD relevant for interstellar chemistry (appendix C). The association processes of CH_n^+ (n=3,5) and some of their deuterated analogues with HD and H_2 (originally planned as a publication), are described in chapter 4 together with some overview and additional unpublished information about these interesting phenomena.

Chapter 2

Experimental

2.1 Principles of ion trap experiments

The experimental results in this work have been obtained with two different ion trap machines containing as the central part a low-temperature 22-pole ion trap. For this reason, the general principles of trapping experiments are explained with the help of figure 2.1 before giving some more details about the Chemnitz machine in the next section.

Figure 2.1: General principle of a tandem mass spectrometric ion trap experiment

Usually, an ion trap machine consists of an ion **source**, a first **mass filter**, the ion **trap**, followed again by a second **mass filter** and finally the ion **detector**. The experiments are conducted in a pulsed mode. The pulse of ions generated in the ion source is mass filtered for the ionic species to be investigated in the first filter and then injected into the ion trap. Here the ions can be stored and cooled. The cooling of the translational and internal degrees of freedom usually happens by inelastic collisions with a cold buffer gas, mostly helium. After relaxation, the ions are allowed to interact with neutral molecules or a laser beam (not shown in figure 2.1) admitted to the trap. After the storage period, the result of the interaction can be observed as a function of product mass and trapping time by releasing the total trap content into the second mass filter and counting the mass-filtered ions in the detector.

One pulse of ions as described above contains around 1000 parent ions which are finally stored in the 22-pole ion trap. This number is of course subject to statistical fluctuations. Furthermore, with one such bunch only **one** trapping time and **one** product mass is registered at a time. To get a better counting statistics and the time dependence of all observed product masses, the pulses are repeated many times (about 20 times) for each product mass and typically for twenty different storage times.

2.2   22-pole ion trap machine

The details of 22-pole ion trap machines have been described thoroughly by Gerlich [ger92] and many PhD thesis' [sor94, pau96, hau97, les00, luc01, wan01, ric02], so these facts are not repeated here. Only recent changes, topics important for this work and those facts elemental for understanding are explained. There are currently two 22-pole setups in Chemnitz, the one used in this work is shown in figure 2.2.
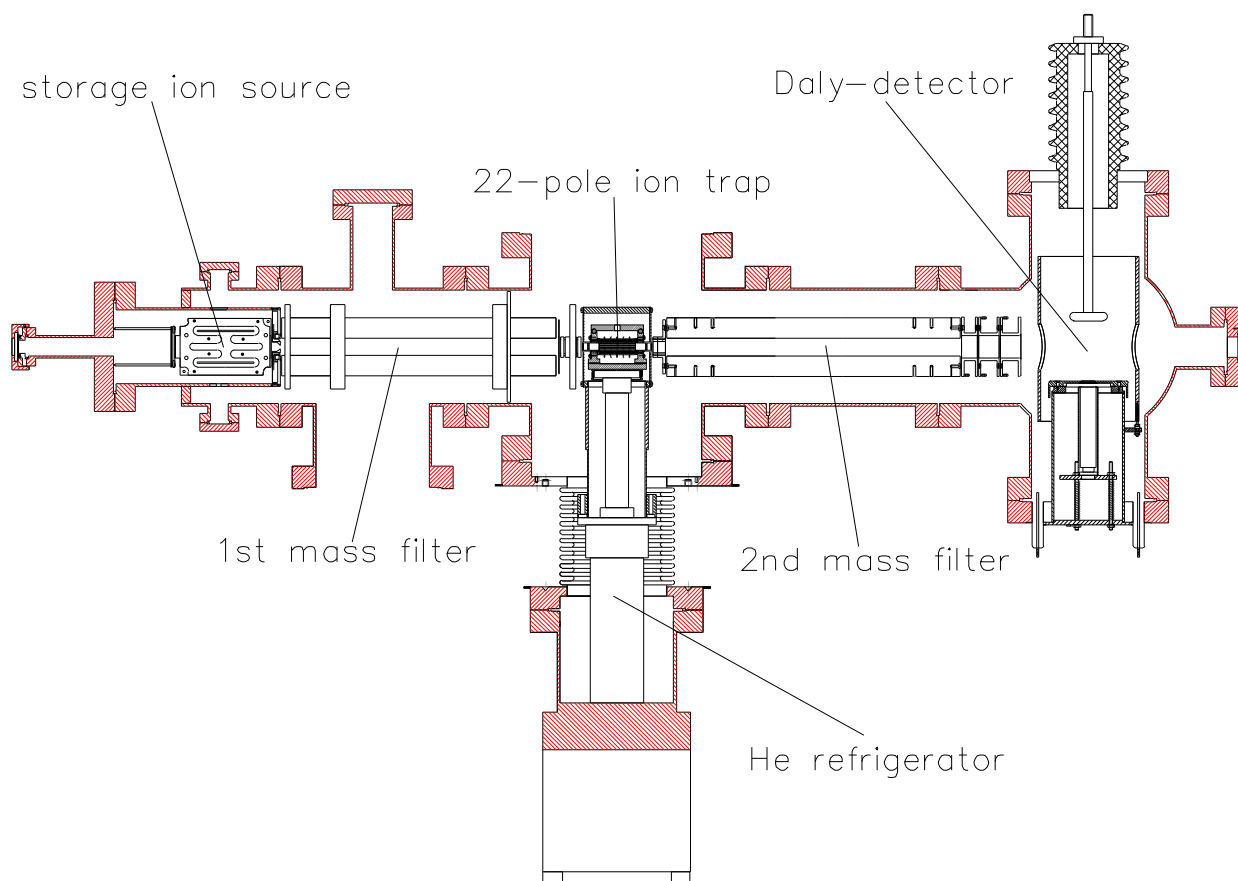
Figure 2.2: The setup of the 22-pole ion trap apparatus

The **ion source** is a storage ion source which is itself an ion trap consisting of a stack of 8 rectangular RF-electrodes. These electrodes have cut-outs inside to store the species generated by electron impact of a neutral precursor gas. After generation, the ions are trapped in an environment where they can cool by collisions to the source temperature (around 350K), or if desired, react with other neutral molecules to the desired species. Variation of the trapping parameters, precursor gas mixture and pressure permits a good control over the generated ion composition. Furthermore, the storage property of the source allows low pressures to be used, so as to keep the precursor gas pressure in the main chamber as low as possible.

The **mass filters** mentioned in section 2.1 are both quadrupole mass spectrometers. The first quadrupole mass filter is 245mm long and the second 260mm. One such quadrupole

mass filter consist of 4 rods each of d=18mm diameter circumscribing an inner circle of r_0=7.8mm radius. RF- and DC-voltages (plus floating voltage) are applied to these four rods. By properly selecting the amplitudes of the applied voltages, the transversal trajectories of some masses get unstable [daw76], so that a selected mass or mass range is only transmitted to the end of the mass filter. In our case, the second mass spectrometer is operated in mass-selective mode driven by a commercial 1.6MHz RF power supply, while the first mass filter is operated in either mass-selective or low-pass mode driven by home-built RF power supplies. More facts about the operation modes of the first quadrupole mass spectrometer are given in section 2.2.2.

The heart of the experiment is the **22-pole ion trap** which is mounted onto a closed cycle He refrigerator. Trapping of the ions in the radial direction is achieved by applying a suitable RF voltage (typically $f \approx 17$MHz, $V_0 \approx 50$V) to the 22 poles (the 22 rods are each of of 1mm diameter and 36mm long, uniformly circumscribing an inner circle of 1cm diameter) of the trap, while trapping in the longitudinal direction and control of the ion storage time is done by pulsed entrance and exit electrodes. The unique wide field free region of the 22-pole trap [ger92] makes experiments at low collision temperatures possible. Reactant and buffer gases are introduced into the trap by pre-cooled tubes, reaching the final trap temperature before entering the interaction region. The translational and internal degrees of freedom of the injected ions are coupled to the cold environment by inelastic collisions with the (continuous or pulsed) buffer gas or via radiation.

The **He refrigerator** consists of a 2-stage coldhead (Leybold RGD 210) and a He compressor (Leybold RW2). The first stage of the coldhead cools the radiation shield surrounding the trap while the second stage is in good thermal contact with the 22-pole ion trap. The system permits the trap to be cooled down to approximately 15K within 1 1/2 hours. The trap temperature can be adjusted with heater wires winded around the trap holder and measured with carbon resistors.

Ions transmitted through the second quadrupole mass spectrometer enter the **Daly-detector** [dal60] where they are counted with high efficiency. This is done by accelerating them onto an electrode held at -30kV, where secondary electrons are emitted on impact. These electrons are accelerated in the same high voltage field to a grounded scintillator on the opposite side where they are converted into photons. The photons are finally detected by a photomultiplier tube located outside of the vacuum chamber. The generated pulses of the photomultiplier tube have a width on the order of 10ns, usually the maximum count rate is kept below 10MHz to avoid saturation. This detection scheme allows only cations to be detected, but on the other side it bears many advantages. Except the aforementioned high efficiency (up to 100%), the detector setup does not degrade with successive ventings, has nearly no mass discrimination, and allows the possibility of introducing a laser beam into the 22-pole machine, as all detector components are transversally located.

2.2.1 Vacuum system

The former vacuum system of the 22-pole machine consisting of rotary vane backing pumps, turbo pumps and diffusion pumps has been replaced in the year 2001 by two magnetically levitated turbo pumps and an oil-free diaphragm pump of the company Pfeiffer. Later in August 2002 a drag pump was added to the system to increase the compression ratio. Please refer to figure 2.3 for the actual pumping system setup and the

pumping speeds of respective device.

Good vacuum plays a crucial role in trapping experiments, especially if long trapping times are desired for sensitive measurements, as the only practical limitation to ion storage is due to parasitic reactions with background molecules. With the new system, a background pressure on the order of 10^{-10} mbar is obtained after bakeout (usually 2 days at a temperature not exceeding 60°C). The background molecules are mostly H_2O and H_2 and their number density has been determined by reactions with known rate coefficients to be roughly 1×10^7 cm^{-3} for H_2O at 300K (see for example the measurement in figure 4.3) and 1×10^8 cm^{-3} for H_2. Operating the coldhead decreases the H_2O number density inside the trap by about 2 orders of magnitude, the H_2 background number density doesn't change remarkably.

The pressure in the vacuum chamber is measured by two ion gauges, one in the region of the first quadrupole mass spectrometer, the other mounted to the main chamber (see figure 2.3). The vacuum interlock system is connected to the latter ion gauge, shutting down all sensitive power supplies when the pressure in the chamber exceeds 10^{-4} mbar. There is also a spinning rotor gauge connected to the inside of the 22-pole trap by a stainless steel tube to measure accurately the number density of reactant molecules (see section 2.3.1).

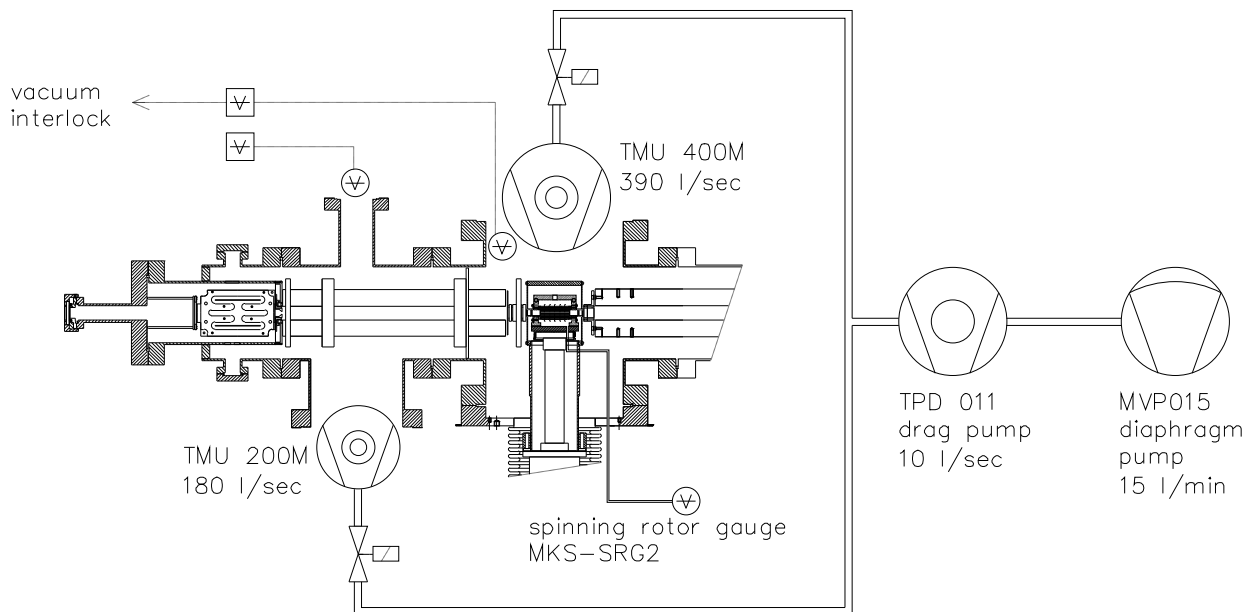Figure 2.3: New vacuum system of the 22-pole machine. The pumping speeds for nitrogen N_2 are indicated in the figure for each pump. The corresponding compression ratios are $> 10^{10}$ for the two main turbo pumps and 3×10^6 for the drag pump. The compression ratios of the turbo pumps for hydrogen H_2 are 5×10^4 for TMU 400M, 5×10^5 for TMU 200M and 3×10^2 for the drag pump TPD 011.

2.2.2 Operation of quadrupole mass spectrometers

A quadrupole mass spectrometer consists of four cylindrical rods to which in alternating order voltages of the form $\pm(U_0 - V_0 \cos \Omega t)$ are applied. The principles of such a device are best explained with the stability parameters a_2 and q_2 defined by [ger92, daw76]

$$a_2 = \frac{8 \cdot U_o \cdot q}{m \cdot \Omega^2 \cdot r_0^2} \tag{2.1}$$

$$q_2 = \frac{4 \cdot V_o \cdot q}{m \cdot \Omega^2 \cdot r_0^2} \tag{2.2}$$

with the variables

$\Omega = 2\pi f$	frequency of RF power supply
r_0	inscribed radius of quadrupole system
m	ion mass
q	elementary charge
U_o, V_o	DC voltage and and RF-amplitude .

These two parameters are in principle expressions for the normalized amplitudes of the RF- and DC- voltages applied to the quadrupole rods. Depending on these two parameters the transversal motion of an ion in a quadrupole mass spectrometer can be stable or unstable, as indicated in the stability diagram 2.4 with the axes being a_2 and q_2. If the set of parameters (a_2, q_2) is located within the triangle-shaped region, the ions will survive the pass through the quadrupole, otherwise they are unstable and will eventually hit the rods and be lost. Now, depending on exactly where in the diagram we operate
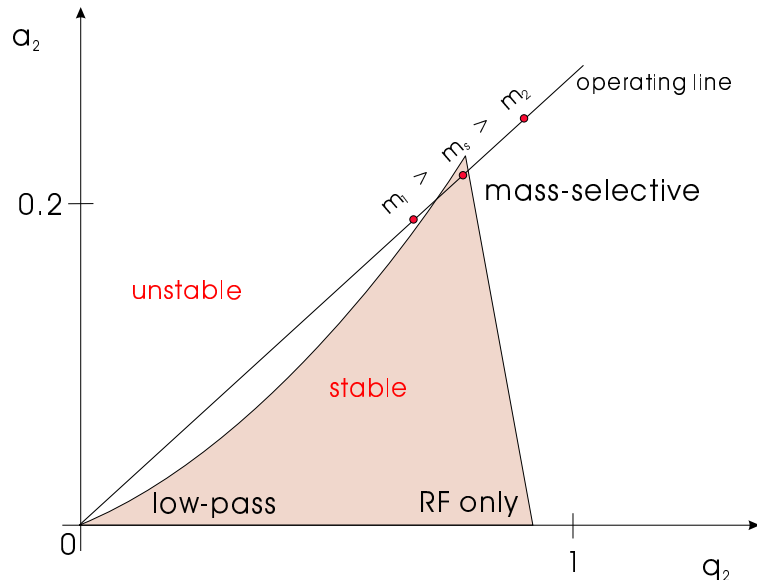

Figure 2.4: Different operation modes of a quadrupole mass spectrometer and their location in the stability diagram. The parameter a_2 is a measure for the applied DC voltage while q_2 is a measure for the RF amplitude.

the quadrupole for mass selection, we distinguish between two different regions in the stability diagram 2.4 called **mass-selective** and **low-pass** mode.

If only one mass should be transmitted, we adjust the set (a_2, q_2) for the selected mass m_s to be inside the stability region close to the tip at (0.237,0.706). All other masses are outside the stability region located on the operating line as shown in the diagram 2.4. Please note that in the relation 2.1 and 2.2 the two stability parameters a_2 and q_2 are reciprocal to the ion mass m, so the order of the masses on the line is as indicated in the figure. If we would like to select another mass in the quadrupole, we change a_2 and q_2 in a proportional manner (by changing the voltages U_o and V_o) so that the desired mass is shifted into the stability region and all other masses shifted out along the line. If the operating line in figure 2.4 is lowered, i.e. we apply just a small DC voltage U_0 to the quadrupole rods, we operate the filter in the low-pass mode. In this case, the operating line cuts the stability region in the lower part of the left boundary. As indicated on the line, higher masses will lie in the unstable region, while beginning from some cutoff value, a range of lower masses will be stable. If we finally don't apply any DC voltage at all, the operating line will coincide with the q_2-axis and the quadrupole is said to operate in the RF-only mode. In this thesis, the mass-selective and low-pass mode were applied for the first quadrupole. More details about these two modes are given in the following two subsections.

Low-pass mode

For driving the first quadrupole in low-pass mode, we used a self-made RF-power supply of the push-pull-type. Since these electron tube based simple oscillators are very robust, they are still widely used to drive RF traps and guides, as reviewed by Jones, Gerlich and Anderson [jon97, jon00]. With the quadrupole load connected, it had a frequency of f=11.7 MHz. The use of this relatively high frequency allows to inject the ions into the trap under adiabatic conditions, i.e. the transversal energy of the ions after leaving the quadrupole is kept as low as possible. The low-pass boundary region (left boundary of triangle-shaped stability region in figure 2.4) is described by the relation $a_2 \approx 1/2 \cdot q_2^2$ [ger92, daw76], and replacement of a_2 and q_2 by formulae 2.1 and 2.2 gives the low-pass cutoff mass

$$m_c = \frac{q \cdot V_o^2}{\Omega^2 \cdot r_0^2 \cdot U_o} \qquad . \qquad (2.3)$$

Application of this relation is shown in figure 2.5, where the CH_n^+-mixture coming from the storage ion source was cut off after mass 15, here predominantly CH_3^+. The RF-amplitude V_o used was usually in the range of 150V. This together with r_0=7.8 mm and angular frequency $\Omega = 2\pi f$ =73.5 MHz gives us a DC voltage of only U_o=0.4 V, using the above relation with m_c=15.5 u. Please note that the calculated DC voltage means that 0.4 V is applied to one pair of quadrupole rods, while -0.4 V is applied to the other pair. Without using this DC voltage, the CH_4^+-peak (mass 16) in the spectrum is usually slightly higher than the CH_3^+-peak (mass 15), i.e. by using the low-pass mode in figure 2.5 mass 16 is suppressed by a factor of at least 10^3 more than mass 15.
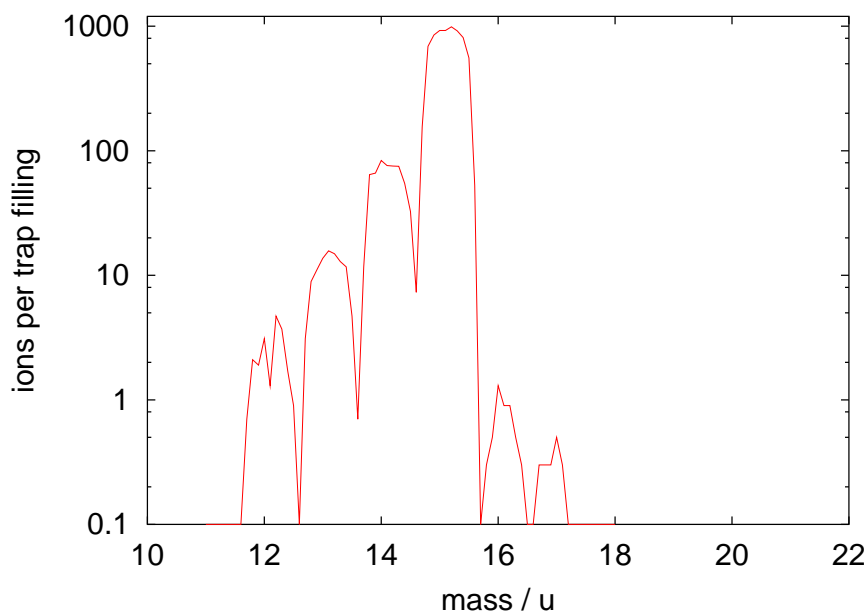
Figure 2.5: Mass spectrum scanning the second quadrupole with first quadrupole operated in low-pass mode. This spectrum was recorded after 100 ms trapping time and no reactant or buffer gases in the 22-pole ion trap.

Mass-selective mode

As mentioned, the low-pass mode allows to inject the ions with well-defined low kinetic energies into the 22-pole ion trap due to the high frequencies used. But on the other side, if the co-transmitted lower masses obscure the reactions to be investigated, full mass selection is desired. For this, we have to put our operating point in the stability diagram 2.4 close to the tip at (0.237,0.706). Application of the relation 2.2 with the parameters as given above shows, however, that for this purpose we would need RF-amplitudes in excess of V_o=1000V even for very low masses. So a lower frequency f had to be applied. For this we used a modified RF-power supply shown in scheme 2.6. The heart of this circuit is a double tetrode tube type VALVO QQE 06/40 driving an LC-circuit shown in the upper part of the figure. With a value of $L = 37\mu$H calculated with the coil-parameters given in the figure and $C = 0.5$nF (two capacitors of 1nF in series), we obtain an estimated frequency of $f = 1/(2\pi\sqrt{LC})$=1.2MHz. Together with the quadrupole load (the first quadrupole has a capacity between the rods of approximately 70pF), we measure f=1.3MHz. The double tetrode tube is forced to run at this frequency by the feedback circuit leading to the gates marked g1 and g1'. The filament circuit is supplied with 6V (max. 2A). Typical parameters for the Anode voltage (supplied from an external power supply) are 100V DC with a current of 19.6mA, giving an RF output amplitude of V_o=115V. The DC-voltages are applied to the quadrupole rods with the small additional circuit shown on the upper left part of figure 2.6. The aforementioned DC difference voltage U_o is applied as $2U_o$ to the inputs marked as '+' and '−' from an external floatable DC power supply. Except this voltage, also a float voltage U_{4PI} must be applied to all quadrupole rods. This voltage defines the kinetic energy of the ions in
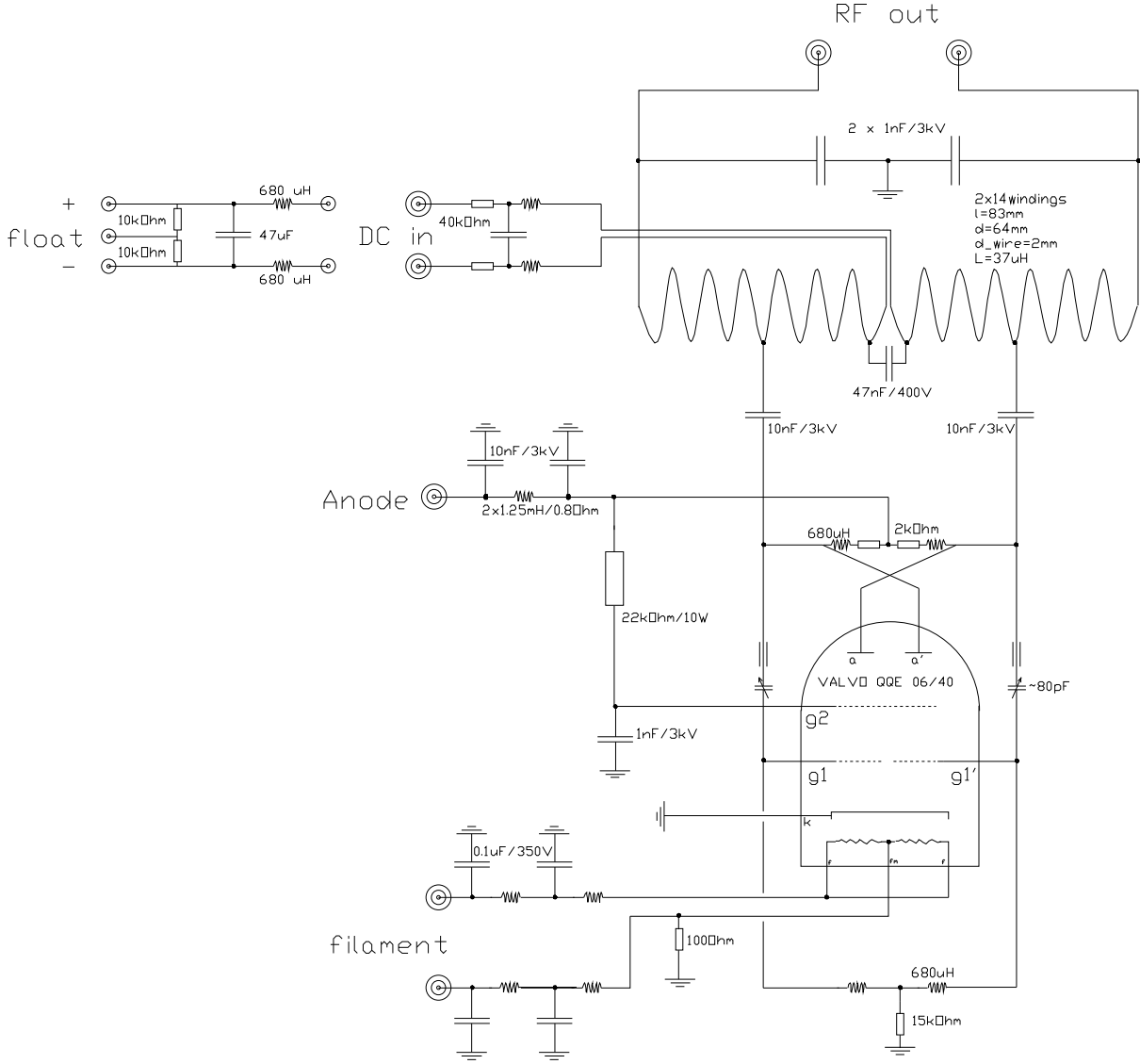
Figure 2.6: 1.3MHz RF generator for driving the first quadrupole in mass-selective mode.

the quadrupole. The DC voltages are decoupled from the RF-circuit part (lower part in scheme 2.6) by capacitors. The total signal generated by the RF-supply at the 2 BNC-outputs is $U_{4PI} \pm (U_o - V_o \cos \Omega t)$.

Let's make a small illustrating example: If we would like to select m=20u with the parameters as given above, then with f=1.3MHz, (a_2,q_2)=(0.237,0.706), r_0=7.8mm, we obtain U_o=26.2 V and V_o=156.2 V. This means we have to use an anode voltage of approximately 136V and a voltage of $2U_o$=52.4 V applied to the DC-inputs of the RF-power supply. The float voltage U_{4PI} is optimized to obtain a maximum count of ions with low kinetic energies. A typical value is $U_{4PI} = -0.4$V. The voltage values given above are in good agreement with the voltages adjusted in practice. Usually, mass selection is achieved by first applying the calculated RF-voltage V_o with no DC-voltage U_o applied, and then observing the mass spectrum as scanned by the second quadrupole mass analyzer. Then the DC-voltage U_o is slowly turned on so that the transmitted mass range is slowly
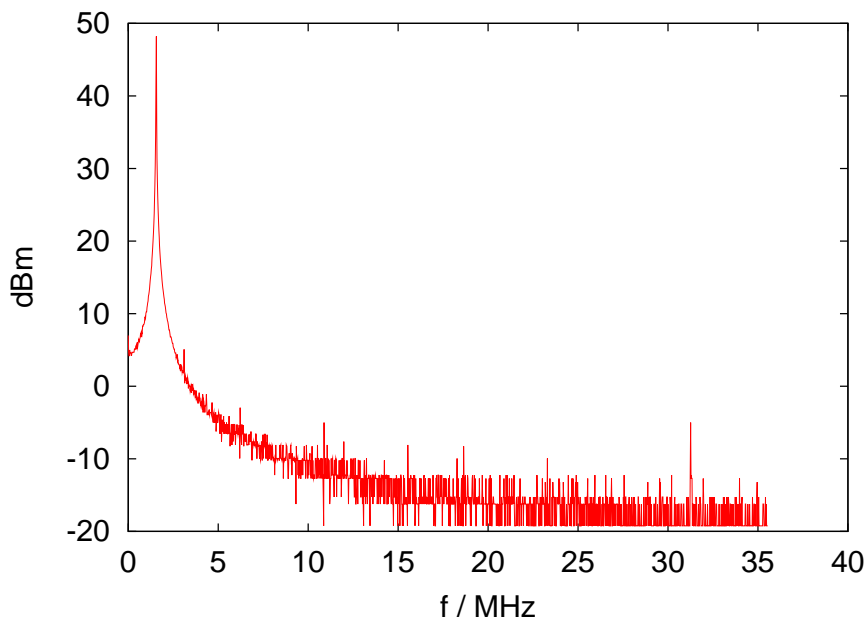
Figure 2.7: FFT power spectrum of 1.3MHz RF-generator

narrowed down, until finally only the desired mass peak is left over after minor adjustments to both V_o and U_o.

The performance of the RF-generator is illustrated in figure 2.7 showing the Fast Fourier Transform (FFT) power spectrum of the RF-generator taken with a rectangular window. In this measurement, a 1:10 probe was connected directly from a LeCroy Oscilloscope to the outputs, so that the measured frequency f=1.56MHz is somewhat higher due to the missing capacitive quadrupole loads. As can be seen, the circuit 2.6 supplies a clean RF-signal for quadrupole operation. There are also some higher harmonics visible, but they are suppressed by several orders of magnitude.

2.2.3 Data processing

What one likes to know in our investigations is the rate coefficient of an ion-molecule reaction of type 1.1 where the ion A^+ is reacting with the neutral molecule B to produce the ion C^+. The rate coefficient k, a measure of the speed of the reaction, is best defined by the relation

$$\dot{N}(t) = -N(t) \cdot k \cdot n \tag{2.4}$$

where N is the number of parent ions A^+ and n is the number density (in cm^{-3}) of the neutral reaction partner B. As we can see from this relation, the unit for the rate coefficient k is $cm^3 s^{-1}$. Integration of the equation 2.4 for $N(t)$ yields an exponential decay of the number of parent ions A^+.

But usually, there is not just a single ion-molecule reaction occurring in the ion trap, instead there is a total number m of parallel and/or subsequent reactions going on. Thus in the most cases the time-dependence of the parent and product ions is not just a simple

single-exponential one. To obtain the rate coefficient k_i $(i = 1, \ldots, m)$ of every contributing reaction step, all occurring parent and product masses are recorded as a function of time. Then these recorded time dependencies are fitted with theoretical curves based on a set of m coupled reactions. Analytical solutions to the corresponding set of coupled equations in more complex cases are not always feasible, so numerical calculations have to be used. For this, we first assume some reasonable initial conditions for the number of ions at time zero, and then do small time steps Δt using the infinitesimal form of relation 2.4,

$$\Delta N_i = -N_i \cdot k_i \cdot n \cdot \Delta t \qquad i = 1, \ldots, m \qquad , \qquad (2.5)$$

where after every small time step Δt we subtract $|\Delta N_i|$ from the number of parent ions N_i of the reaction i and add the same amount to the corresponding product ion, so that the total number of ions is conserved. These time steps have to be small enough for the numerical calculation not to lead to erroneous results, i.e.

$$\Delta t \ll \frac{1}{k_i \cdot n} \qquad i = 1, \ldots, m \qquad . \qquad (2.6)$$

To satisfy this condition, usually between 1000 and 10000 time steps are used. The result of such a numerical simulation is then the time dependence of the ionic species for a certain set of k_i $(i = 1, \ldots, m)$ and a fixed number density n. These k_i are then varied until a reasonable fit to the measured time dependencies is obtained. In this thesis, the numerical calculations were done using *awk* scripts on a *linux*-platform, but any other simple programming language will also do. Examples for recorded ion mass time dependencies and theoretical fits can be found in the figures in chapter 4.

2.3   Test measurements

2.3.1   Measurement of neutral density

As seen in equation 2.4 of the preceeding section, the reliable measurement of rate coefficients k depends on the accuracy in counting the number of ions N and measuring the number density n of the neutral reaction partner. Pressures and number densities are normally indicated by ion gauges, but for our purposes more accurate pressure meters are needed, for example capacitance manometers (Baratrons) or spinning rotor gauges. The Chemnitz 22-pole machine uses a spinning rotor gauge type MKS SRG2, in the following called Viscovac. It is located outside the apparatus and measures the number density n inside the 22-pole ion trap by a stainless steel tube connection. This Viscovac is specified to be accurate within 5%. Unfortunately, it can be applied only to densities not lower than 10^{-7} mbar and is very sensitive to vibrations, for example caused by the moving displacer of the coldhead or accidentally slammed doors. The main chamber ion gauge doesn't have these disadvantages, hence, it can be calibrated against the Viscovac. Please confer figure 2.3 for the locations of the two pressure meters.

Viscovac calibration

The calibration of the ion gauge against the Viscovac is dependent on the applied gas as will be explained below and thus has to be performed for every reactant gas to be
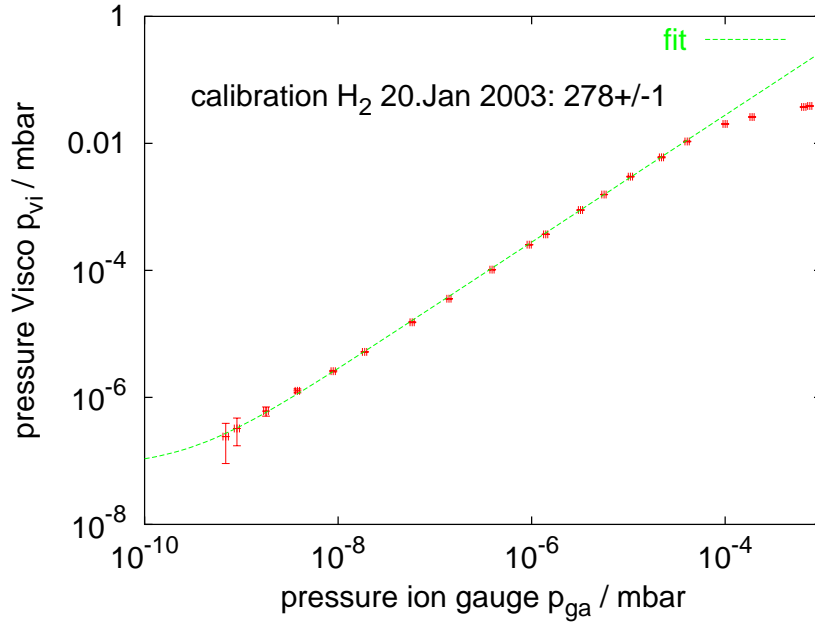
Figure 2.8: Calibration of ion gauge against Viscovac for H_2 gas. The errors for the Viscovac pressure p_{vi} are standard deviations for 20 measurements. See text for further details.

used. The calibration procedure is simply done by introducing the gas to be calibrated into the 22-pole ion trap and measuring both pressure meter readings (designated in the following p_{vi} and p_{ga}) at 300K, as shown in figure 2.8 for H_2. As can be seen in the figure, there is a proportional relation between the two readings which can be fitted by $p_{vi} = \mathcal{C} \cdot p_{ga} + p_{off}$ giving a calibration factor of $\mathcal{C}=278$ for H_2. The term p_{off} is a tiny residual pressure offset of the Viscovac at low pressures seen in figure 2.8. The visible deviation from the linear fit at pressures p_{vi} exceeding 10^{-2} mbar is due to intrinsic non-linearities of the Viscovac in the transition region from free molecular flow to continuum gas flow [mks90, wut97]. Table 2.1 summarizes the calibration factors $\mathcal{C}$ obtained for the 4 gases used in this work, namely H_2, HD, D_2 and He. The calibration factors $\mathcal{C}$ originate from the pressure drop through a small aperture of area A between the inside of the ion

gas	H_2	HD	D_2	He
calibration factor $\mathcal{C}$	278	352	444	1233
relative sensitivity	0.3-0.45		0.35	0.13-0.18
pumping speed S / l/s	280			350

Table 2.1: Measured gas calibration factors $\mathcal{C}$. Included in the table are also ion gauge sensitivities relative to nitrogen N_2, and pumping speeds S of the main chamber turbo pump TMU400M for the different gases (data taken from [pfe00]). The nominal pumping speed of this pump for N_2 is 400l/s. The gas calibration factors given here are valid for a selected ion gauge sensitivity of 19 mbar^{-1}.

trap and the main chamber, but also the sensitivity (ionization probability) of the ion gauge to different gases has to be considered. Typical sensitivities of ion gauges relative to N_2 for the gases used are also included in table 2.1. The mentioned ratio between the pressures in the trap and the chamber can be estimated using the factor

$$1 + \frac{S}{\alpha A} \sqrt{\frac{2\pi m}{k_B T}} \tag{2.7}$$

knowing the pumping speed S, the molecular mass m and the transmission probability α for molecules through a small tube of area A. For this formula we assume the trap and the chamber to be at same temperature T. Using this relation and the ion gauge sensitivities from table 2.1 gives reasonable relative agreement between the different calibration factors $\mathcal{C}$.

Determination of neutral density

With the above measured calibration factors $\mathcal{C}$ we can determine the pressure of the neutral reactant inside the 22-pole ion trap if the ion gauge (ga) and the trap (tr) are at the same temperature. But usually in most experiments the trap is cooled down to low temperatures $T_{tr} = 15$K while the point at which we measure the pressure is still at $T_{ga} = 300$K. In this case, we have to use the relation [laf98]

$$\frac{p_{tr}}{p_{ga}} = \sqrt{\frac{T_{tr}}{T_{ga}}} \tag{2.8}$$

and taking into consideration the different temperatures. Introduction of the calibration factor $\mathcal{C}$ and solving for the number density n_{tr} in the ion trap gives us

$$n_{tr} = \frac{p_{tr}}{k_B T_{tr}} = \mathcal{C} \frac{p_{ga}}{k_B \sqrt{T_{tr} T_{ga}}} \tag{2.9}$$

and insertion of the value of the Boltzmann constant k_B and $T_{ga}=300$K gives us the final practical relation

$$n_{tr} = \mathcal{C} \cdot 4.18 \times 10^{17} \cdot \frac{p_{ga}}{\sqrt{T_{tr}}} \quad \text{cm}^{-3} \tag{2.10}$$

for determining the number density n_{tr} of the neutral reactant inside of the 22-pole ion trap, with the density given in cm^{-3}, the temperature in units of K and the pressure in mbar.

Some words should also be said about the accuracy of the measurement of the neutral density n_{tr}. The Viscovac is specified to be accurate within 5%, but the calibration factors are also slightly sensitive to the performance of the backing pumps and can therefore change slightly in time. Furthermore, the determination of n_{tr} depends also on the trap temperature T_{tr} (see relation 2.10), and hence also the temperature uncertainties have to be considered. Finally, there is not a constant neutral density throughout the trap, rather there is a density distribution with a maximum in the trap center with decreasing densities approaching the two trap ends [kae89]. In total, the overall accuracy for the determination of n_{tr} is rather in the range 10% to 15%.

2.3.2   Measurement of HD-purity

Deuterium hydride, HD, was extensively used in the ionic hydrocarbon experiments described in chapter 4. It was purchased from Cambridge Isotope Laboratories Inc. who specify the purity to be 97%, the rest being H_2 and D_2. The gas was contained in a 460ml carbon steel lecture bottle with a content corresponding to 5 normal liter, i.e. the pressure in the small cylinder was 10.8 bar. According to the manufacturer [rob02], at pressures exceeding 70 bar HD can react to form a statistical mixture of H_2, HD and D_2, this process being negligible below 50 bar. We wanted to confirm the above specification and tested the purity of HD with 2 different reactions described below. No modification of the 22-pole machine setup was necessary for this purpose. The HD gas from the bottle was lead to the interaction region inside the 22-pole trap via an adapter (CGA 110 to Swagelock), a leakage valve and a stainless steel tube.

Reaction $Ar^+ + H_2$

Argon cations generated in the source were injected into the trap containing HD and the small impurities of H_2 and D_2. If we first assume the simple case of pure H_2 (or D_2) as the reaction partner, there are two primary reaction channels,

$$Ar^+ + H_2 \quad \longrightarrow \quad ArH^+ + H \tag{2.11}$$
$$\longrightarrow \quad Ar + H_2^+ \qquad , \tag{2.12}$$
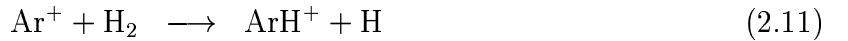
an H-atom abstraction channel (about 85%) and a charge transfer channel (15%). In the bath of H_2 these products react further to give

$$ArH^+ + H_2 \quad \longrightarrow \quad Ar + H_3^+ \tag{2.13}$$
$$H_2^+ + H_2 \quad \longrightarrow \quad H + H_3^+ \tag{2.14}$$

leading finally in everything ending up in H_3^+. Injecting Ar^+ in pure HD, these processes get a little bit more complicated due to the two possibilities of H-atom or D-atom abstraction, but the reaction sequences similar to 2.11 through 2.14 end in the products H_2D^+ and HD_2^+. These in turn react in the HD bath to deuterated H_3^+-analogues, i.e. there will be an equilibrium distribution ranging from H_3^+ to D_3^+, depending on the temperature. But we are interested here in the determination of the H_2 impurities contained in HD. For this we use the charge transfer channel 2.12. As stated, this channel yields H_2^+ (mass 2) if the argon ion encounters an H_2 molecule and HD^+ (mass 3) if it encounters deuterium hydride. Assuming equal rates for the charge transfer channel for H_2 and HD, this gives us a measure of the H_2 contamination as shown in figure 2.9. For clarity, only masses 2 and 3 are shown and those for Ar^+, ArH^+, ArD^+, etc. are omitted. The H_3^+ arising in that figure is due to the above mentioned reactions leading to an equilibrium distribution of H_3^+-analogues. This measurement gives us less than 1% of H_2 contained in HD. It is not possible to measure the D_2 impurities with this method, because it is obscured by H_2D^+, but it is assumed that it is abundant in the same amount as the H_2 impurities. The following method gives us the possibility to measure both the H_2 and D_2 contamination.
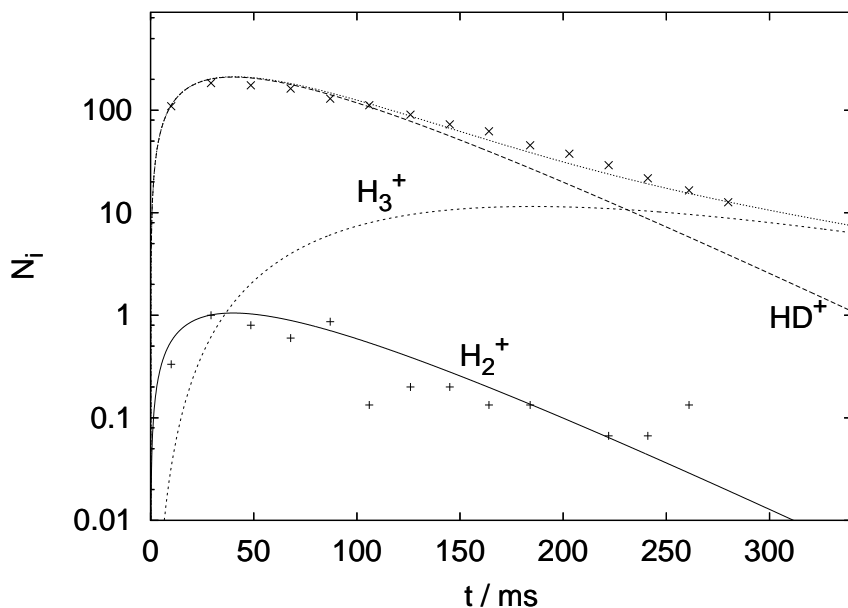
Figure 2.9: HD-purity measurement with reaction $Ar^+ + HD/H_2$ at a trap temperature of 20K. Shown are only the products with mass 2 (H_2^+) and mass 3 (HD^+ and H_3^+). The lines represent the numerical solution of an adequate rate equation system like discussed in section 2.2.3. The signal from H_2^+ is 2 orders of magnitude lower than HD^+. The H_3^+ originates from the reaction sequence $H_3^+ + HD \rightleftharpoons H_2D^+ + HD \rightleftharpoons HD_2^+ + HD \rightleftharpoons D_3^+ + HD$ leading finally to equilibrium at longer storage times (not shown in this figure). At 20K, the equilibrium distribution is about 0.01% H_3^+, 0.51% H_2D^+, 11.25% HD_2^+ and 88.23% D_3^+.

Association $CD_3^+ + HD$

If CH_3^+ is injected into the trap containing HD at low temperatures, it will first undergo three fast deuteration reactions resulting in CD_3^+, which will then further react by radiative or ternary association (please confer figure 4.4 in section 4.3 for an overview of these processes):

$$CD_3^+ + HD \longrightarrow CHD_4^+ + h\nu \tag{2.15}$$

$$CD_3^+ + 2HD \longrightarrow CHD_4^+ + HD \quad . \tag{2.16}$$
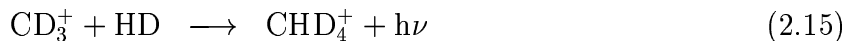
These association reactions resulting in CHD_4^+ (mass 21) can be observed in the mass spectrum of figure 2.10 as well as the subsequent much slower association step to the cluster ion $CHD_4^+(HD)$ (mass 24). The impurities of H_2 and D_2 give rise to similar association reactions detectable as side peaks of mass 21 in the spectrum. Taking for simplicity equal radiative and ternary rate coefficients for the association with H_2, HD and D_2 (these types of reactions and their dependence on isotopic configuration are discussed in section 4.4), one can estimate from the peak intensities that the total impurity of H_2 and D_2 contained in the HD gas is less than 3%.

26
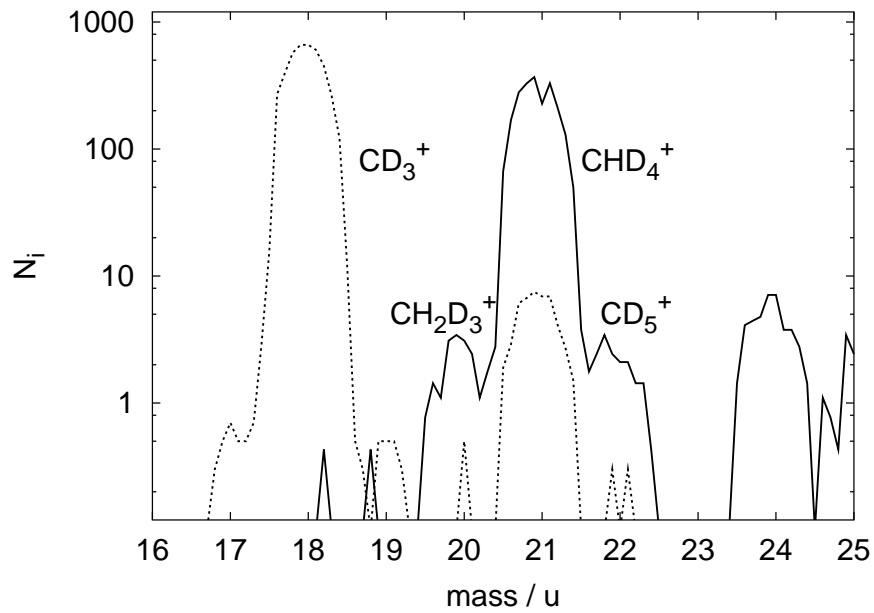
Figure 2.10: Mass spectrum showing the association of CD_3^+ with HD at two different number densities of $[HD]=3.5 \times 10^{10}$ cm^{-3} (dotted line) and $[HD]=3.5 \times 10^{12}$ cm^{-3} (solid line). The CD_3^+ was produced by injecting CH_3^+ into the trap and 3 fast deuteration steps in HD. The association products CHD_4^+ (mass 21) and $CHD_4^+(HD)$ (mass 24) are visible, but there are also satellite peaks to the first association peak due to H_2 and D_2 impurities. This mass spectrum was taken at a temperature of 15K and 1s trapping time.

Chapter 3

Protonated water clusters $H^+(H_2O)_n$

3.1 Introduction

3.1.1 A small history of $H^+(H_2O)_n$

Protonated water clusters $H^+(H_2O)_n$ are not only of general interest in physical chemistry, but also play important roles in the interstellar medium, atmospheric chemistry and biological systems. This interest comes surely from the high abundance of water on earth, and also from the ease of formation of smaller clusters, as the water molecule has a high proton affinity of 165 kcal/mol [hun98] to form H_3O^+, the simplest species in this series with n=1.

Experiments with these clusters go back to the 1970s when the Kebarle group [cun72, lau82] and Meot-Ner and coworkers [meo86] investigated the equilibrium of these clusters in pulsed high pressure mass spectrometric experiments and deduced the bond energies and other thermochemical quantities from the temperature dependence of the equilibrium constants. First low-resolution infrared spectra of gas-phase water cluster mixtures have been reported by Schwarz in 1977 [sch77], but it was only after the use of the corona discharge source [sea74] for production of internally cold clusters and the application of mass selection that many detailed spectroscopic investigations could be conducted. The Y.T. Lee group investigated small protonated water clusters (n=2..4) in the free OH-stretching region (i.e. 3500 to 3800 cm^{-1}) first with the H_2-messenger technique (Okumura et al. [oku86]) and later with the infrared multi photon dissociation (IRMPD) method (Yeh et al. [yeh89]). These investigations have been extended to larger clusters [jia00, wan97] by applying predissociation spectroscopy revealing many structural information up to n=8 in the free and bonded OH-stretching regions (2700 to 3900 cm^{-1}). For these highly solvated cluster the spectral assignment becomes increasingly difficult due to the manifold of structural isomers. Recently, Asmis and coworkers [asm03] obtained the gas-phase spectrum of the protonated water dimer (n=2) in the far infrared (620 to 1900 cm^{-1}) using the IRMPD technique.

Of special interest have also been the bond energy deviations from the smooth sequence indicating special stable structures or shell closures. The first shell closure at n=4 was already observed by Kebarle and the special stability of this cluster can be observed in many experiments. The $H^+(H_2O)_n$ cluster with n=21 is also observed to have special stability (see e.g. [sch96]) and this is ascribed to a 'clathrate' cluster structure. In the last years many measurements of the bond energies have been done with different approaches

[lov00, mag91, shi93] in the range up to n=28, although there are still some discrepancies left. Lovejoy and coworkers [lov00, lov01, cur01] demonstrated the feasibility of determining the bond energy of small clusters by measuring the dissociation rates in a He buffer bath gas at various temperatures together with calculations of the internal energy. They performed their experiment for protonated water clusters with n=3,4 using a Paul trap at temperatures around 300-500K. This work (see paper appendix A) represents an extension of their method to lower temperatures, allowing to study the weaker bonded clusters n=4..10.

3.1.2   Protonated water clusters and water ice in the ISM

Protonated water clusters $H^+(H_2O)_n$ and mixed clusters of the type $H^+(H_2O)_n(H_2)_m$ (as an example) can also be found in dense interstellar clouds. As summarized by Duley [dul96], they are most probably formed by cosmic-ray-induced desorption from dust grains which are known to be covered with an ice layer consisting of H_2O, CO, methanol and dissolved H_2. Ejection of rather large ($n \leq 50$) water cluster ions have also been measured in the laboratory on impact of He^+-ions and electrons on ice. Once in the gas phase, these water clusters can undergo electron-ion recombination and influence the complex chemistry of the ISM.
Water molecules accreted on grains forming an ice layer have also an important impact on the synthesis of molecules which are known to form very inefficiently in the gas phase, the most prominent example being the production of H_2 (Pirronello et al. [ros02, pir97]). The water ice on such grains is thought to be amorphous in nature [ros02], containing many micropores. Interstellar H-atoms can stick on such a surface and recombine catalytically to molecular hydrogen either after migration on the surface or by being hit by another H-atom coming from the gas-phase.

3.2   Spectroscopy and structure of $H^+(H_2O)_n$

The water molecule H_2O consists of 3 atoms and has thus 3 vibrational modes, one asymmetric OH-stretch at 3756 cm^{-1}, one symmetric OH-stretch at 3657 cm^{-1} and one bending mode at 1595 cm^{-1}. If we incorporate these water molecules into protonated water clusters $H^+(H_2O)_n$, we will certainly be able to observe these vibrations, although at somewhat modified frequencies due to the hydrogen-bonding interaction. Some selected structural isomers of the water clusters $H^+(H_2O)_n$ for n=5..8 are depicted in figure 3.1 together with their infrared predissociation spectra taken in the OH-stretching region [wan01, jia00]. As can be seen, each protonated water cluster has a core consisting either of an H_3O^+ or $H_5O_2^+$, around which the water molecules can cluster. The clustering close to the core is dominated by charge-dipole interactions and the bonds are consequently rather strong, while the water molecules in outer solvation shells are bonded by the weaker hydrogen bonding (see paper in appendix A). One water molecule can be hydrogen-bonded to 1, 2 or 3 other water molecules in the cluster (called 1-, 2- or 3-coordinated) and this can also be observed in the free OH-stretching region above 3600 cm^{-1} in the spectra 3.1. Water molecules which act as a single proton acceptor, for instance like the 3 outer water molecules in isomer 5I, will have their two H-atoms free to stretch and this will give rise to an asymmetric and symmetric peak in the spectra located around 3740 cm^{-1}
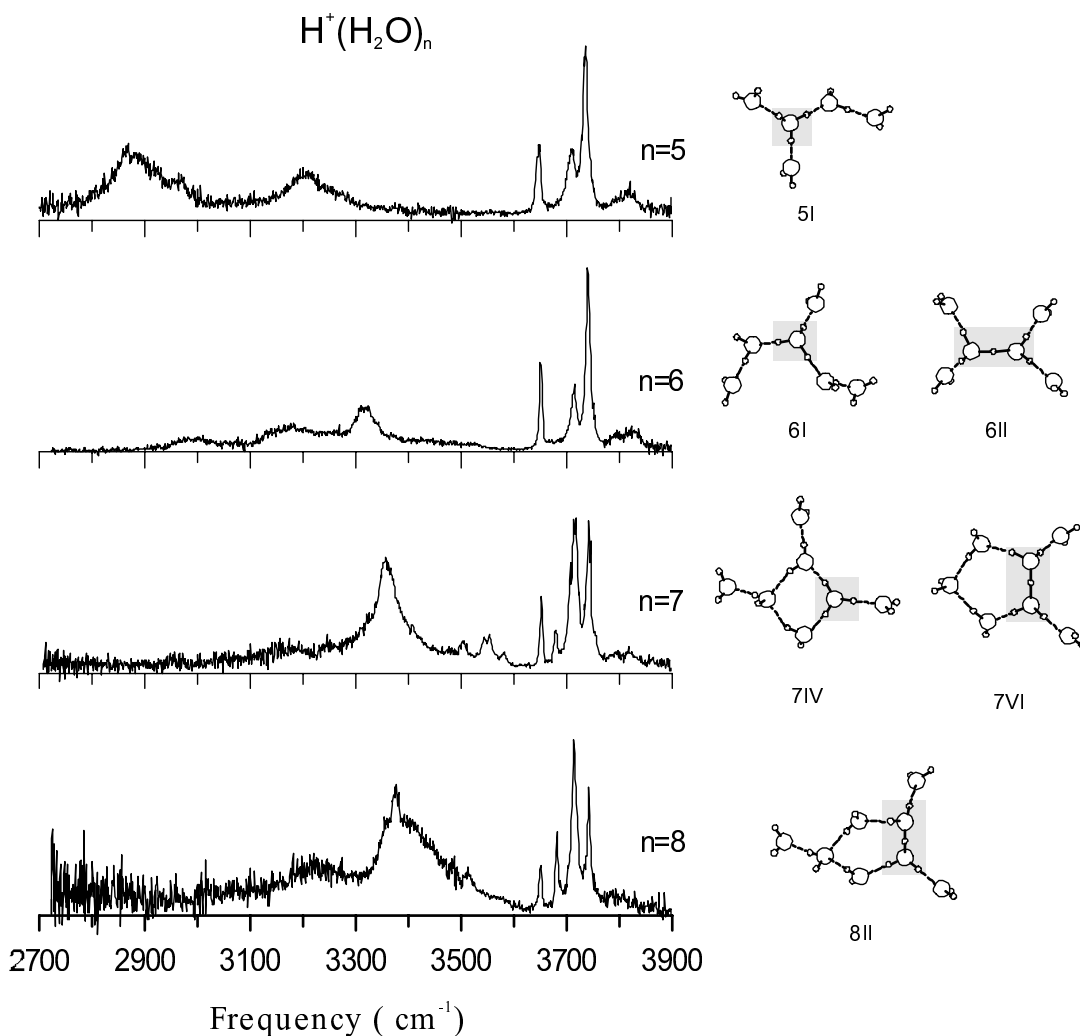
Figure 3.1: Vibrational predissociation spectra of $H^+(H_2O)_n$ n=5..8 in the bonded and free OH-stretching region (2700 cm^{-1} through 3900 cm^{-1}). The most probable isomers for each degree of solvation n are also shown. Figure adapted from [wan01].

and 3650 cm^{-1}. 2-coordinated acceptor-donor water molecules have only 1 free OH-bond and this is observable as a single absorption around 3715 cm^{-1}. Finally, 3-coordinated water molecules with one unbonded H-atom have also a clear signature at 3680 cm^{-1}. The appearance of this free OH-stretching of 3-coordinated water can be observed very nicely in the spectra by going from n=6 to n=7. Isomers 6I and 6II contain only 1- and 2-coordinated water molecules, whereas isomer 7IV contains one 3-coordinated water molecule.

The bonded OH-vibrations are redshifted and can be found in the frequency region below 3600 cm^{-1} together with the vibrations due to the cluster cores. More recent details about the structure and IR-spectra of ionic water clusters can be found in [wan97], [jia00], [cha01], [wan01] or [asm03] and references therein.

3.3 Experimental: Production of $H^+(H_2O)_n$ in a corona discharge source

The Taipei 22-pole machine has been used to investigate the protonated water clusters as reported in appendix A. The corona discharge source used for these experiments to produce a continuous beam of $H^+(H_2O)_n$ is explained in this section with the help of figure 3.2. It is very compact and simple as it is built from a Swagelock reducing union and a BNC-feedthrough. The design is identical to that described by Niedner-Schatteburg [gns96]. An ordinary stainless steel sewing needle tip is set to high voltage (around 500V
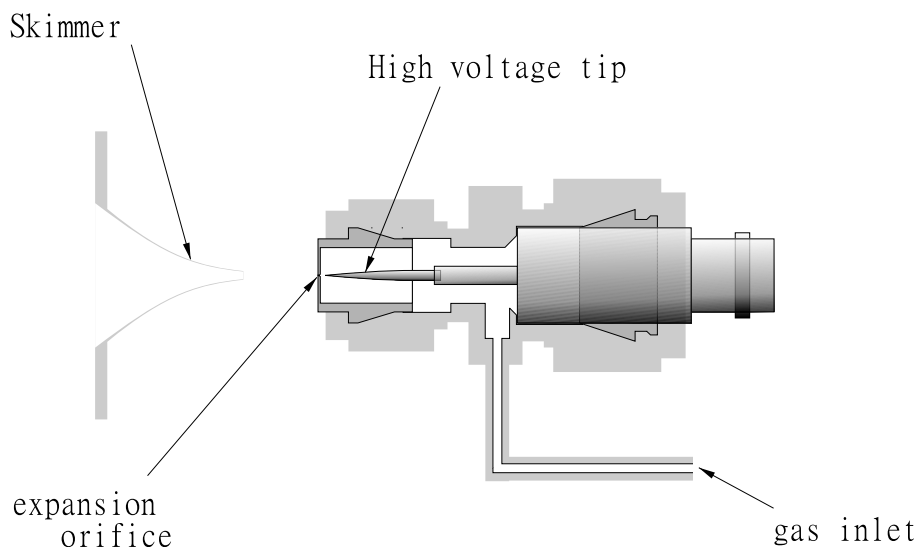
Figure 3.2: Corona discharge source, figure adapted from [wan01]

to 700V), and the potential difference between this tip and the source body initiates a discharge in the supplied H_2/H_2O gas mixture (around 50 Torr of a 20:1 mixture). The resulting discharge current is usually in the range of $30\mu A$. The ionic species generated in the discharge undergo many collisions with the neutral precursor gas at room temperature and are thus internally cooled before they can leave the source through the $75\mu m$-orifice. The subsequent supersonic expansion provides further cooling down to temperatures of the range of 150K so that clustering can take place. The 1mm diameter skimmer selects the center part of the beam to be admitted to the high-vacuum region of the 22-pole machine. This skimmer is floated not more than 1.5V below the source body potential to avoid collision-induced heating of the $H^+(H_2O)_n$ clusters.

The power supply scheme of the corona discharge source is also quite simple: A low voltage power supply floats the source body and also a high voltage power supply. This high voltage power supply in turn provides the potential difference between the source body and the needle tip. In the electric circuit between the source body and the needle there are also two resistors, one limiting resistor ($1M\Omega$) to avoid accidental overheating of the corona discharge source and another resistor to measure the discharge current ($1k\Omega$). The reactions inside the source body and in the supersonic expansion leading finally to $H^+(H_2O)_n$ (n=4..10..) could proceed like following (see also [wan01]). First, the H_2

molecules are ionized by the discharge:

$$H_2 + e^- \longrightarrow H_2^+ + 2e^- \tag{3.1}$$

The formed H_2^+ ions encounter the abundant H_2 molecules leading to following reaction

$$H_2^+ + H_2 \longrightarrow H_3^+ + H \tag{3.2}$$

which is exothermic by around 1.7eV. Clustering of H_2 molecules to the produced H_3^+ to yield $H_3^+(H_2)_n$ is very unlikely due to the low binding energies of the hydrogen clusters and the relatively high temperature of the source of roughly 300K. The H_3^+ can transfer a proton to a water molecule

$$H_3^+ + H_2O \longrightarrow H_3O^+ + H_2 \tag{3.3}$$

and release the energy of 2.82eV. The reaction leading to H_3O^+ could also go directly by the following reaction, which is more exothermic (4.52eV) due to the high proton affinity of water,

$$H_2^+ + H_2O \longrightarrow H_3O^+ + H \tag{3.4}$$

but is more unlikely, because H_2O is present in a low concentration in the precursor gas mixture. The H_3O^+ are relatively stable and will not do any further reactions except clustering. This clustering can only happen in the expansion region due to the lower prevailing temperatures,

$$H_3O^+ + H_2O + M \longrightarrow H^+(H_2O)_2 + M \tag{3.5}$$
$$H^+(H_2O)_{n-1} + H_2O + M \longrightarrow H^+(H_2O)_n + M \tag{3.6}$$
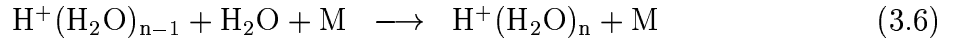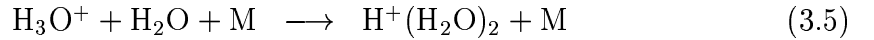
with M being either H_2 or H_2O.

3.4 Theory: Calculation of internal energies

In this section important relations for the calculation of internal energies and heat capacities for the vibrational and rotational motions of molecules are derived. These relations are used in the calculation of the mean vibrational energy of protonated water clusters $H^+(H_2O)_n$ at a defined temperature T (appendix A and section 3.5), and also in the conversion between bond energies and bond enthalpies (3.4.3). Many of the equations below have also been summarized by Ochterski [och00].

3.4.1 Vibrational energy E_{vib} and heat capacity C_{vib}

Vibrational energy

The water clusters $H^+(H_2O)_n$ consist of $\mathcal{N} = 1 + 3 \cdot n$ atoms and thus have $m = 3 \cdot \mathcal{N} - 6 = 9 \cdot n - 3$ vibrational normal modes. If we take now one of these vibrational modes $\overline{\nu}_i$ ($i = 1..m$) with its well-known harmonic oscillator energy levels

$$E_i(v) = hc\overline{\nu}_i \cdot \left(v + \frac{1}{2}\right) \tag{3.7}$$

with the vibrational quantum number v (v= 0,1,2,..), we obtain the following distribution for the occupation of the vibrational levels at temperature T:

$$\frac{N_i(v)}{N} = \frac{1}{Z_{vib}} \cdot e^{-\frac{hc\overline{\nu}_i v}{k_B T}} = \left[1 - e^{-\frac{hc\overline{\nu}_i}{k_B T}}\right] \cdot e^{-\frac{hc\overline{\nu}_i v}{k_B T}} \tag{3.8}$$

with the vibrational partitioning function Z_{vib} given as

$$Z_{vib} = \sum_{v=0}^{\infty} e^{-\frac{hc\overline{\nu}_i v}{k_B T}} = \frac{1}{1 - e^{-\frac{hc\overline{\nu}_i}{k_B T}}} \qquad . \tag{3.9}$$

The term $\frac{1}{2}$ representing the zero-point vibrational energy (ZPVE) in the expression for $E_i(v)$ in equation 3.7 cancels out in the relation 3.8. The ZPVE will also further be omitted in the following expressions as one is just interested in the energy above the zero-point vibrational level. The ZPVE is usually included in *ab initio* calculations.

The total energy $E_{vib,i}$ (without ZPVE) in the ith vibrational mode of an ensemble of N protonated water clusters $H^+(H_2O)_n$ at temperature T is thus:

$$E_{vib,i} = \sum_{v=0}^{\infty} E_i(v) \cdot N_i(v) \tag{3.10}$$

$$= N \sum_{v=0}^{\infty} (hc\overline{\nu}_i v) \cdot \left[1 - e^{-\frac{hc\overline{\nu}_i}{k_B T}}\right] \cdot e^{-\frac{hc\overline{\nu}_i v}{k_B T}} \tag{3.11}$$

$$= N(hc\overline{\nu}_i)\left[1 - e^{-\frac{hc\overline{\nu}_i}{k_B T}}\right] \cdot \sum_{v=0}^{\infty} v e^{-\frac{hc\overline{\nu}_i v}{k_B T}} \tag{3.12}$$

$$= Nhc\overline{\nu}_i \left[1 - e^{-\frac{hc\overline{\nu}_i}{k_B T}}\right] \cdot \frac{e^{-\frac{hc\overline{\nu}_i}{k_B T}}}{\left(1 - e^{-\frac{hc\overline{\nu}_i}{k_B T}}\right)^2} \tag{3.13}$$

$$= Nhc\overline{\nu}_i \cdot \frac{e^{-\frac{hc\overline{\nu}_i}{k_B T}}}{1 - e^{-\frac{hc\overline{\nu}_i}{k_B T}}} \tag{3.14}$$

$$= Nhc\overline{\nu}_i \cdot \frac{1}{e^{\frac{hc\overline{\nu}_i}{k_B T}} - 1} \tag{3.15}$$

using the following relation to solve the sum given above

$$\sum_{n=0}^{\infty} nx^n = \frac{x}{(1-x)^2} \quad \text{for } x < 1 \qquad . \tag{3.16}$$

Expression 3.15 is only the energy in the ith (i=1..m) vibrational mode. To obtain the total vibrational energy at temperature T contained in all m vibrational modes we use summation

$$E_{vib}(T) = \sum_{i=1}^{m} E_{vib,i} = \sum_{i=1}^{m} Nhc\overline{\nu}_i \cdot \frac{1}{e^{\frac{hc\overline{\nu}_i}{k_B T}} - 1} \tag{3.17}$$

which can be done numerically. As mentioned, the only necessary input for this calculation is the set $\overline{\nu}_i$ (i=1..m) of *ab initio* calculated vibrational frequencies.

Vibrational heat capacity

The heat capacity at constant volume is in general defined by

$$C_{\mathrm{V}} = \frac{\partial E(T)}{\partial T} \tag{3.18}$$

and we can use this relation to derive the vibrational heat capacity at constant volume from equation 3.17

$$C_{\mathrm{V},vib} = N/k_B \cdot \sum_{i=1}^{m} e^{\frac{hc\overline{\nu}_i}{k_B T}} \cdot \left(\frac{hc\overline{\nu}_i/T}{e^{\frac{hc\overline{\nu}_i}{k_B T}} - 1} \right)^2 \tag{3.19}$$

and with $C_{\mathrm{p}} = C_{\mathrm{V}} + k_B$ one gets also the heat capacity at constant pressure.

The just derived relations should be illustrated with the example of the most stable isomer of $H^+(H_2O)_4$ (isomer 4I, see reference [jia00]) for which the vibrational energy 3.17 and the heat capacity at constant volume 3.19 are shown in figure 3.3. This cluster has $\mathcal{N} = 1 + 3 \cdot 4 = 13$ atoms and thus $m = 3 \cdot 13 - 6 = 33$ vibrational modes in the range of $\overline{\nu}_1 = 62\text{cm}^{-1}$ through $\overline{\nu}_{33} = 3730\text{cm}^{-1}$ (*ab initio*-calculated, [jia01]). As can be seen in both
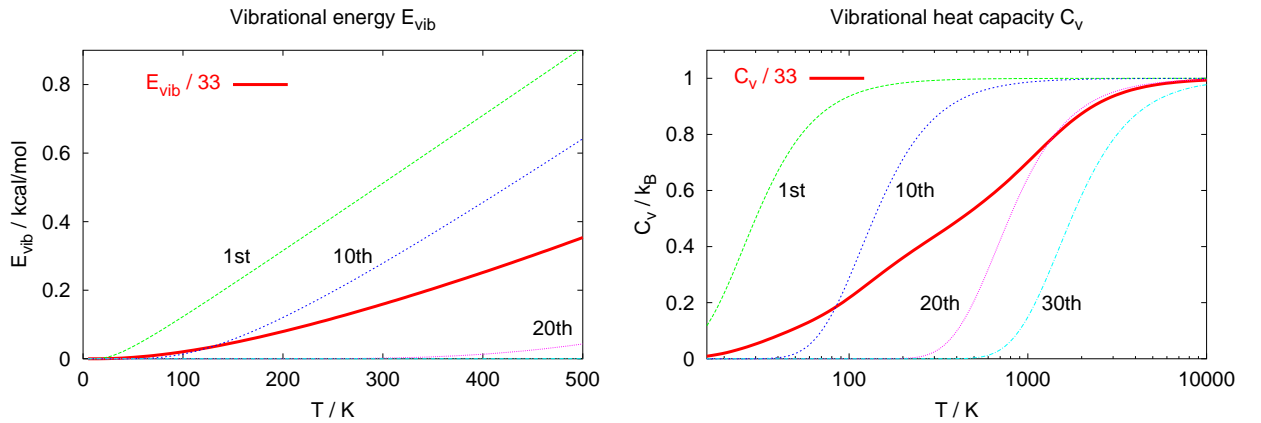

Figure 3.3: Calculated vibrational energy $E_{vib}(T)$ (without ZPVE) and heat capacity $C_{\mathrm{V},vib}(T)$ for the cluster $H^+(H_2O)_4$. The fat lines represent the total energy and heat capacity which have been divided by m=33 for comparison with the values for selected vibrational modes. The respective values for the 1st, 10th, 20th and 30th vibrational mode are shown. Please note the different temperature axes.

graphs, at low temperatures, the vibrational modes with low frequency contribute most to the energy (excluding ZPVE) and heat capacity, whereas the higher vibrational modes are activated only at high temperatures. For example, in the temperature range of the left graph (T=0 to 500K), for the 1st vibrational mode with $\overline{\nu}_1$=62cm^{-1} the vibrational energy is roughly proportional with temperature, whereas the 30th vibrational mode with $\overline{\nu}_{30}$=3631cm^{-1} is not yet contributing to the internal energy. If a vibrational mode is activated ($hc\overline{\nu}_i \ll k_B T$), it contributes the Boltzmann constant k_B to the heat capacity as claimed by the equipartition theorem. So only when all modes are switched on ($T > 3000$K in this case) we get a total heat capacity of $C_{\mathrm{V}} = 33k_B$ as depicted in the right graph.

3.4.2 Rotational energy E_{rot} and heat capacity C_{rot}

Similar to the case of discrete vibrational levels, the energies and heat capacities for the rotational motion are now derived. For the simple case of a diatomic molecule, the quantum mechanical rotational energies and degeneracy is given by

$$E(J) = \Theta k_B J(J+1) \tag{3.20}$$
$$g(J) = 2J+1 \tag{3.21}$$

with the characteristic rotational constant Θ (given in K), the Boltzmann constant k_B and the rotational quantum number J (J=0,1,2,..). The rotational distribution, the partition function Z_{rot} and the rotational energy E_{rot} are then calculated similar to the vibrational values as:

$$\frac{N(J)}{N} = \frac{2J+1}{Z_{rot}} \cdot e^{-\frac{\Theta J(J+1)}{T}} \tag{3.22}$$

$$Z_{rot} = \sum_{J=0}^{\infty} (2J+1) e^{-\frac{\Theta J(J+1)}{T}} \tag{3.23}$$

$$E_{rot}(T) = \sum_{J=0}^{\infty} E(J) \cdot N(J) \qquad . \tag{3.24}$$

Unfortunately, the sums in the equations above cannot be evaluated as easily as in the vibrational case, so approximations (like $Z_{rot} = T/\Theta$ for high temperatures) or numerical calculations are necessary. The rotational heat capacity is then given according to definition 3.18 as

$$C_{V,rot} = \partial E_{rot}(T)/\partial T \qquad . \tag{3.25}$$

Such an exact numerical evaluation of the heat capacity is shown in figure 3.4 for the diatomic molecules HD and H_2. The calculations were conducted by using solely the *gnuplot* plotting utility on a *linux* platform. The rotational constants of $\Theta(HD)$=65.3K and $\Theta(H_2)$=86.9K were taken from the book of Herzberg [her65]. These molecules were chosen as examples because they were extensively used in the Chemnitz experiments at low temperatures. Of special interest is here the hydrogen molecule H_2 as it is known to consist of 25% para-H_2 (even J) and 75% ortho-H_2 (uneven J) giving rise to interesting effects at low temperatures. As in the case of the vibrational motion, the rotational heat capacity reaches the classical limit at high temperatures. For $T \gg \Theta$, the rotational heat capacity for the diatomic molecules HD and H_2 settles at $2 \cdot k_B/2$ for the 2 rotational degrees of freedom. It has to be stressed here that the equations 3.20 and 3.21 and the following derivations are only valid for diatomic and linear polyatomic molecules and that more complex formulas exist for other molecules (see for example [hol96]). In any case, the given relations can help to estimate the rotational energies and heat capacities of non-linear molecules.

Protonated water clusters $H^+(H_2O)_n$ (n=4..10) for example have relatively huge moments of inertia $I_i = \sum mr^2$ around all principal axes (i=1,2,3) and thus very small characteristic rotational constants $\Theta_i = \hbar^2/2I_i k_B \ll$ 1K. In this case one can assume to a good approximation the classical relations $E_{rot}(T)$=3/2$k_B T$ and $C_{V,rot} = 3/2k_B$ for all temperatures accessible the experiment.
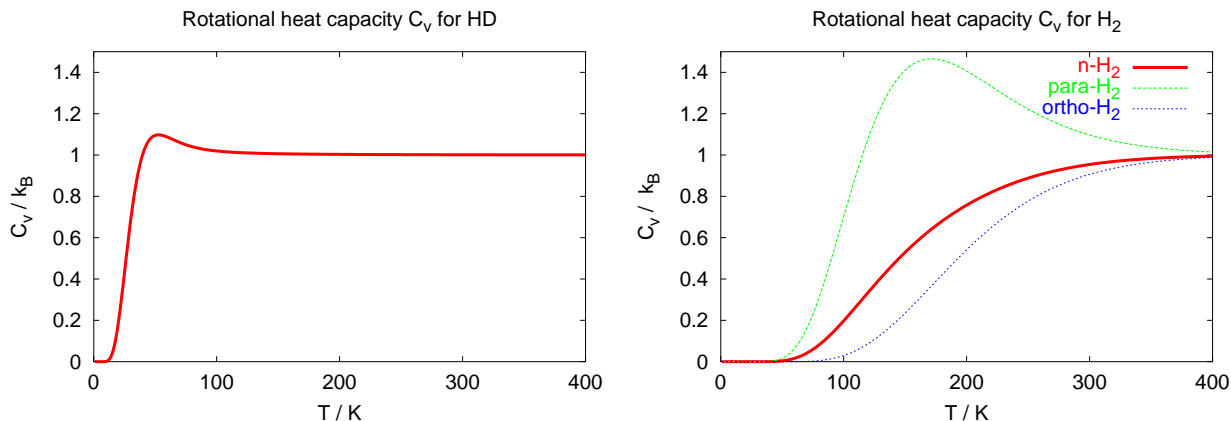
Figure 3.4: Calculated rotational heat capacities $C_{V,rot}$ for HD and H_2. Normal-H_2 (fat line in right graph) consists of 25% para-H_2 and 75% ortho-H_2. The characteristic rotational constants are $\Theta(HD)$=65.3K and $\Theta(H_2)$=86.9K.

The water molecule H_2O as a further example, has characteristic rotational constants of Θ_1=13K, Θ_2=20K and Θ_3=40K (values taken from Herzberg [her65]). One could treat this molecule as a classical object and assume in first approximation $E_{rot}(T)$=3/2k_BT and $C_{V,rot} = 3/2k_B$ (the thermochemistry routines in *Gaussian* do this, [och00]). But as can be seen in figure 3.4, the rotational heat capacity $C_{V,rot}$ tends toward zero for $T \ll \Theta_i$. In this case, the rotational energy at temperature T will be somewhat lower than the assumed $3/2k_BT$. A rough estimation with the relations given above for diatomic molecules yields a rotational energy of 0.865kcal/mol at T=298K for the water molecule instead of the expected $3/2k_B \cdot$ 298K=0.889kcal/mol and even greater relative deviations at lower temperatures.

3.4.3 Bond energy vs. bond enthalpy

In the literature, sometimes bond energies and sometimes bond enthalpies are reported for the water clusters $H^+(H_2O)_n$. For being able to compare the bond energies obtained in appendix A with literature values one has to apply a conversion. In the following lines the small difference between bond energies and enthalpies, and the corresponding conversion procedure are explained. Let's take for example the dissociation reaction

$$H^+(H_2O)_5 \longrightarrow H^+(H_2O)_4 + H_2O \qquad . \qquad (3.26)$$
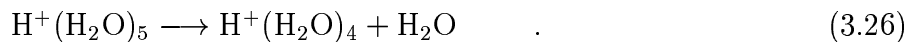
The bond energy E_{diss} is defined as the energy for the dissociation if we consider the reactants and the products to be in the ground states, i.e. without inner energy (but including ZPVE) at 0K. If one takes a molecular system with inner Energy E, then the enthalpy is defined as $H = E + pV$, so one obtains

$$\left(\frac{\partial H}{\partial T}\right)_p = \frac{\partial E}{\partial T} + k_B = C_V + k_B = C_p \qquad (3.27)$$

with the total heat capacity at constant volume $C_V = C_{V,vib} + C_{V,rot} + C_{V,trans}$. The heat capacities for the vibrational and rotational motion were given in the preceding sections,

the heat capacity for the translational motion is $C_{\mathrm{v},trans} = 3/2k_B$ for all T.

Enthalpies are given usually at a defined temperature of 298.15K. To obtain the enthalpy for the dissociation reaction 3.26 from the known bond energy at 0K, one can imagine the temperature to be raised slowly from 0K to 298.15K and calculate the enthalpy

$$H^{298} = \int_{0K}^{298K} C_{\mathrm{p}}\, dT = E_{vib} + E_{rot} + E_{trans} + k_B T \qquad (3.28)$$

for all product and reactant molecules. The dissociation enthalpy is then finally given by the difference

$$\Delta H^{298} = E_{diss} + H^{298}_{products} - H^{298}_{reactants} \qquad . \qquad (3.29)$$

This conversion has been done for the dissociation reaction 3.26 and the ingredients for this calculation are listed in table 3.1. Please note that according to relation 3.28 also the term $k_B T$ has to be considered. The vibrational energies in table 3.1 are calculated as described in section 3.4.1. The vibrational energy of H_2O at T=298K is comparably low because its three vibrational modes have relatively high frequency (lowest mode has 1595 cm^{-1} as already mentioned in section 3.2). The translational and rotational energies are all $3/2k_B T$, except the rotational energy of water, where a somewhat lower value of 0.865kcal/mol has been taken. The difference between products and reactants is then $H^{298}_{products} - H^{298}_{reactants}$=0.40kcal/mol and with the dissociation energy E_{diss}=12.1kcal/mol one finally obtains ΔH^{298}=12.5kcal/mol according to relation 3.29.

	$H^+(H_2O)_5$	$H^+(H_2O)_4$	H_2O
E_{vib}	7.15	5.20	0.0021
E_{rot}	$3/2k_B T$=0.889	$3/2k_B T$	$\sim 3/2k_B T$=0.865
E_{trans}	$3/2k_B T$	$3/2k_B T$	$3/2k_B T$
$k_B T$	$k_B T$=0.59	$k_B T$	$k_B T$
$H^{295} = \Sigma$	9.52	7.57	2.35

Table 3.1: Calculation of enthalpies of product and reactant molecules of reaction 3.26 from the vibrational, rotational and translational energies at a temperature T=298K. The energies are given in units of kcal/mol. The enthalpy difference between product and reactant molecules is 0.40kcal/mol (last row). This value is used in the conversion between bond energy and bond enthalpy according to relation 3.29.

3.5 Determination of bond energies E_{diss}

For the determination of the dissociation energies E_{diss} of the protonated water clusters $H^+(H_2O)_n$ in the work presented in appendix A, relation

$$E_{diss} = E_a + \langle E_{vib}\rangle(T_m) + ak_B T_m \qquad (3.30)$$

is applied. For this sum, one has to measure the activation energy E_a for the dissociation process in the He bath gas,

$$E_a = -\frac{\partial ln(k)}{\partial(1/k_B T)} \qquad , \qquad (3.31)$$

calculate the mean vibrational energy of the water cluster $\langle E_{vib} \rangle (T_m)$ at the mean temperature T_m according to equation 3.17

$$\langle E_{vib} \rangle (T_m) = E_{vib}(T_m)/N = \sum_{i=1}^{m} hc\bar{\nu}_i \cdot \frac{1}{e^{\frac{hc\bar{\nu}_i}{k_B T_m}} - 1} \tag{3.32}$$

and finally add a small empirical correction term $ak_B T_m$ introduced by Lovejoy and coworkers [lov01, lov00, cur01]. A rigorous derivation of relation 3.30 exceeds the scope of this section, so just some illustrative remarks are made below. A stringent treatment of relations similar to 3.30 for the case of unimolecular dissociation induced by low-intensity infrared radiation has been given by Dunbar [dun91, dun94].

With $a = 0$, relation 3.30 takes the more simple form of the Tolman theorem [dun94, tol20] stating that in a thermally driven reaction, the activation energy is equal to the average energy of the reacting (in this case dissociating) molecules minus the average of the entire population. This is illustrated in figure 3.5 showing a Maxwell-Boltzmann distribution of the total vibrational energy of an ensemble of molecules which is truncated at the dissociation energy E_{diss}. By collisions with the He bath gas, the water cluster molecules $H^+(H_2O)_n$ can do small steps on the energy ladder (x-axis) and those clusters exceeding E_{diss} will dissociate. In this simple picture, the Tolman theorem (a=0) can be derived by assuming the rate coefficient k for dissociation to be proportional to the fraction of clusters sitting just below the threshold E_{diss} and differentiating k according to relation 3.31 [dun91].
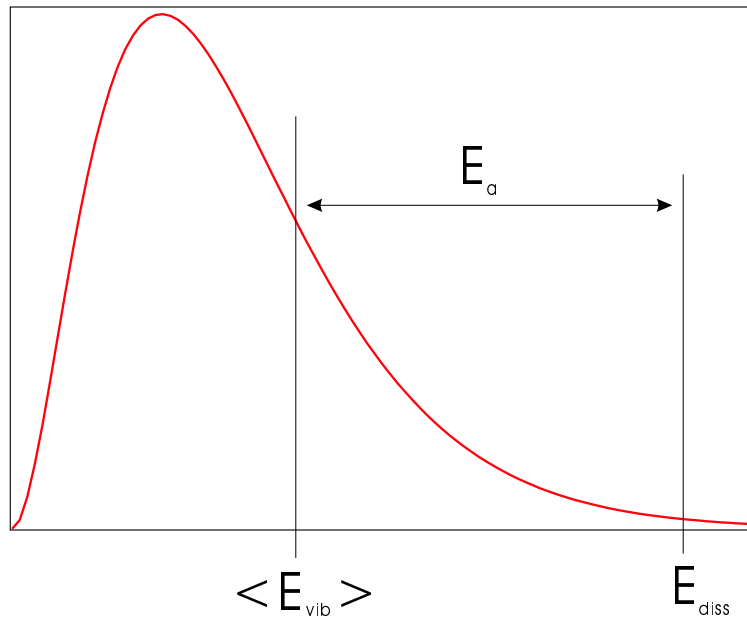

Figure 3.5: truncated Maxwell-Boltzmann distribution for internal (vibrational) energy of a molecular system at temperature T.

Chapter 4

Ionic hydrocarbons CH_n^+

This work has been written in a cumulative manner with the investigations about the reactions of CH_n^+ (n=3..5) with H_2, HD and D_2 contained in the appendices B and C. Therefore just some overview is given in this chapter and additional information about the association processes is summarized in section 4.5.

4.1 Structure and properties of CH_n^+

The following paragraphs summarize some properties of the studied CH_n^+ for n=3,4,5. Belonging to the family of carbocations, these species play important roles as short-lived intermediates in chemical reactions, as discovered by Olah (Nobel prize 1994 [ola94]). Beginning with n=3, the electron-deficient carbon atom in CH_3^+ is bonded to three other hydrogen atoms by sp^2-orbitals. Therefore it is a flat ionic molecule with a trigonal structure. The remaining p-orbital, perpendicular to the molecular plane, is not occupied by electrons. This is the reason for the inertness of this molecular ion toward the reaction with H_2, as shown in the following section 4.2.

Although methane is one of the simplest molecules, known from high-school chemistry textbooks to have a tetrahedral structure with one electron pair for each carbon-hydrogen chemical bond, when taking away one electron from this system, the resulting methane radical cation, CH_4^+, is not so simple. The first rotationally resolved spectrum of CH_4^+ was reported only recently in 1999 by Signorell and Merkt [sig99, sig00] using ZEKE spectroscopy. Their investigation and other theoretical studies indicate that the CH_4^+ is subject to Jahn-Teller effect, distorting the geometry of the methane cation from a tetrahedral one to a C_{2v} minimum structure. Low barriers between a manifold of such equivalent minimum C_{2v}-structures allow for pseudorotations of this molecule. It seems that CH_4^+ is a fluxional ionic molecule [sig00], like is also the case for CH_5^+, as discussed next.

Maybe the most interesting small ionic hydrocarbon is CH_5^+, sometimes called the 'Holy Grail' of spectroscopy. Although easy to make and known for many decades (at least since 1952), first spectra of the solvated species $CH_5^+(H_2)_n$ (n=1,2,3) have been reported by Boo and Lee [boo95] in 1995 and it wasn't until the year 1999 that a part of the infrared spectrum of CH_5^+ could be inferred in Oka's spectroscopy laboratory in Chicago [whi99] having started the search in 1983. Nearly 1000 lines have been resolved in a very narrow spectral range from about 2800 to 3100 cm^{-1}. But despite this incredible amount
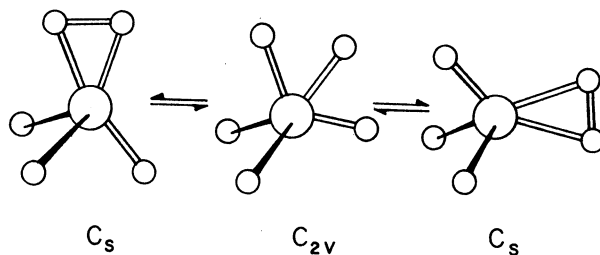
$$C_s \qquad C_{2v} \qquad C_s$$

Figure 4.1: Intermolecular rearrangement between two CH_5^+ ions of C_s symmetry. In the C_s configuration three H-atoms are attached by conventional chemical bonds to the carbon center while the remaining two H-atoms are involved in a 'three center - two electron' bond. Figure adapted from Sefcik et al. [sef74].

of information it was not possible to link the spectrum of CH_5^+ to any structure and to do any assignment. This is due to the 'floppy' nature of this molecule which doesn't seem to have a fixed structure like all other well-behaved molecules. For this reason it has also been the subject of many theoretical considerations (see for example [kom87], [mul97], [mar99]). Most of these investigations indicate that there are only tiny barriers hindering the scrambling movements of the H-atoms, like is also the case for CH_4^+. Recent theoretical calculations of this non-classical molecule confirm the near equivalency of the H-atoms, obtaining a barrier height of only 3.4 kJ/mol (Müller et al. [mul97]) for the C_{2v}-transition between two minima of C_s point group symmetry, as depicted in figure 4.1.

4.2   Reactions with H_2

This section starts with simple reactions, namely those of small ionic hydrocarbons CH_n^+ with hydrogen. The reactions are shown in scheme 4.2 in which the abstraction and association reactions beginning from C^+ leading to CH_5^+ and further clustering to $CH_5^+(H_2)_n$ are summarized. At low temperatures, the pathway towards CH_5^+ proceeds by H-abstraction reactions of the type

$$CH_n^+ + H_2 \longrightarrow CH_{n+1}^+ + H \tag{4.1}$$

except in 2 steps (for n=0 and n=3) due to endothermic barriers. In those cases the much slower radiative or ternary association prevails:

$$CH_n^+ + H_2 \longrightarrow CH_{n+2}^+ + h\nu \tag{4.2}$$

$$CH_n^+ + 2H_2 \longrightarrow CH_{n+2}^+ + H_2 \ . \tag{4.3}$$
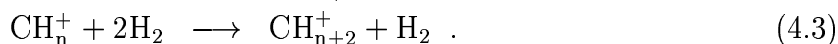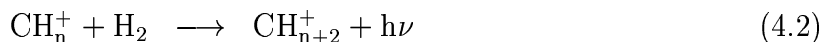
At CH_5^+ the abstraction processes stop. A further abstraction reaction is not possible as there is no known stable molecular ion such as CH_6^+. All following reactions are association reactions with the H_2 molecules clustering around the CH_5^+-core leading to $CH_5^+(H_2)_n$. For completeness, one should mention that the resulting clusters $CH_5^+(H_2)_n$ can also fragment in collisions with H_2.
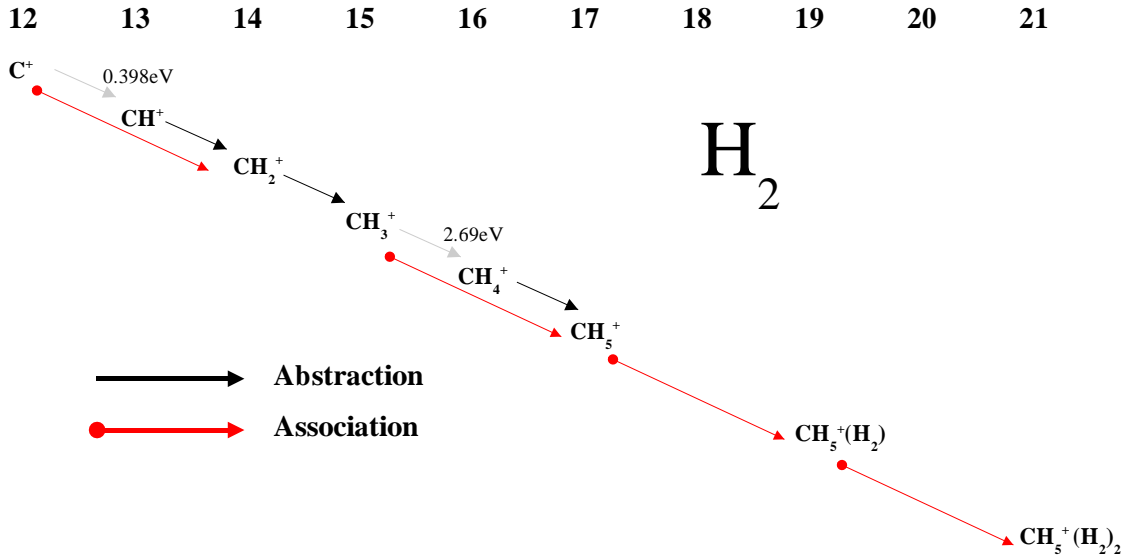
Figure 4.2: Reactions of CH_n^+ in H_2 at low temperatures. Only H-atom abstraction reactions (black arrows) and association reactions (red arrows) occur. The abstraction reactions leading to CH^+ and CH_4^+ are endothermic by the indicated energies and therefore do not occur at low temperatures (gray arrows), instead the slow association process proceeds. All abstraction processes stop at CH_5^+ and clustering of H_2 molecules around the CH_5^+ ion core begins.

The formation of small ionic hydrocarbons in the gas phase of the ISM is thought to proceed by just the above outlined reactions, as was also shown in figure 1.1. Bottlenecks in this reaction chain are of course the slow association processes. Due to the low H_2-density prevailing in the ISM they can just proceed by radiative association (reaction 4.2).

Most of the reactions described above have been investigated by several authors, for example by Sorgenfrei (n=0,3 [sor94]), Adams and Smith (n=0..4 [ada77]) and Kim et al. (n=1,2,4 [kim74]). In this thesis, new surprising results for the temperature dependence of the abstraction reaction $CH_4^+ + H_2$ have been obtained; the measurements can be found in figure 4.3 and more details in appendix B. The investigations concerning association reactions for n=3,5 are given in section 4.4.

As an example measurement, the reaction of CH_4^+ with H_2 is shown for T=15K and 300K in figure 4.3. At both temperatures, the main reaction is abstraction leading to CH_5^+ on mass 17. As mentioned, this reaction exhibits a strong negative temperature dependence, with a rate coefficient increasing from $k = 3.3 \times 10^{-11}$ cm^{3}s^{-1} at 300K to $k = 4.0 \times 10^{-10}$ cm^{3}s^{-1} at 15K (see paper in appendix B). But there are also some other small details to discover in these measurements. At 15K (upper part), there are some impurities (about 1.1%) in the injected beam which don't react with H_2, giving rise to the offset in the otherwise exponentially falling signal on mass 16. These impurities are $^{13}CH_3^+$, of which we have just seen in scheme 4.2 that it doesn't react with H_2, and CH_2D^+. The reaction of CH_2D^+ with H_2 to CH_3^+ is endothermic by roughly 370K and thus does not happen at 15K. This is of course different at 300K (lower part), where the product CH_3^+ appears at mass 15 with a measured rate coefficient of $k = 2 \times 10^{-10}$ cm^{3}s^{-1} (a value also

given by [smi82]). Due to the large endothermicity (see scheme 4.2), the 0.9%-impurity of $^{13}CH_3^+$ still doesn't react even at 300K. Noteworthy are also the signals on mass 19 and 20. Mass 19 is stemming from proton transfer of all ionic hydrocarbons to H_2O present in the vacuum chamber while mass 20 is due to proton transfer to singly deuterated water HDO. There are of course also small amounts of doubly deuterated water D_2O in the machine, but the corresponding proton transfer signal on mass 21 (HD_2O^+) has not been recorded. Singly and doubly deuterated water has been detected in our vacuum chamber in many experiments. It comes most probably from catalytic deuteration of H_2O on the vacuum chamber surfaces after usage of HD or D_2 in the machine.
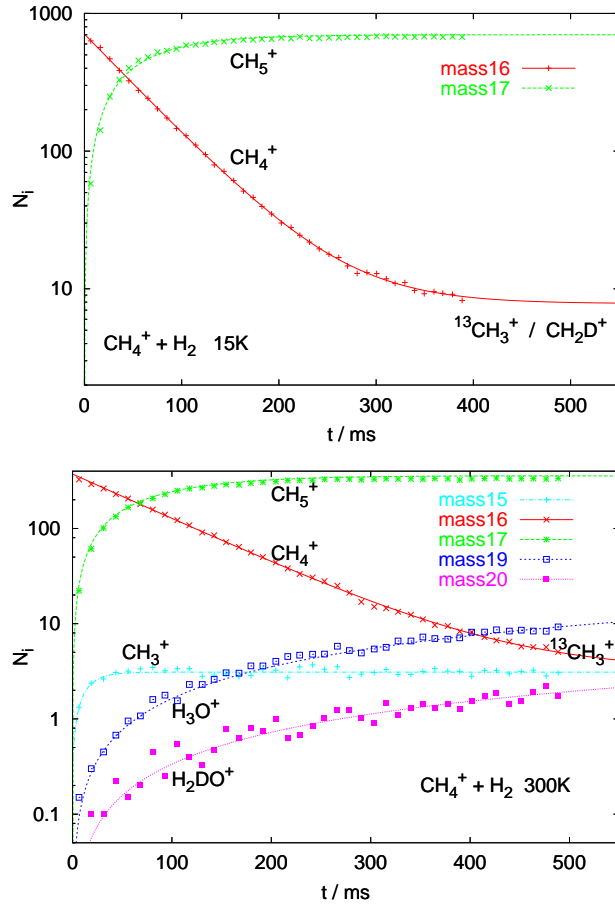
Figure 4.3: Reaction of CH_4^+ with H_2 at 15K (upper part) and 300K (lower part). The neutral number densities are $[H_2]=4.3\times10^{10}$ cm^{-3} (15K) and $[H_2]=3.4\times10^{11}$ cm^{-3} (300K), and also He pulses have been used to cool the CH_4^+ ions on entering the trap. Each data point has been measured 40 times. The lines are solutions to an adequate rate equation system (see section 2.2.3) leading to the rate coefficients $k = 4.0 \times 10^{-10}$ cm^{3}s^{-1} at 15K and $k = 3.3 \times 10^{-11}$ cm^{3}s^{-1} at 300K for the production of CH_5^+ (mass 17). Masses 19 and 20 (lower part) are due to proton transfer to (deuterated) water contained with a background number density of $[H_2O]=2 \times 10^7$ cm^{-3} in the vacuum chamber. Mass 21 (trace amounts of HD_2O^+) was not recorded in this measurement. See text for further details.

4.3   Reactions with HD

Now the reactions of CH_n^+ with HD are considered (see scheme 4.4). These proceed in the same manner as the reactions with H_2 in the section before, except that in the case of abstraction there are now two possibilities: H-atom abstraction or D-atom abstraction. Also some ionic species can undergo deuterium exchange reactions of the type

$$CH_nD_m^+ + HD \longrightarrow CH_{n-1}D_{m+1}^+ + H_2 \tag{4.4}$$
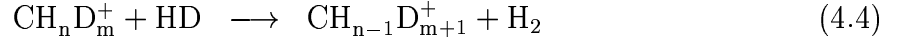
in the cases where endothermic abstraction reactions are inhibited at low temperatures. These deuterium exchange reactions have been measured to be very fast at 15K for CH_3^+ with rate coefficients of $k = 1.6 \times 10^{-9}$ cm^{3}s^{-1}, while CH_5^+ is not seen to deuterate in our experiments and we give an upper limit of 5×10^{-18} cm^{3}s^{-1} (see discussion in appendix C). So beginning from the CH_5^+-analogues, exchange reactions (blue arrows in scheme 4.4) are not longer possible and the only process occurring is clustering of HD-molecules around the CH_5^+-analogue-cores.
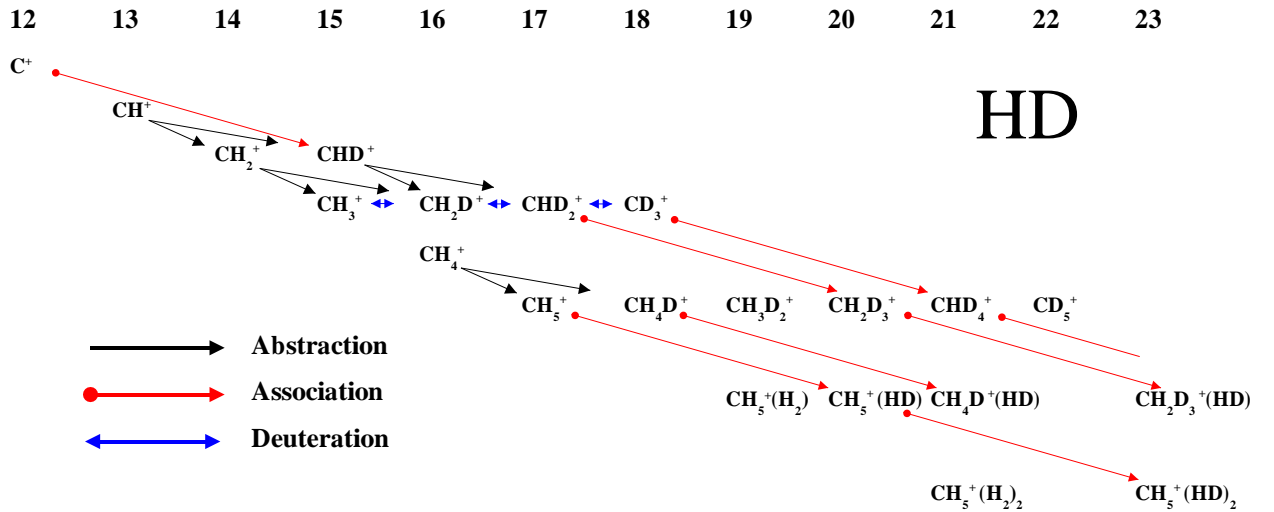
Figure 4.4: Reactions of CH_n^+ (and deuterated analogues) with HD at low temperatures. The columns contain species of equal mass while all deuterated analogues of one species CH_n^+ are listed in the horizontal. The reactions are marked as H- or D-abstraction reactions (black arrows), association reactions (red arrows) or deuterium exchange reactions (blue arrows). The reactions inhibited at low temperatures are omitted as well as deuterium exchange reactions for CH_5^+-analogues, as it was found in this work that these are very improbable (see text for details).

These processes have been observed many times in the ion trap. Injecting for example CH^+, CH_2^+ or CH_3^+ in the trap containing HD, will in any case lead to CD_3^+ at 15K, which will undergo association first to CHD_4^+ and then to CHD_4^+(HD) etc. One such example has already been shown in figure 2.10. In these processes, association of CHD_2^+ with HD

is in principle possible, as indicated by the red arrow, but is very improbable, because association reactions of CH_3^+-analogues are at least three orders of magnitude slower than the deuterium exchange in CH_3^+.

Interesting in the abstracting reactions are also the branching ratios for the H-atom and D-atom channel. As an example, figure 4.5 shows the abstraction reaction of CH_2^+ with HD and the subsequent deuteration of the produced CH_3^+-analogues as also sketched in the 3rd and 4th row of scheme 4.4. The CH_2^+ is reacting at the collision limit of
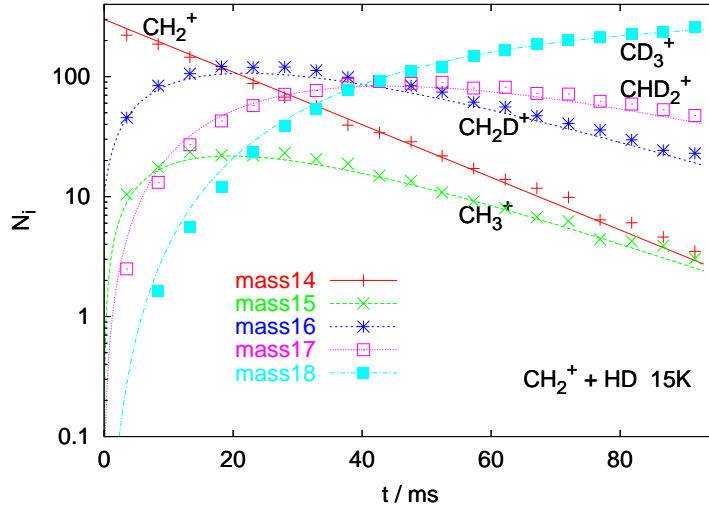
Figure 4.5: Reaction of CH_2^+ (mass 14) with HD at 15K and a neutral number density of [HD]=3.2×10^{10} cm^{-3}. The lines are solutions to an adequate rate equation system leading to the rate coefficient $k = 1.6 \times 10^{-9}$ cm^{3}s^{-1} for the production of CH_2D^+ (80%) and CH_3^+ (20%). These primary product ions are both CH_3^+-analogues and will therefore undergo H-D-exchange with the HD gas (see scheme 4.4) leading finally to CD_3^+ (mass 18) at low temperatures. All involved reaction steps are exothermic and proceed close to the collision limit. To guarantee that also the secondary reactions are measured at thermal equilibrium (T=15K), continuous cooling of the (nascent) ions is mandatory. Therefore He buffer gas with a number density on the order of [He]=1×10^{13} cm^{-3} is continuously admitted to the trap.

k=1.6×10^{-9} cm^{3}s^{-1} with HD to yield as products 80% CH_2D^+ (mass 16) and 20% CH_3^+ (mass 15). The subsequent deuteration leads completely to CD_3^+ (mass 18). So in this case the D-atom abstraction is preferred. This has to be contrasted to the reaction of CH_4^+ with HD (5th and 6th row of scheme 4.4), in which case H-atom abstraction is preferred leading to 68% of the products being CH_5^+ at 15K. The explanation for this interesting observation is based on the different reaction mechanisms for both collision systems. The CH_2^+ reacts with H_2-analogues by fast direct abstraction, while CH_4^+ first forms a collision complex with the H_2-analogue (confer paper appendix B).

4.4 Reactions with D_2

The ionic hydrocarbons CH_n^+ can react with D_2 by D-atom abstraction (for instance CH^+, CH_2^+ or CH_4^+), deuterium exchange reactions (CH_3^+ deuterates very fast to CD_3^+) or slow association reactions (for example association of CH_5^+ with D_2). In this work, only the D-atom abstraction reaction $CH_4^+ + D_2$ shown in figure 4.6 has been investigated. Similar to
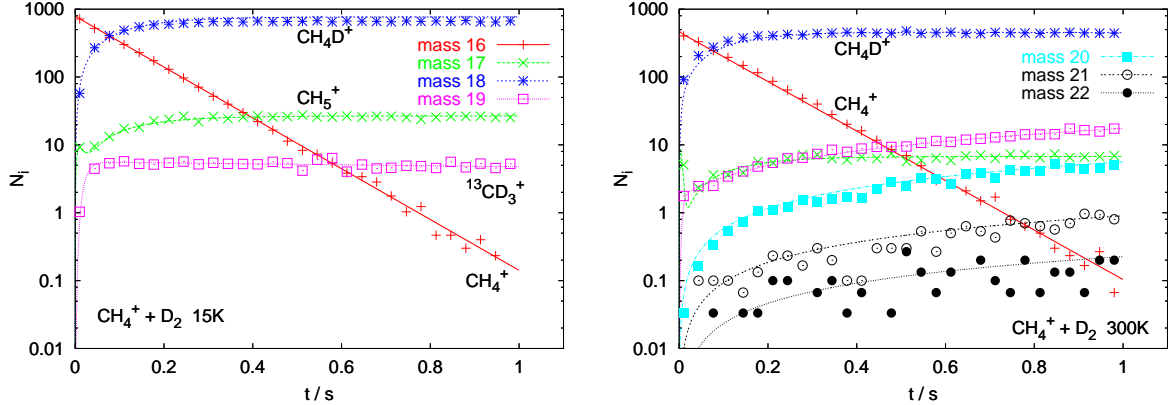

Figure 4.6: Reaction of CH_4^+ with D_2 at 15K (left figure) and 300K (right figure). The neutral number densities are $[D_2] = 8.3 \times 10^{10}$ cm^{-3} (15K) and $[D_2] = 8.3 \times 10^{11}$ cm^{-3} (300K). Each data point has been measured 30 times. He pulses with number densities reaching up to 10^{15} cm^{-3} have been used to cool the CH_4^+ ions on entering the trap. The lines are solutions to an adequate rate equation system (see section 2.2.3) leading to the rate coefficients $k = 1.2 \times 10^{-10}$ cm^{3}s^{-1} at 15K and $k = 1.1 \times 10^{-11}$ cm^{3}s^{-1} at 300K for the production of CH_4D^+ (mass 18). The small bumps at early times of mass 17 are due to fast deuterium exchange reactions of small impurities contained in the injected beam (see text). At 300K, deuterated H_3O^+-analogues appear on masses 19 through 22.

the temperature dependence of the reaction $CH_4^+ + H_2$ in section 4.2, the formation of the product CH_4D^+ (mass 18) has a rate coefficient increasing from $k = 1.1 \times 10^{-11}$ cm^{3}s^{-1} at 300K to $k = 1.2 \times 10^{-10}$ cm^{3}s^{-1} at 15K. Please note the lower rate coefficients in this case as compared to the reaction with H_2 (discussion appendix B). The exchange reaction leading to CH_3D^+ has not been observed in the experiment and an upper limit of $k < 1.0 \times 10^{-12}$ cm^{3}s^{-1} is determined (see appendix B). At 15K (left part of figure 4.6), besides the production of CH_4D^+ also other side reactions can be observed due to $^{13}CH_3^+$ and CH_2D^+ (both mass 16) contained in the injected beam. The first reacts by fast exchange reactions to $^{13}CD_3^+$ (mass 19) and the latter to CD_3^+ on mass 18. Small impurities of H_2 (0.9%) contained in the target gas give rise to CH_5^+ (mass 17) forming in the trap. Essentially the same processes are occurring at 300K (right part in figure 4.6) with (deuterated) water being present in the vacuum chamber. H_2O, HDO and D_2O can abstract a proton or a deuteron from the ionic hydrocarbons giving rise to H_3O^+ through D_3O^+ on masses 19 to 22.

4.5 Association processes with H_2 and HD

Association processes have already been shortly introduced in 4.2 (formulae 4.2 and 4.3). Now a closer look is taken at the radiative and ternary association processes of the systems $CH_3^+ + H_2$ and $CH_5^+ + H_2$ as well as for some of its deuterated versions. The determination of the radiative and ternary rate coefficients from density dependent measurements allow to estimate the lifetimes of the collision complex against decay back into reactants and the lifetime for radiative stabilization. This, on the other hand, gives insights into the structure and internal motions of the intermediate complexes.

A typical measurement for this purpose is shown in figure 4.7 where the number of
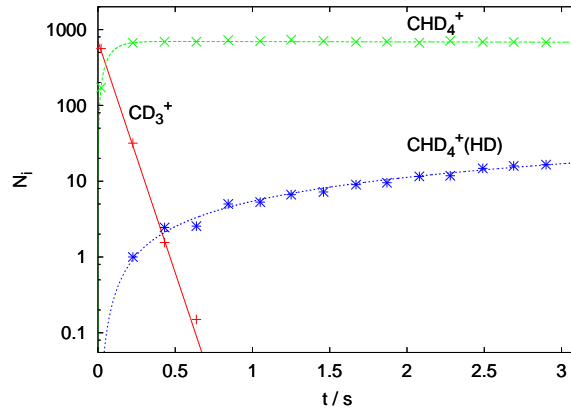

Figure 4.7: The number of molecular ions, N_i, plotted as a function of the storage time t. The 22-pole ion trap is filled with deuterium hydride with a number density [HD]$=2.8 \times 10^{12}$ cm^{-3} at a temperature of $T = 15$K. Under these conditions, CD_3^+ undergoes association to CHD_4^+ which in turn associates to yield CHD_4^+(HD). CD_3^+ is generated in the ion trap itself by injecting CH_3^+ and three fast subsequent H-D-exchange reactions; this process is too fast to be visible on the timescale of the figure. The solid lines are solutions of an adequate rate equation system leading to a set of two effective rate coefficients k_{eff}. They are $k_{eff} = 5.0 \times 10^{-12}$ cm^{3}s^{-1} for $CD_3^+ +$ HD and $k_{eff} = 3.0 \times 10^{-15}$ cm^{3}s^{-1} for $CHD_4^+ +$ HD. These values are included in figure 4.8 for the respective collision system.

ionic species is plotted as a function of time. CH_3^+ was injected into the 22-pole trap at a temperature $T = 15$K. In general, special care has been taken for the He cooling pulse not to be too intense to induce ternary reactions during the injection period. HD is supplied as the neutral reaction partner at a high number density [HD]$= 2.8 \times 10^{12}$ cm^{-3}. Under these conditions, CH_3^+ converts in three fast exchange reactions to CD_3^+ within less than 10 ms as explained in section 4.3. On the timescale of figure 4.7 the association processes of CD_3^+ with HD become visible. Formation of CHD_4^+ is happening on a timescale of 100ms, followed by the much slower association with HD to yield the cluster ion CHD_4^+(HD). The timescale for this process is on the order of 100s.

In order to determine the rate coefficients of the corresponding association processes, the kinetics of this sequential growth of clusters has been simulated (see section 2.2.3). In general, all growth and also fragmentation steps have to be included into the system of rate equations, although at the conditions present in figure 4.7, association dominates

fragmentation and good fits to the temporal evolution of the number of stored cluster ions have been obtained using $k_{\text{eff}} = 5.0 \times 10^{-12}$ cm^{3}s^{-1} for CD$_3^+$ + HD and $k_{\text{eff}} = 3.0 \times 10^{-15}$ cm^{3}s^{-1} for CHD$_4^+$ + HD. In comparison, the rate coefficients for fragmentation are much smaller and could be neglected. For larger (fragile) clusters and higher number densities, this assumption no longer holds and significant deviations of the fit curves from the measured number of ions have been found which could only be remedied when including fragmentation and further cluster growth into the simulations.

Measurements of this type have been performed for several reaction systems as a function of the number density n of the neutral reaction partner (either H$_2$ or HD) ranging from about 10^{10}cm^{-3} to 10^{14}cm^{-3} and reaction times ranging from 100ms to 20s. As a result, the rate coefficients for the association processes of CH$_3^+$-analogues are summarized in the left part of figure 4.8 and the ones for association reactions of CH$_5^+$-analogues in the right. As a general trend, k_{eff} for the CH$_3^+$ systems is larger by at least two orders of magnitude for all densities than the values for the CH$_5^+$ systems. It is also evident that in both cases the deuterium-containing species associate faster than the hydrogen-containing ones.

The effective bimolecular rate coefficients k_{eff} are composed of two contributions as
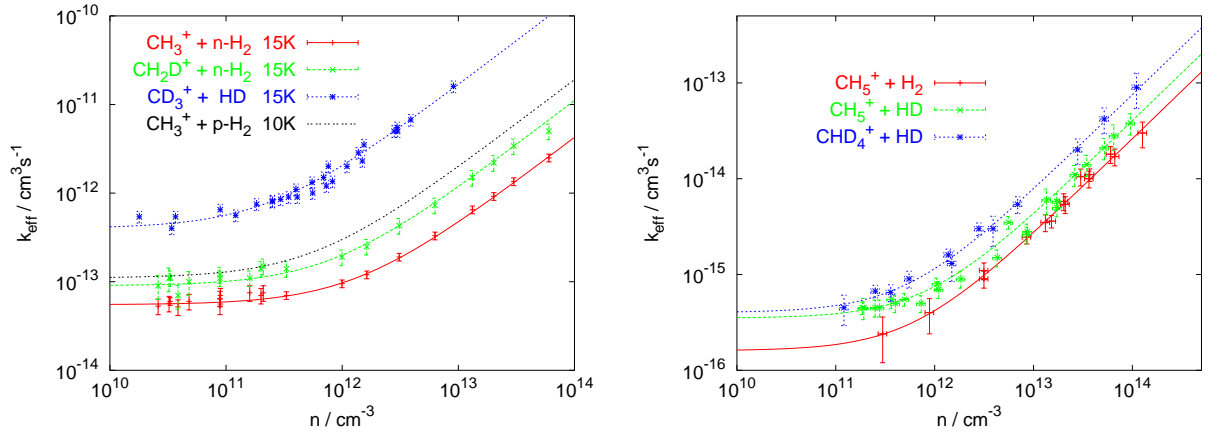
Figure 4.8: Effective rate coefficients k_{eff} for the indicated collision system as a function of neutral number density n (either H$_2$ or HD) at a temperature of 15K. Left: CH$_3^+$+H$_2$ analogues, Right: CH$_5^+$+H$_2$ analogues. Please note the different scales for k_{eff}. The effective rate coefficients k_{eff} have been extracted from measurements of the type like shown in figure 4.7. The line for CH$_3^+$ + p-H$_2$ (T = 10K) is adapted from [sor94] for comparison. The errors of around 10% for the rate coefficients are mostly coming from uncertainties in determining the neutral number density. They are somewhat higher (up to 20%) for the system CH$_3^+$ + H$_2$ and CH$_2$D$^+$ + H$_2$ at low pressures as fast exchange reactions with HD impurities make the determination of the association reactions more difficult (see text). The effective rate coefficients have been fitted with $k_{\text{eff}} = k_r + k_3 \cdot n$. The corresponding radiative and ternary rate coefficients k_r and k_3 can be found in table 4.1.

shown in figure 4.8. For low densities collisions with the neutral partner are relatively scarce and k_{eff} approaches a constant, as expected for a bimolecular process. For higher densities, k_{eff} is proportional to the density n which indicates a ternary process. As has been described several times [pau95, ger92a], association can be understood as a two-step process. First a collision complex is formed. This collision complex is highly excited as its

total energy is above the dissociation limit. Therefore it is very likely that this complex redissociates back into reactants at a rate $1/\tau_d$ (τ_d lifetime of the complex). Alternatively, the complex can be stabilized. In the bimolecular process this happens via the emission of a photon. This radiative association happens at a rate $1/\tau_r$ where τ_r is the radiative lifetime of the excited state. If the excited complex encounters a third body during its lifetime, it can also be stabilized by collision. Stabilization of the complex is only achieved with an efficiency f, $f < 1$, while in $(1-f)$ cases it will redissociate upon collision. As seen in figure 4.8 this ternary association is dominant for higher number densities n. In effect, the rate coefficient of association, k_{eff}, is the sum of the rate coefficient for radiative association, k_r, and the one for ternary association, k_3, times the density of the third body, n,

$$k_{\text{eff}} = k_r + k_3 \cdot n \ \ . \tag{4.5}$$

This equation has been used to extract k_r and k_3 from the experimental values of k_{eff} displayed in figure 4.8. The results are summarized in table 4.1 for the different collision systems studied. According to the two-step model discussed above [ger92a], the rate coefficients k_r and k_3 are intimately related to the radiative lifetime τ_r and the lifetime of the complex with respect to dissociation τ_d by

$$\tau_d \ = \ \frac{k_3}{k_c^2 f} \tag{4.6}$$

$$\tau_r \ = \ \frac{k_3}{k_c k_r f} \tag{4.7}$$

with k_c being the rate coefficient for collisions between the ion and the neutral reactant. Lower limits for the lifetimes can be determined when using the Langevin rate coefficient, k_L, for the collision rate coefficient, k_c. A fixed stabilization efficiency of f=0.1 has been used for the determination of τ_d and τ_r (although f will be higher for the CH_3^+-system than for the CH_5^+-system). This value has been adapted from the hydrogen cluster ions [pau95] since it is expected that these clusters exhibit similar properties, as binding energies, densities of states, etc. as the present case of CH_n^+. Results on the basis of these assumptions are also presented in table 4.1.

Some remarks should be made concerning the measurements leading to the values in the first five rows of table 4.1. These have been obtained by injecting CH_3^+ into the trap containing H_2 with HD in its natural fractional abundance of 3×10^{-4}. As the association is slow at low number densities, the H-D-exchange with HD can compete with association and both processes can be observed simultaneously. These process have been measured by Sorgenfrei [sor94] for p-H_2 and n-H_2 at 10K, and the resulting values are included in the table. In the analysis of Sorgenfrei it was assumed that CH_5^+-like ions undergo H-D-exchange and that all isotopic variants of CH_3^+ have the same rate coefficient for association. With the knowledge gained in this work, these assumptions cannot be longer maintained, thus the measurements have been repeated with better quality in order to extract more information about the association of CH_2D^+ and CHD_2^+ with H_2 as shown in table 4.1. These numbers are important for astrochemical models as the deuterated versions of CH_3^+ are thought to undergo radiative association with the abundant H_2 in

Process	k_r / cm^{3}s^{-1}	k_3 / cm^{6}s^{-1}	k_L / cm^{3}s^{-1}	τ_r/ms	τ_d/ns	Remarks
CH$_3^+$+n-H$_2$	$(5.5 \pm 0.8) \times 10^{-14}$	$(4.2 \pm 0.5) \times 10^{-26}$	1.58×10^{-9}	4.8	168	this work
CH$_3^+$+n-H$_2$	$(5.0 \pm 2.0) \times 10^{-14}$	$(6.0 \pm 1.2) \times 10^{-26}$	1.58×10^{-9}	3.9	120	[sor94],10K
CH$_3^+$+p-H$_2$	$(1.1 \pm 0.1) \times 10^{-13}$	$(1.9 \pm 0.2) \times 10^{-25}$	1.58×10^{-9}	5.7	390	[sor94],10K
CH$_2$D$^+$+n-H$_2$	$(9.0 \pm 4.0) \times 10^{-14}$	$(1.1 \pm 0.3) \times 10^{-25}$	1.57×10^{-9}	7.8	444	this work
CHD$_2^+$+n-H$_2$	$(1.9 \pm 0.9) \times 10^{-13}$	$(1.4 \pm 0.4) \times 10^{-25}$	1.57×10^{-9}	4.7	569	this work
CD$_3^+$+HD	$(4.0 \pm 0.6) \times 10^{-13}$	$(1.6 \pm 0.4) \times 10^{-24}$	1.30×10^{-9}	31	9404	this work
CH$_5^+$+n-H$_2$	$(1.6 \pm 0.6) \times 10^{-16}$	$(2.6 \pm 0.6) \times 10^{-28}$	1.57×10^{-9}	10	1.1	this work
CH$_5^+$+HD	$(3.5 \pm 0.5) \times 10^{-16}$	$(4.0 \pm 0.6) \times 10^{-28}$	1.31×10^{-9}	8.7	2.3	this work
CHD$_4^+$+HD	$(4.5 \pm 0.4) \times 10^{-16}$	$(7.5 \pm 1.5) \times 10^{-28}$	1.29×10^{-9}	13	4.5	this work

Table 4.1: Radiative and ternary association rate coefficients k_r and k_3 for the indicated collision systems at a temperature of 15K as obtained from fitting equation 4.5 to the data shown in figure 4.8. The radiative and complex lifetimes τ_r and τ_d are calculated using equations 4.7 and 4.6 with the listed Langevin collision rate coefficients k_L and assuming a collisional stabilization efficiency f=0.1. The values from [sor94] are included for comparison. For the CH$_3^+$+n-H$_2$ system, the uncertainties of k_r and k_3 increase with the degree of deuteration of the CH$_3^+$ ion due to the increasing insensitivity to these parameters (confer reaction scheme 4.9).

the ISM, thus producing deuterated CH$_5^+$-analogues [mil89]. The measurements for four different H$_2$(HD) number densities are shown in the lower part of figure 4.9. The data have been fitted consistently by numerical solutions of a rate equation system including the 14 reactions indicated in the upper part of the same figure. These fits have been guided by the known rate coefficients for the deuteration processes and the previously measured association of CH$_5^+$ with H$_2$ (see table). Interesting is the observation in the numerical simulations of the data that reasonable fits are only obtained if the rate coefficient for deuteration of CH$_3^+$ with HD is lower than the previously measured value of 1.6×10^{-9} cm^{3}s^{-1} in pure HD (assuming that the natural fractional abundance of HD in H$_2$ of 3×10^{-4} is not modified by the low temperature environment of the ion trap). The simulated solid lines in figure 4.9 suggest a lower value of 1.3×10^{-9} cm^{3}s^{-1}. This effect is most probably due to the surrounding n-H$_2$ environment which contains 75% o-H$_2$ (J=1). These species can heat the CH$_3^+$ ions by effective exchange collisions. These 'heated' CH$_3^+$ ions seem to have a lower rate coefficient for H-D-exchange with HD than cold CH$_3^+$ embedded in a pure HD environment (for a further discussion see appendix C).

As can be seen in table 4.1, the radiative lifetimes for all systems studied are on the order of several ms while the lifetimes of the complexes range from a few ns up to μs. Although these quantities only contain rather integral information about each system under consideration, their absolute value and their relation comparing systems of different complexity (CH$_5^+$ vs. CH$_5^+$(H$_2$)-analogues) or systems with equivalent atoms or inequivalent atoms (CH$_5^+$ vs. CHD$_4^+$), can help understanding part of the internal dynamics of these systems.
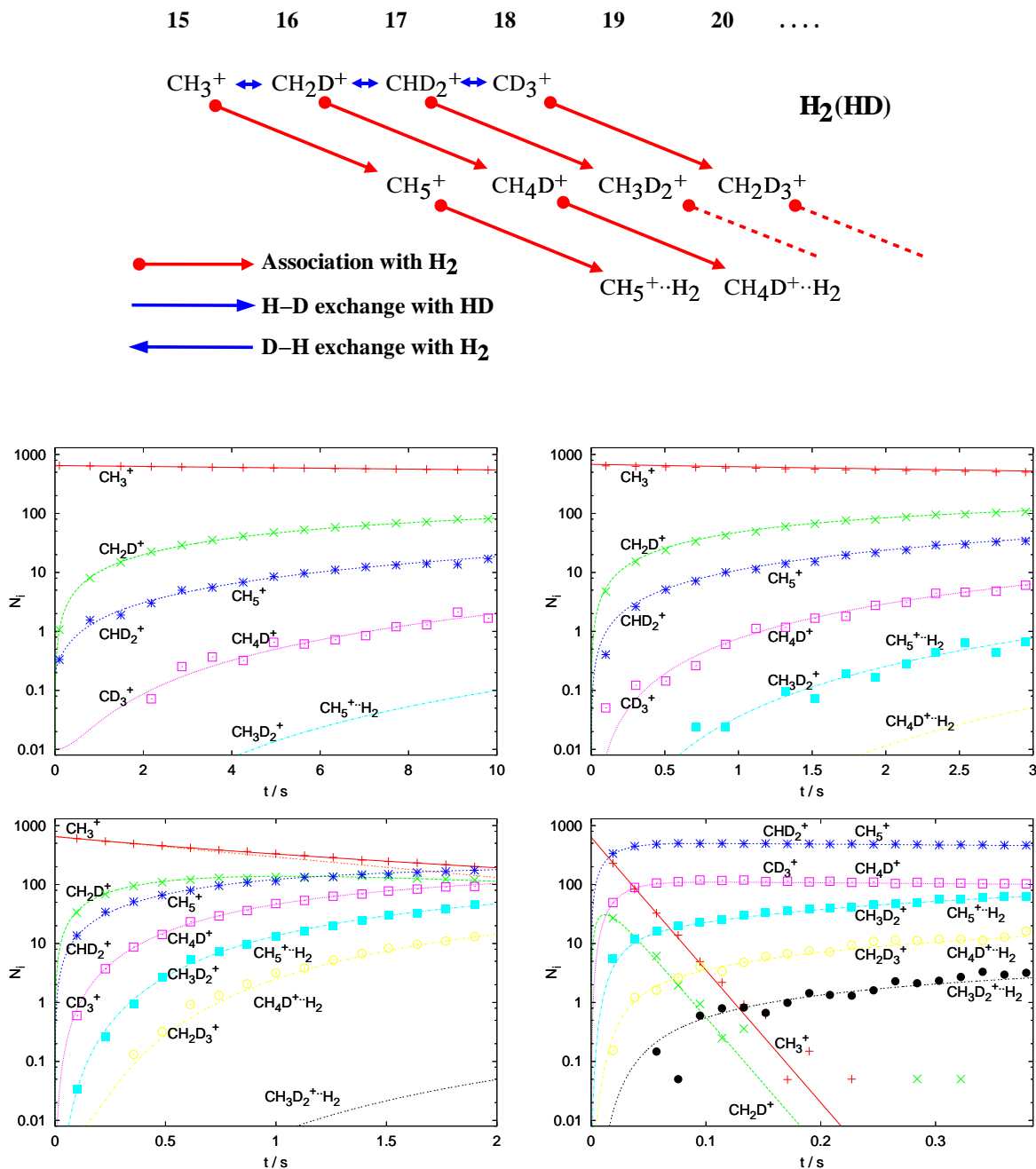
Figure 4.9:

Upper Part: Scheme for CH_3^+ when reacting with H_2 containing HD as a natural impurity. As known from other experiments (see appendix C), H-D-exchange with HD is only possible for CH_3^+-analogues.

Lower Part: Measurements for CH_3^+ + n-H_2(HD) using increasing H_2 number densities (from upper left to lower right: 3.3×10^{10} cm^{-3} , 2.0×10^{11} cm^{-3}, 1.6×10^{12} cm^{-3} , 3.0×10^{13} cm^{-3}) at T=15K. Please observe the different time scales. The data have been fitted consistently using up to 14 reactions shown in the upper part. Fragmentation and further association of the clusters could be neglected at the number densities used. Visible in the lower left measurement is a non-exponential time-dependence of the primary CH_3^+-ions due to back-reaction of CH_2D^+ with H_2 to yield CH_3^+ with a rate coefficient of 3.3×10^{-13} cm^{3}s^{-1}.

Radiative lifetimes in the ms range are typical for vibrational-rotational transitions. The excited complexes formed are composed of two entities approaching one another. As such the nuclei of the complex are largely displaced from their ground state equilibrium positions. Therefore vibrational transitions indeed play a dominant role in the relaxation of the collision complex. The absolute values for τ_r are therefore in agreement with the expectations based on the internal motion of the newly forming molecule. Differences for deuterated and undeuterated CH_5^+-analogues are much larger than those among $CH_5^+(H_2)$-analogues. This will be discussed below.

Much larger differences are observed for the dissociation lifetimes. First of all, the lifetime is shortened by more than two orders of magnitude when forming $CH_5^+(H_2)$ rather than CH_5^+. This effect is typical for systems of decreasing binding energies. The H_2 in CH_5^+ is bound by more than 1eV (1.8eV [mul97], 1.72eV [kom87]) and should therefore be considered as a molecule rather than a cluster. Partly due to the high excitation in this potential well and partly due to the floppiness of this molecule, one expects a very high density of states for the complex formed. This leads to a long lifetime with respect to dissociation. In contrast, the H_2 unit is bound by less than 0.1eV [boo95a] to the CH_5^+-core in $CH_5^+(H_2)$. Its lifetime is only a few ns at 15K. The density of states at the energy level of reactants in the shallow potential well is comparably small and therefore there are much fewer possibilities to partition the internal energy of the complex among the different degrees of freedom than in the CH_5^+ case.

An increase in lifetime of about a factor four is found between the formation of $CH_5^+(H_2)$ and $CHD_4^+(HD)$. As mentioned, the prolongation of a lifetime can be due to a higher density of states. It is also well known that the lifetime of a complex increases with decreasing temperature. All the experiments have been carried out at 15K. Despite this fact at this low temperature HD is only populating the rotational ground state (J=0) while n-H_2 contains 75% o-H_2 (J=1) instead. Therefore in principle the effective temperature of the complexes will certainly be different if there is a way to release a fraction of the internal energy of the o-H_2. However, ΔJ=1 transitions of hydrogen are rather unlikely and their contribution to heating the cluster is considered to be small. Instead, scrambling collisions in which the (J=1) molecule is incorporated into the molecule while two other hydrogen atoms form a (J=0) H_2 can lead to an effective heating of the cluster. Detailed analysis of the deuteration process in collisions of CH_5^+ + HD (appendix C) show that an HD exchange is slower than 5×10^{-18} cm^{3}s^{-1}. Therefore scrambling is also a rather inefficient process for this cluster. In summary, internal heating of the $CH_5^+(H_2)$ complex can most probably not be made responsible for the increased lifetime in case of the isotopomers $CH_5^+(HD)$ and $CHD_4^+(HD)$. Instead, the increase of lifetime is attributed to an increase in the number of accessible states in the complex, just as is the case in the comparison of the CH_5^+ and $CH_5^+(H_2)$-analogues. As has been found by Smith et al. [smi82], the replacement of hydrogen atoms by deuterium atoms leads to a much smaller spacing of the involved rotational and vibrational levels, thus increasing the density of states and consequently the lifetime of the complex.

The differences in lifetime τ_d among the $CH_5^+(H_2)$ analogues are much smaller than the ones among the CH_5^+ analogues. First of all, there is a tripling of the lifetime when p-H_2 (J=0) is used instead of n-H_2 in collisions with CH_3^+. As these two cases do not have isotopic differences, this indicates that in $CH_3^+\cdots H_2$ there is indeed a way to heat (or cool) the complex by scrambling collisions. The effectiveness of these exchange collisions has

already been demonstrated for the case CH_3^++HD in section 4.3 (also appendix C). This ability of scrambling is strongly correlated to the fluxional nature of this molecule [mar99] as introduced in section 4.1. Therefore, in contrast to the formation of $CH_5^+(H_2)$, an effective exchange is possible in the collision of CH_3^+ with H_2.

An even larger prolongation of the complex lifetime is observed for the formation of the CHD_4^+ isotopomer. Its lifetime should be compared to the case $CH_3^+ + p$-H_2, since HD in the $CD_3^+ + HD$ collision is also most likely in J=0 at 15K. Still the lifetime is larger by about a factor of 25. In this case the density of states increases considerably when taking four deuterium atoms instead of hydrogen atoms. This is surely related to the deep well of 1.8eV in this system. Indeed, a look in the table reveals that the increase is not so pronounced for the loosely bound CH_5^++H_2 collision systems even when replacing five hydrogen atoms by deuterium.

Besides the astrochemical interest in the systems studied, the data revealed a wealth of information about the processes occurring in ion-molecule collisions. It seems that not only the exothermic H-D-exchange collisions boost deuterium enrichment in the ISM, but also the association processes to form more complex molecules are faster for deuterium containing species. Several future studies will help to complete the picture. Insightful will surely be further investigations with p-H_2. It is not expected that the use of p-H_2 instead of n-H_2 will change a lot in collisions with CH_5^+, but surely it will increase the complex lifetime in collisions with the isotopomers of CH_3^+. In a dedicated experiment CD_3^++p-H_2 for example, not only the slow D-H-exchange with the cold p-H_2 can be observed, but also the association process which can then be compared to the case CD_3^++HD listed in table 4.1. It is expected that the association rate of CD_3^+ with p-H_2 is only slightly lower than with HD, as both neutral reaction partners have J=0 at low temperature. As a further isotopic variant adding to the collision systems in table 4.1, the system CH_4D^++HD is experimentally accessible by injecting CH_4^+ into the trap containing HD and letting it react to CH_4D^+ (with a branching fraction of 30%, appendix B). Unfortunately, association processes of CH_3^++HD are unobservable, as H-D-exchange is orders of magnitude faster than association. Concerning the absence of H-D-exchange in collisions of CH_5^+ with HD, a further sensitive experimental test would consist of generating the corresponding cluster ion $CH_5^+(HD)$ in the 22-pole ion trap, store it for several seconds there, and then confirm by collision induced dissociation (CID) during the extraction period that the ion core is still the undeuterated CH_5^+.

Systematic spectroscopic studies of CH_n^+ and their isotopomers could help to learn more about the structure and dynamics of these interesting species. Especially measurements dedicated to CH_5^+, the 'Holy Grail', will be challenging. One aim is to extend the work of White et al. [whi99] on CH_5^+ and Boo et al. [boo95, boo95a] on solvated ions $CH_5^+(H_2)_n$ to the far infrared regime utilizing the method of laser induced reactions (LIR, [les00, sch02]). This wavelength region is of special importance, as soft bending modes and also the scrambling motion of CH_5^+ reveal their fingerprints in this regime.

Chapter 5

Summary and Outlook

In this work, 22-pole ion trap machines have been applied to investigate protonated water clusters $H^+(H_2O)_n$ (n=4..10) and ionic hydrocarbons CH_n^+ (n=2..5) at low temperatures.

Protonated water clusters $H^+(H_2O)_n$ play an important role in atmospheric chemistry and in interstellar space. The Taipei 22-pole ion trap machine has been applied to kinetic and spectroscopic investigations of these clusters produced from a supersonic expansion in a corona discharge source. Using low-pressure He buffer gas for collisional thermalization, refrigeration of the ion trap by liquid nitrogen allows a good control of the cluster temperature over the range $80K-350K$. This method provides an accurate means of determining the dissociation energies of the cluster ions by measuring their dissociation rates as a function of temperature and calculating their internal energies from vibrational frequencies provided by density functional theory. Results of the thermochemical measurements at well-defined cluster temperatures have been given for $H^+(H_2O)_n$, n=4..10. The feasibility of using the ion trap to acquire temperature-dependent infrared spectra is presented.

The deuteration and abstraction reactions of small ionic hydrocarbons CH_n^+ (n=2..5) with H_2, HD and D_2 and the subsequent association processes have been explored at temperatures down to 15K in the Chemnitz 22-pole apparatus. The reactions of the investigated ionic species and their isotopic variants are important for understanding ion-molecule processes in the ISM. One of the starting points of the research program was the question whether protonated methane, CH_5^+, is subject to H-D-exchange in collisions with HD at low temperatures. It turns out that the rate coefficient for this deuteration process is smaller than 5×10^{-18} cm^3s^{-1}, whereas CH_3^+ deuterates with HD by three subsequent fast exchange reactions to CD_3^+ at a temperature of 15K. The latter process is very efficient and happens close to the collision limit. The methane cation, CH_4^+, on the other hand, shows also some interesting features in collisions with H_2, HD and D_2. It exhibits an inverse temperature dependence with the rate coefficient increasing at least one order of magnitude going from 300K to 15K. Furthermore, reacting with HD at the temperature of 15K, the reaction channel leading to CH_5^+ is preferred over the D-atom abstraction channel (isotope effect). This behavior is tentatively explained with a longer complex lifetime at low temperatures. Tunneling, like in the case of the iso-electronic system $NH_3^+ + H_2$, is most probably not responsible for this interesting observation.

The combination of an ion trap with laser radiation is a very sensitive tool to study

the vibrational structure of molecular ions. Several methods have been developed for this purpose, for example predissociation spectroscopy ([wan97, jia00], appendix A), infrared multi photon dissociation (IRMPD, [yeh89, asm03]), or laser induced reaction (LIR, [sch02]). Most of these experiments have been performed with laser radiation in the infrared (IR) wavelength region. Future research programs will extend the observations to the far infrared (FIR) and submillimeter region, as many molecules show their unmistakable chemical signature at these wavelengths. Intense laser sources to perform these experimental tasks, as for example the free electron laser for infrared experiments FELIX in Rijnhuizen (Netherlands), are available, and there are also other high emittance IR- and FIR-lasers under construction, for instance the ELBE-source in Rossendorf (Germany). Also in astrophysics there is a rising interest in FIR and submillimeter observations due to the capability of detecting cold objects and stars obscured by dust nebulae. In 2007, the European Space Agency will launch the satellite Herschel for observations in this wavelength range.

The hydronium ion H_3O^+ and water cluster ions $H^+(H_2O)_n$ will certainly be prime targets of future projects with the 22-pole ion trap, as water is a key ingredient in many astrophysical environments. Structural isomers can be identified and their thermal or non-thermal composition in the trap can be investigated using LIR with one of the above mentioned laser sources. Also intra-cluster processes such as isomerization or chemical reactions in heterogeneous clusters can be studied and help to understand the transition from small molecular species towards bulk systems.

Appendix A

Investigations of protonated and deprotonated water clusters using a low-temperature 22-pole ion trap

Y.-S. Wang, C.-H. Tsai, Y. T. Lee, and H.-C. Chang, J. C. Jiang,
O. Asvany, S. Schlemmer, D. Gerlich

Investigations of Protonated and Deprotonated Water Clusters Using a Low-Temperature 22-Pole Ion Trap

Y.-S. Wang, C.-H. Tsai, Y. T. Lee, and H.-C. Chang*

Institute of Atomic and Molecular Sciences, Academia Sinica, P.O. Box 23-166 Taipei, Taiwan, ROC, and Department of Chemistry, National Taiwan University, Taipei, Taiwan 106, ROC

J. C. Jiang

Department of Chemical Engineering, National Taiwan University of Science and Technology, Taipei, Taiwan 106, ROC

O. Asvany, S. Schlemmer, and D. Gerlich

Institute of Physics, Chemnitz University of Technology, 09107 Chemnitz, Germany

Received: September 26, 2002; In Final Form: January 7, 2003

A new tandem mass spectrometer, containing a temperature-variable 22-pole ion trap, has been constructed. It is applied, as a first application, to kinetic and spectroscopic investigation of charged water clusters produced from a supersonic expansion. Using low-pressure He or H_2 as buffer gas for collisional thermalization, refrigeration of the ion trap allows a good control of the cluster temperature over the range $77-350$ K. It provides an accurate means of determining the dissociation energies of both protonated and deprotonated water cluster ions [$H^+(H_2O)_n$ and $OH^-(H_2O)_m$] by measuring the dissociation rates at various temperatures along with their internal energies calculated from vibrational frequencies provided by density functional theory calculations. In this report, results of the thermochemical measurements for $H^+(H_2O)_{4-10}$ and $OH^-(H_2O)_{3-7}$ at well-defined cluster temperatures are presented. The feasibility of using this ion trap to acquire temperature-dependent infrared spectra of charged water clusters is also demonstrated with $H^+(H_2O)_6$.

Introduction

An important parameter to measure and to control in the study of ion chemistry[1] and spectroscopy[2] is the ion temperature. Conventional thermometers, thermocouples for example, provide accurate measurements of the temperature of solid and liquid samples over a wide range. For the temperature determination of high-pressure gas, one can measure the temperature of their sample vessel because collisional motions will fully thermalize the gas with its surroundings. The temperature of gas-phase ions in a high vacuum system is more difficult to measure (and to control) because the ions are intentionally isolated from the vacuum chambers to avoid charge transfer. As a result, the temperature of gas-phase ions is often far above 300 K owing to the heating effect during ionization, which can create unwanted reactions as well as spectral complications. Several techniques have thus been developed for the reason of temperature control, mainly to lower the temperature of the intentionally isolated ions, such as adiabatic expansion,[3] evaporative cooling,[4] sympathetic cooling,[5] laser cooling,[6] and cooling by collisions with cold buffer gas.[7]

The collisional cooling method, as to be discussed in this report, is one of the most universal ways for the temperature control (particularly for the internal degrees of freedom) of gas-phase ions. In a storage cell, the buffer gas fills more or less the entire region at a well defined temperature and pressure, producing a thermal "bath". Ions in the storage cell are confined translationally by a time-varying electric field and thermalize both internally and kinetically with the bath by collisions. Temperature control of the storage cell can therefore be performed to change the ion temperature. In the 1980s, Gerlich and co-workers[8-10] developed multipole radio frequency (RF) ion traps, which serve as ion storage cells and can easily be combined with lasers.[8] Integration of the trap to a refrigeration system enables active temperature control of the storage cell, thereby allowing studies of the temperature dependence of ion-molecule interactions[9] as well as the thermodynamic and kinetic properties of gas-phase ions and cluster ions.[10]

In this paper, a temperature-variable 22-pole ion trap integrated into a tandem mass spectrometer is used for investigation of charged water clusters, in both protonated [$H^+(H_2O)_n$] and deprotonated [$OH^-(H_2O)_m$] forms, produced from a supersonic expansion. These cluster ions are chosen because water is not only of general interest in physical chemistry but also plays important roles in interstellar space[11] and in the atmosphere.[12] The importance of the latter surely stems from the high abundance of water on earth and the ease of charge separation of the water molecule within clusters,[13] as H_2O has a high proton affinity of 165 kcal mol^{-1} and basicity of 157 kcal mol^{-1} in the gas phase.[14]

Experiments with the water cluster ions [$H^+(H_2O)_n$] go back to the 1970s when the Kebarle group[15] first investigated these ions in a pulsed high-pressure mass spectrometer and deduced the cluster bond energies and other thermochemical quantities from the temperature dependence of equilibrium constants. After
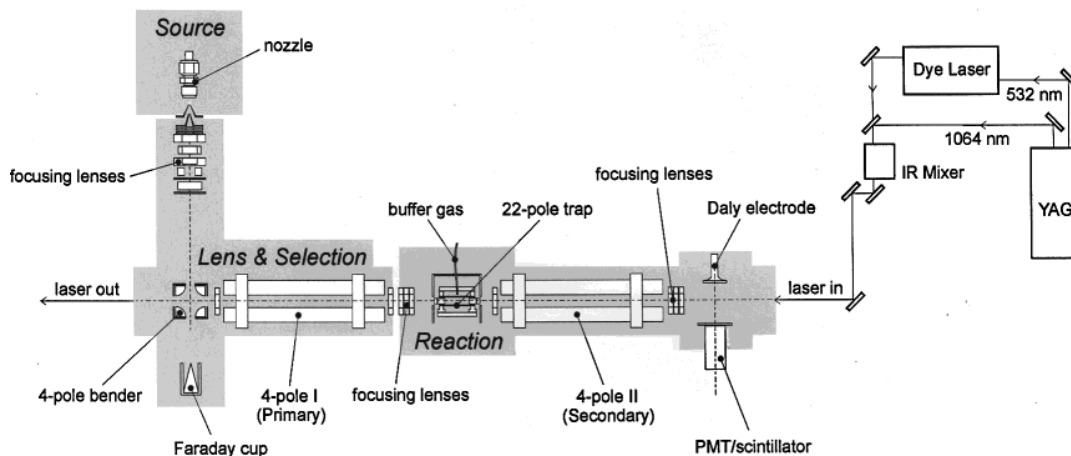
Figure 1. Experimental layout of the temperature-variable 22-pole ion trap mass spectrometer. Shown on the right is the pulsed infrared laser system.
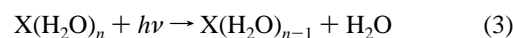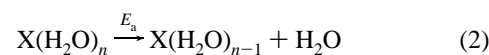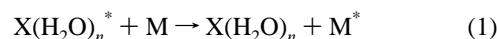
emergence of the corona discharge source[3] for production of internally cold clusters, detailed spectroscopic investigations followed,[16-18] revealing important structural information for cluster ions of a size up to $n = 8$. Productions as well as spectral assignments of larger clusters become much more difficult because of the complex manifold of structural isomers. Of special interest in the measurements of Kebarle[15] and other groups[19-22] is the deviation of the cluster bond energy from a smooth sequence, an indication for the existence of stable structures involving shell closures. The first shell closure was found to occur at $n = 4$ for $H^+(H_2O)_n$,[15,19] and the special stability of this cluster ion has since been observed in a number of experiments, including the vibrational predissociation spectroscopic measurements of Yeh et al.[16]

In addition to the aforementioned bond energy measurements, the temperature-variable 22-pole ion trap also opens new possibilities to obtain temperature-dependent infrared spectra, from which the population of various isomers as a function of temperature can be inferred. For the cluster ions of interest in this work, there exist many structurally as well as energetically similar isomers, and these isomers are separated by barriers with heights comparable to the strength (a few kcal mol^{-1}) of the hydrogen bonds that link the water molecules together. Therefore, up to a certain temperature, structural isomerization can occur. Accompanied with this isomerization, the intracluster proton may migrate (through tunneling) and it can either localize at a site close to one water molecule, forming an H_3O^+ (or OH^-) ion core, or delocalize between two water molecules, forming an $H_5O_2^+$ (or $H_3O_2^-$) ion core.[18,23,24] By monitoring the evolution of the spectral changes with temperature, one may investigate the intracluster proton-transfer process closely.

Theoretical analysis for the structural transformation of $H^+(H_2O)_n$ (refs 25 and 26) and $OH^-(H_2O)_m$ (refs 27 and 28) has been carried out at various levels of computation. Singer et al.,[26] for example, employed basin-hopping Monte Carlo simulations, examined the topology of $H^+(H_2O)_8$ as a function of temperature, and concluded that the tree-like topology with chains of H_2O molecules emanating from a H_3O^+ core is favored by Gibbs free energies at room temperature. The conclusion is in accord with the spectroscopic observations of Jiang et al.[18] for $H^+(H_2O)_{5-8}$ produced in a molecular beam. However, in the beam experiment, the workable cluster temperature range is very limited, only about 140–200 K, disallowing a test of the simulations. The temperature-variable 22-pole ion trap clearly offers an excellent opportunity to study the isomeric transitions under equilibrium conditions over a much wider

temperature range, potentially from 4 to 400 K. Furthermore, the possibility of collision-induced isomerization can be explored.

In the kinetic and spectroscopic measurements of this work, the reactant ions are first thermalized with buffer gas and then analyzed as a function of both trapping time and laser frequency as

$$X(H_2O)_n^* + M \rightarrow X(H_2O)_n + M^* \tag{1}$$

$$X(H_2O)_n \xrightarrow{E_a} X(H_2O)_{n-1} + H_2O \tag{2}$$

$$X(H_2O)_n + h\nu \rightarrow X(H_2O)_{n-1} + H_2O \tag{3}$$

where X is H^+ or OH^-. The third body M in eq 1 is nothing but a medium for energy transfer, and it can be either He or H_2 because they are light and chemically inert. The method of such cluster bond energy measurements has recently been demonstrated by Lovejoy and Bianco[29] for small water cluster ions $H^+(H_2O)_{3,4}$ using a three-dimensional quadrupole ion trap (Paul trap) at elevated temperatures, i.e., around 300–500 K. The present study represents an extension of their work to larger clusters at lower temperatures.

Experimental and Computational Sections

A. Experimental. The temperature-variable ion trap mass spectrometer is composed of three differentially pumped vacuum regions, denoted respectively by "Source", "Lens & Selection", and "Reaction". The heart of this spectrometer is the 22-pole ion trap, as shown schematically in Figure 1. The trap consists of 22 stainless steel rods with a diameter of 1 mm and a length of 36 mm equally spaced on an inscribed radius of 5 mm. Pulsed electrodes at the entrance and exit of the trap confine the ions along the axial direction. The design of this trap is identical to that described in detail in ref 9.

We produced the charged water cluster ions by a supersonic expansion of corona-discharged H_2/H_2O (99/1) mixtures through a room-temperature nozzle (~100 μm in orifice diameter) at a backing pressure of ~100 Torr. The typical discharge voltage used is 700 V and the resulting discharge current is about 30 μA. Downstream the nozzle, the ion beam is skimmed, focused, and bent 90° toward the first quadrupole mass spectrometer for mass selection. With this mass filter, we select clusters with a specific solvation number n (or m) out of the mixture $H^+(H_2O)_n$

TABLE 1: Determination of the Dissociation Energies (kcal mol^{-1}) of H$^+$(H$_2$O)$_{4-10}$ and OH$^-$(H$_2$O)$_{3-7}$ from Their Components at the Mean Trap Temperature T_m (K) and Comparison with Literature Values

			this work			literature values[c]
clusters	T_m	E_a	$\langle E_{vib} \rangle^a$	$ak_BT_m{}^b$	E_{diss}	E_{diss}
H$^+$(H$_2$O)$_4$	325	10.2 ± 0.4	6.0 ± 0.4	0.97 ± 0.24	17.2 ± 0.7	17.3, 17.4
H$^+$(H$_2$O)$_5$	227	6.8 ± 0.1	4.6 ± 0.4	0.68 ± 0.17	12.1 ± 0.5	12.3, 11.1
H$^+$(H$_2$O)$_6$	203	4.9 ± 0.1	5.0 ± 0.5	0.61 ± 0.15	10.5 ± 0.6	11.2, 10.7
H$^+$(H$_2$O)$_7$	181	4.0 ± 0.1	4.9 ± 0.8	0.54 ± 0.13	9.4 ± 0.9	10.2, -
H$^+$(H$_2$O)$_8$	164	4.0 ± 0.1	5.0 ± 0.4	0.49 ± 0.12	9.5 ± 0.5	-, -
H$^+$(H$_2$O)$_9$	155	4.2 ± 0.1	u.d.	0.46 ± 0.11		-, -
H$^+$(H$_2$O)$_{10}$	150	4.0 ± 0.1	u.d.	0.45 ± 0.11		-, -
OH$^-$(H$_2$O)$_3$	323	10.3 ± 0.1	4.9 ± 0.4	0.96 ± 0.24	16.2 ± 0.5	-, 15.5
OH$^-$(H$_2$O)$_4$	254	6.9 ± 0.1	4.3 ± 0.5	0.76 ± 0.19	12.0 ± 0.6	-, 11.2
OH$^-$(H$_2$O)$_5$	216	6.0 ± 0.1	4.3 ± 0.6	0.64 ± 0.16	10.9 ± 0.7	-, 10.7
OH$^-$(H$_2$O)$_6$	203	6.3 ± 0.1	4.6 ± 0.4	0.61 ± 0.15	11.5 ± 0.5	-, 10.4
OH$^-$(H$_2$O)$_7$	192	6.9 ± 0.1	u.d.	0.57 ± 0.14		-, 9.6

^{a} Internal energies of H$^+$(H$_2$O)$_9$, H$^+$(H$_2$O)$_{10}$, and OH$^-$(H$_2$O)$_7$ are undetermined (u.d.). ^{b} Adopting $a = 3/2$ and assuming an error of 25%. ^{c} Values adapted from thermochemical measurements (refs 15 and 19), following the procedures described in ref 29.

[or OH$^-$(H$_2$O)$_m$] coming from the source. After passing through the filter, the selected ions are injected with low kinetic energy into the 22-pole RF ion trap, which contains buffer gas at a fixed pressure and temperature. While being stored, the ions are thermalized by collisions with the cold buffer gas for either kinetic or spectroscopic measurements.

Low temperatures of the ion trap are achieved by using a liquid-nitrogen-cooled coldfinger counter-heated by a heating wire winded around the trap holder. The temperature is measured by two thermocouples (type E) attached directly to the body of the 22-pole trap. The temperature range thus obtainable is from 77 to 300 K, and above 300 K (using only the heater without liquid nitrogen). The error in the absolute temperature measurements is about ±1 K, calibrated against the liquid-nitrogen temperature.

Pressures of the buffer gas (either He or H$_2$) inside the 22-pole ion trap are measured using a conventional ion gauge outside the storage cell. The ion gauge does not have the accuracy of, for example, a spinning rotor gauge or a Baratron, but in our application, we need only relative pressure readings for determination of the bond energies (see below) and/or in spectroscopic measurements. In assessing the molecular number densities in the trap, we have to include the sensitivity factor of the ion gauge for the used buffer gas [e.g., $f_{He} = S(He)/S(N_2) \approx 0.15$ and $f_{H2} = S(H_2)/S(N_2) \approx 0.4$] and the correction for the Knudsen effect[30]

$$n_t = \frac{p_g}{k_B\sqrt{T_tT_g}} \qquad (4)$$

where n_t and T_t are the number density and the temperature of buffer gas in the trap, p_g and T_g are the pressure and the temperature of buffer gas in the gauge, respectively, and k_B stands for the Boltzmann factor. The typical value of n_t used in this experiment is 2×10^{13} cm^{-3}, which suggests a collision frequency of $\sim 10^4$ s^{-1} between the trapped ions and the buffer gas atoms (or molecules).

A RF amplitude (zero-to-peak) of $V_0 = 50$ V from a home-built power source[31] is applied to the 22 rods of the ion trap at the fixed frequency $\Omega/2\pi = 10$ MHz. Short dc pulses applied to the retarding electrodes control the entrance and exit of the ions to be investigated. Operating under these conditions, the ion trap allows storage of ions over a wide mass range; it keeps the fragment as well as the parent ions of the reactions described by eqs 2 and 3 for subsequent analysis. In the kinetic

measurements, the second quadrupole mass filter located just behind the trap (cf. Figure 1) is set to the *parent* ion, from which we monitored its decay in a time range up to 200 ms. The typical repetition rate of the ion pulses, generated by the trap entrance gating, in this cluster bond energy measurement is 5 Hz. In the spectroscopic measurements, infrared laser pulses are introduced into the ion trap to pump the collisionally cooled cluster ions to the first vibrationally excited state at a repetition rate of 20 Hz. The laser beam with an energy of $\sim$2 mJ/pulse is generated by difference frequency mixing of the Nd:YAG fundamental photon (1064 nm) and the $\sim$760 nm output of a tunable dye laser using a LiNbO$_3$ crystal. After vibrational excitation, the *product* ions are extracted from the ion trap and selected by the second mass filter to obtain the infrared action spectra. The typical storage time of the ions in the trap before the laser excitation is 10 ms. The ion signals in both experiments are detected by either a Daly detector (for positive ions) or an electron multiplier (for negative ions) operated in an ion counting mode.

We emphasize that, compared to the Paul trap, our 22-pole storage cell has a wide field-free region, which effectively avoids RF excitation and collisional defocusing of the trapped ions. The feature is critically important for experiments conducted at lower temperatures for larger and/or less strongly bound clusters.[10] Lovejoy and Bianco[29] have examined the effect of the applied trap driving voltage on the measured decomposition rate constants for H$^+$(H$_2$O)$_4$ and other cluster ion systems. Their results show that the RF heating effect is nonnegligible at the parameter $q_z > 0.3$ when using the quadrupole ion trap as a storage cell. For the multipole ion trap, Gerlich[7] has defined an adiabaticity parameter

$$\eta = 2n(n - 1)\frac{eV_0}{mr_0{}^2\Omega^2}\hat{r}^{n-2} \qquad (5)$$

which reduces to q_z at $2n = 4$. Adopting $V_0 = 50$ V, $\Omega/2\pi = 10$ MHz, the center-to-pole distance of $r_0 = 5$ mm, the pole number of $2n = 22$, and the maximum turning radius of $\hat{r} = r/r_0 = 0.8$ for the 22-pole trap used in this experiment, we have $\eta \approx 0.02$ at $m/e = 70$. Because η is inversely proportional to m, the values of this parameter for other ions ($m/e > 70$) listed in Table 1 are all less than 0.02, which is well below the safe operation limit ($\eta < 0.3$) of the multipole RF ion trap.[7]

B. Computational. Theoretically calculated vibrational frequencies and molecular structures are used in assessment of cluster internal energies as well as for spectral assignment. The
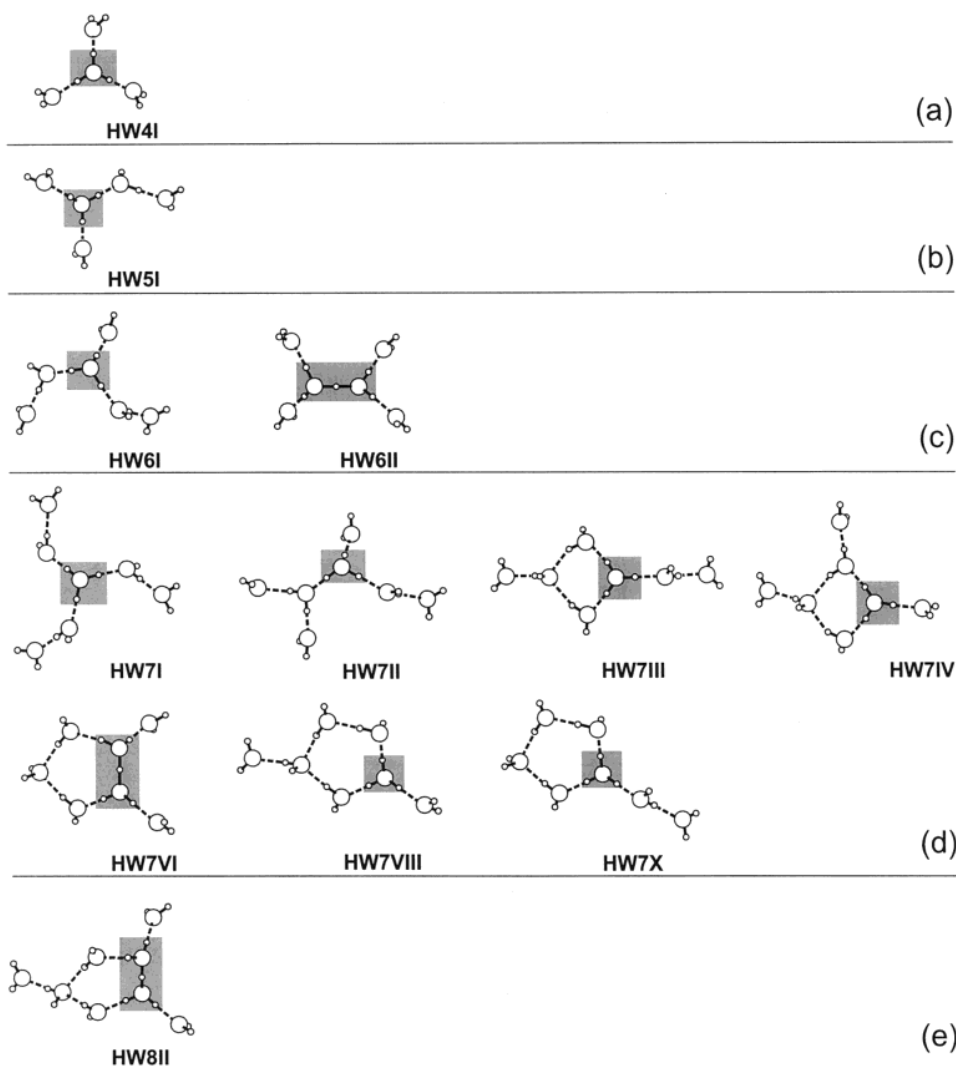
Figure 2. Low-energy isomers of (a) $H^+(H_2O)_4$, (b) $H^+(H_2O)_5$, (c) $H^+(H_2O)_6$, (d) $H^+(H_2O)_7$, and (e) $H^+(H_2O)_8$. The O and H atoms are represented by large open and small open circles, respectively, and the ion cores (either H_3O^+ or $H_5O_2^+$) are shaded for clarity. Shown here are only isomers that have been previously identified in a supersonic expansion (ref 18).

calculations, based on the density functional theory (DFT), are performed using the commercial Gaussian 98 package.[32] Utilizing a standard analytical gradient method, geometries of the cluster ions were optimized without imposing any symmetry constraints at the B3LYP level of computation with the 6-31+G* basis set (denoted as B3LYP/6-31+G*).

A large number of $H^+(H_2O)_{4-10}$ and $OH^-(H_2O)_{3-7}$ potential minima are located in the course of the computation. They correspond to isomers of chainlike, four-membered ring, five-membered ring, double ring, and cage-like structures. The structures and energetics of these isomers have been previously reported.[18,23] We depict in Figure 2 only the isomeric structures of $H^+(H_2O)_{4-8}$ that have been identified in a corona-discharged supersonic expansion at an estimated cluster temperature of 170 K.[16-18] For clusters of $n \leq 6$, they are predominantly the chainlike structures (namely, **HW4I**, **HW5I**, **HW6I**, and **HW6II**), whereas at $n \geq 7$, ring structures (**HW7III**, **HW7IV**, **HW7VI**, **HW7VIII**, **HW7X**, and **HW8II**) exist. Such a preference of five-membered ring formation in $H_3O^+(H_2O)_n$ stands as an interesting contrast to its structural analogue $NH_4^+(H_2O)_n$,[33] of which the formation of symmetric four-membered rings is strongly favored.

Results and Discussions

A. Kinetic Measurements. For bond energy measurements temperature-dependent decays of the cluster ions, in He buffer gas were recorded, as described by eq 2. At higher buffer gas temperatures (>120 K), we observed a simple exponential decay of the stored parent ions as the internal energy of some of them comes close to the dissociation limit, and the collisions with the buffer gas atoms help to overcome this barrier. At lower temperatures (77−120 K), a part of the cluster ions are seen to fragment due to collisions with the buffer gas atoms when they enter the trap. The fragmentation, however, slows down after 20 ms of the storage (with a buffer gas pressure of $p_g = 8 \times 10^{-5}$ Torr) and the number of the detected parent ions gradually stabilizes. In the first 20 ms, the ions undergo about 200 collisions. It is therefore safe to assume that the ions are in thermal equilibrium with the buffer gas at this time. It also suggests that the time scale for the cluster ions to be completely equilibrated in internal (rotational and vibrational) modes is ∼20 ms.

As an example of the measurements done, we show in Figure 3a the exponential decay of $H^+(H_2O)_5$ (mass 91) in He buffer gas at 8 different trapping temperatures (T_t) in the range 190−240 K. The single exponential decays are indications that the
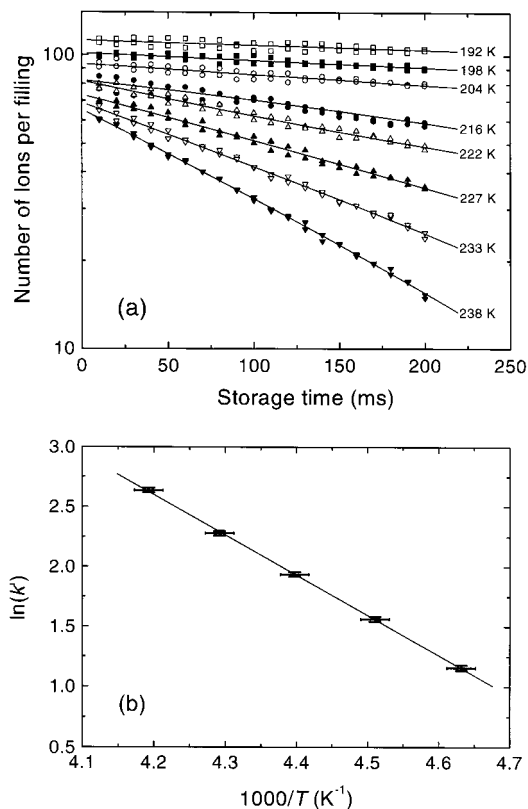
Figure 3. (a) Dissociation of $H^+(H_2O)_5$ in the temperature-variable 22-pole ion trap at various temperatures. (b) Dissociation rate constants of $H^+(H_2O)_5$ as a function of ion trap temperature. The linear line represents the best fit of the experimental data to the Arrhenius equation.

Figure 4. Dependence of the dissociation rate constants of (a) $H^+(H_2O)_n$, $n = 4-10$, and (b) $OH^-(H_2O)_m$, $m = 3-7$, on the ion trap temperature. The linear lines represent the best fits of the experimental data to the Arrhenius equation.

ensemble is in thermal equilibrium to a precision of about 1 K because otherwise the decays would be curved corresponding to a thermalization happening on the time scale of 200 ms. We began the trapping with around 100 cluster ions per filling, which may vary between 70 and 110, depending on the trapping conditions used (for example, different buffer gas temperatures and ion energies). Each data point in the figure consists of an average of 200 ion trap fillings. The multiple data points given for each temperature and storage time come from several iterations to check for the primary beam stability. Exponential fits to these curves give the pseudo-first-order rate constants ranging from $k' = 0.31$ s^{-1} for $T_t = 192$ K to $k' = 7.21$ s^{-1} for $T_t = 238$ K. The statistical errors obtained from the fits, as shown in Figure 3b, are around 1% for the faster decays but become much larger (approximately 20%, not shown) for the slower decays at lower temperatures ($T_t < 200$ K). Such obtained temperature-dependent rate constants follow the well-known Arrhenius relation, $k' = A \exp(-E_a/k_B T)$, where

$$E_a = -k_B \frac{\partial \ln(k')}{\partial(1/T)} \qquad (6)$$

is given as the linear slope in Figures 3b and 4a.

In making these plots, we have taken into account the change of the buffer gas number density n_t with trap temperature as explained in eq 4. To limit the temperature range for later analysis, we considered only the ~5 highest temperature points and made a fit weighted by experimental errors. Another reason to consider only these points is that the residual reactive loss of the water cluster ions (with a rate constant of ~0.1 s^{-1}) due to contaminants in the vacuum chamber influences less the
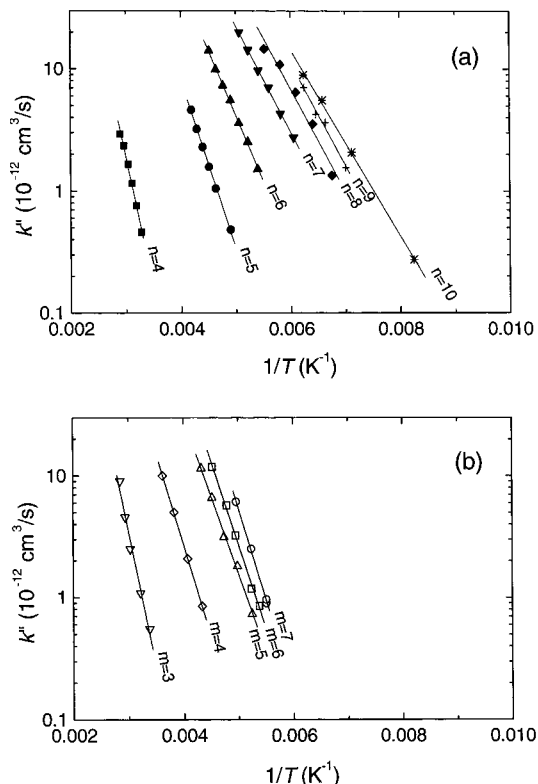
measurements involving faster decays (or a larger k'). From the fit in Figure 3b, we obtain a slope of $-(3407 \pm 50)$ in units of Kelvin, which corresponds to an activation energy of $E_a = 6.8 \pm 0.1$ kcal mol^{-1} for the $H^+(H_2O)_5$ cluster ion.

From eq 6, we see that it is not important for the determination of E_a to know the exact pressure of He in the 22-pole trap. Rather, it is the temperature dependence of k' that matters, because the absolute number density n_t finally cancels out when taking the logarithm and the derivative of k' in relation 6. In this experiment, we were working in (or very near to) the low-pressure limit, where the pseudo-first-order rate constant k' is proportional to the He number density n_t. Tests for the linearity $k' = k'' n_t$, where k'' is the second-order rate constant, have been made independently by varying the pressures. With twice the pressure, for example, a factor of 2 increase in k' was indeed observed. This gives us the magnitude of the k'' to be around 1×10^{-12} cm^3 s^{-1} (cf. Figure 4), but we should allow for an uncertainty factor of 2 for the result because of the limited accuracy of the ion gauge in the He pressure measurements.

To obtain the cluster bond energy, or the cluster dissociation energy E_{diss}, from the kinetics measurements as described above, we use the relation[29,34]

$$E_{diss} = E_a + \langle E_{vib} \rangle + a k_B T_m \qquad (7)$$

which applies to the special case of weak collisions and low pressures; that is, the change of internal energy by one collision is small compared to the total mean internal energy $\langle E_{vib} \rangle$, and if one collision lifts the ionic cluster over the dissociation threshold E_{diss}, it decays faster than the next collision can take place. The correction term $a k_B T_m$ in this relation accounts for

the average energy transferred from the He bath to those clusters sitting just below their dissociation limit and irreversibly lifted over the dissociation barrier by collisions with the He atoms. The temperature dependence of the factors such as the rate coefficient for collision with buffer gas and the collision efficiency are included in this term.[34] Lovejoy and Bianco[29] have carefully examined this term for a variety of (small) cluster ions and found the value of the parameter a may vary from -1 to $+3$, depending on the ionic species, cluster size and experimental conditions.

Theoretical evaluation of $\langle E_{vib} \rangle$ is based on the vibrational frequencies provided by the B3LYP/6-31+G* level of computation. We calculate the internal energies $\langle E_{vib} \rangle$ at the median temperature (T_m) of the temperature range of the ion decay measurements. Continuing with $H^+(H_2O)_5$ as the example, this would be $T_m = 227$ K and the calculated vibrational energy is $\langle E_{vib} \rangle = 4.6$ kcal mol^{-1} for the isomer **HW5I**, which is the only species identified in our previous spectroscopic experiments (cf. Table 1). For the correction term ak_BT_m, Lovejoy and Bianco[29] have suggested two average values, $a = 1.2$ and 1.8, obtained respectively from the harmonic and free rotor treatments for the torsional motions of the clusters. These two numbers give an average difference of $\sim$1 kcal mol^{-1} between the predicted and the literature values of E_{diss} in the temperature range 300$-$500 K. As in our case, except that of $H^+(H_2O)_4$ and $OH^-(H_2O)_3$, the ion trap is typically maintained at a temperature less than 250 K, and the contribution from this correction term to E_{diss} is significantly smaller. We therefore adopt $a = 1.5$ (assuming an error of 25%), namely, only taking into account the three external degrees of freedom of the free neutral water molecule as the first-order approximation in the present treatment.

With the values given above, we obtain a dissociation energy $E_{diss} = 12.1$ kcal mol^{-1} for $H^+(H_2O)_5$. The standard deviation deduced from the activation energy fit in Figure 3b is $\sim$0.1 kcal mol^{-1}, but we have some uncertainties in the determination of T_m, which in turn has a significant influence on the calculation of $\langle E_{vib} \rangle$. In addition to that, we have some uncertainties in the DFT computation of the vibrational frequencies (especially the lower-frequency modes, which are crucial in the temperature range considered here) and also the uncertainties for the coexistence of more than one isomer in the cluster production. A combination of all these factors makes precise determination of $\langle E_{vib} \rangle$ very difficult. So, we would rather assume our total error in the bond energy assessment to be of the order of 0.5 kcal mol^{-1} for this particular cluster ion, $H^+(H_2O)_5$.

For $H^+(H_2O)_n$ of $n = 6-8$, rather than to consider only the lowest energy isomer as in the cases of $n = 4$ and 5, we choose to take into account all isomers that have been identified in our previous experiments for the calculation of E_{diss}. The structures of these isomers for each cluster size are depicted in Figure 2c$-$e. There are seven possible isomers for $H^+(H_2O)_7$, for example, and we have taken the average value of $\langle E_{vib} \rangle$ for all of them in the calculation. As for the clusters with $n = 9$ and 10, identification of the structural isomers in a supersonic expansion has not yet been accomplished. A reasonable assumption to make is that their structures closely resemble those of $n = 7$ and 8, namely they contain only one or two five-membered rings rather than compact cages. It is clear that the calculation for the vibrational energies $\langle E_{vib} \rangle$ of larger clusters would become much less accurate because of the exponentially increasing manifold of possible isomers. We expect the total error in our bond energy assessment to be $\sim$1 kcal mol^{-1} for these high-mass clusters.

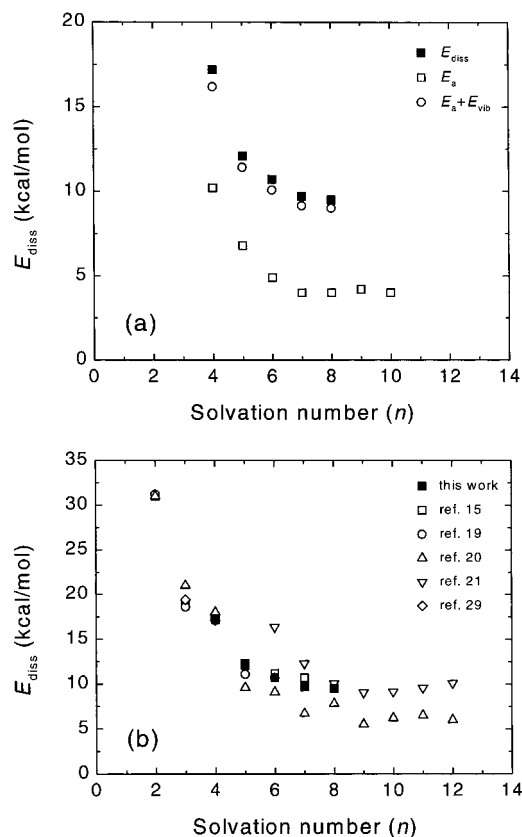**Figure 5.** (a) Variations of the measured dissociation energies and their components with the solvation number of $H^+(H_2O)_n$. (b) Comparison of the dissociation energies E_{diss} obtained in this work with literature values for $H^+(H_2O)_n$ at various n.

We summarize in Table 1 and Figure 5 the measured and the DFT-calculated components of E_{diss} for $H^+(H_2O)_n$ of $n = 4-10$. Figure 5a shows the dissociation energy E_{diss} as a sum of the activation energy E_a, the vibrational energy at the median temperature $\langle E_{vib} \rangle$, and the small correction term ak_BT_m. Going from the large to the small solvation number n, the dissociation energy for $H^+(H_2O)_n$ increases steadily, beginning in the regime of bulk water with an evaporation enthalpy of $\sim$10 kcal mol^{-1}.[35] At $n = 4$, the otherwise smooth sequence of the bond energies makes a noticeable jump. Such a jump is expected if we examine the structure of the most stable isomer for $H^+(H_2O)_4$, i.e., **HW4I**, which is symmetric and consists of a H_3O^+ core with three water molecules surrounding it. For this cluster isomer, the first solvation shell of H_3O^+ has been just filled, and all of the water molecules are predominantly bound to the central ion by strong charge$-$dipole interactions rather than hydrogen bonding as is the case for water molecules in the outer solvation shells. Hence, not surprisingly, it would take relatively more energy (17.2 $\pm$ 0.8 kcal mol^{-1}) to detach a water molecule from $H^+(H_2O)_4$. This shell filling effect has been observed in the earliest experiment of Kebarle and co-workers.[15]

In Table 1, we also include the results of $OH^-(H_2O)_{3-7}$ for comparison with literature values. The listed internal energies of $OH^-(H_2O)_{3-6}$ are averages of the $\langle E_{vib} \rangle$ of DFT-predicted low-energy isomers. We may give an uncertainty of around $\pm$1 kcal mol^{-1} for these values because of the lack of the knowledge of isomers that make contribution to our measurements.[23] Analogous to the case of $H^+(H_2O)_n$, the cluster bond energy of $OH^-(H_2O)_m$ shows a steady decrease from 16.2 kcal mol^{-1} of $m = 3$ to 11.5 kcal mol^{-1} of $m = 6$. However, unlike the cation counterparts, no distinct shell effect is detected for the hydroxide
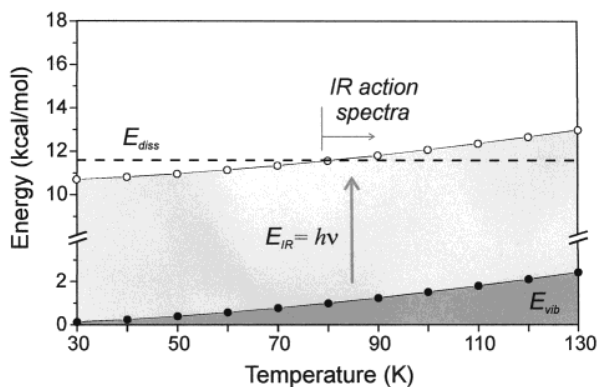
Figure 6. Energy diagram of isomer **HW6II** of the $H^+(H_2O)_6$ cluster. The E_{vib} area represents the DFT-calculated internal energies at different temperatures, E_{IR} is the average photon energy used in this work ($\sim$10.6 kcal mol^{-1}), and E_{diss} is the measured dissociation energy. The infrared action spectra are recorded at temperatures above 77 K.

ion, where filling of the first solvation shell is expected to complete at $m = 3$ for $OH^-(H_2O)_m$, according to Meot-Ner and Speller.[19]

A comparison of our results with other literature values[15,19,20,21,29] is shown in Figure 5b. However, to compare our measured bond energies E_{diss} with the bond enthalpies $\Delta H^0_{n-1,n}(T)$ as given in most publications from thermochemical measurements, we have to calculate the difference in total energies (i.e., translational, rotational, and vibrational energies) of the products and reactants for the dissociation [eq 2] at the given temperature T. Such a conversion based on theoretical heat capacities has been performed (see refs 36 and 37 for details of the calculation), although it is found that the difference between the bond enthalpy and the bond energy is small, typically less than 0.5 kcal mol^{-1}. As shown in Figure 5b, the agreement in E_{diss} among different measurements is very good (within 1 kcal mol^{-1}) except that of ref 20, where the reported bond energies are systematically too low, whereas the bond energies at $n = 6$ and 7 from ref 21 seem to be too high in comparison to ours and other measured values.

B. Spectroscopic Measurements. To obtain the infrared spectra of gas-phase cluster ions, one always requires an intense and stable precursor beam during the entire data-recording period (typically 4 h). For $H^+(H_2O)_n$, as determined by the expansion conditions of our ion source, the size distribution of the precursors in this experiment is often peaking at $n = 6$ and 7. We therefore started the spectroscopic measurement with the protonated water hexamer for the fundamental free-OH stretches over the frequency range 3620–3760 cm^{-1}. Because one quantum of the free-OH vibration corresponds to an energy of $E_{IR} \approx 10.6$ kcal mol^{-1}, which is typically less than the dissociation energy of $E_{diss} \approx 12$ kcal mol^{-1} for most of the cluster ions shown in Table 1, some internal energy must be required for the dehydration of cluster ions under low-temperature conditions when only single photons are absorbed by the individual ions during each trapping cycle. Figure 6 illustrates the correlations of the total vibrational energy $\langle E_{vib} \rangle$ and the ion temperature and the dissociation threshold of $H^+(H_2O)_n$ using the cluster isomer **HW6II** (Figure 2c) as an example.

We employ H_2, rather than He, as the buffer gas in the spectroscopic measurement. This is because the hydrogen molecule contains one internal degree of freedom, which makes it easier to accept the vibrational energies of the trapped ions than the helium atom in a cold environment. Moreover, hydrogen is lighter than helium and so collisional excitation of
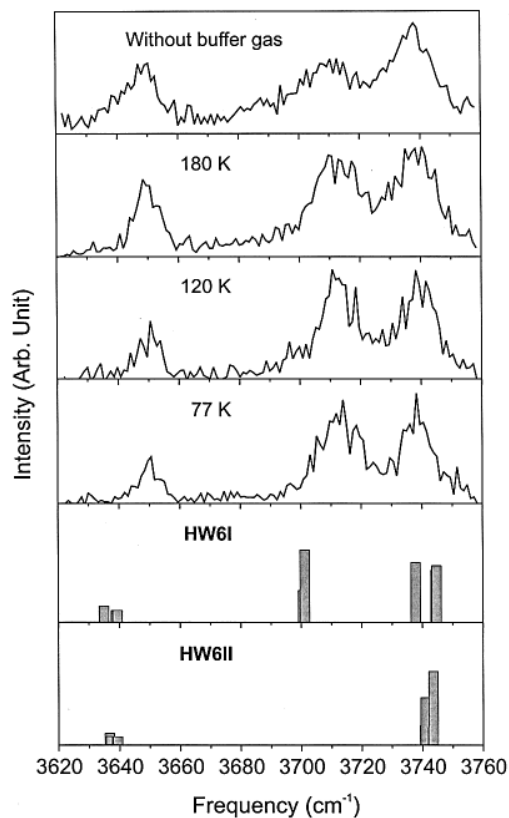

Figure 7. Temperature-dependent vibrational predissociation spectra of $H^+(H_2O)_6$ acquired at 77, 120, and 180 K in the free-OH stretch region. They are compared to the spectrum acquired without buffer gas in the trap held at room temperature. Shown at the bottom are the calculated stick spectra of two lowest-energy isomers, **HW6I** and **HW6II** (cf. Figure 2c).

the trapped species can be minimized. In this experiment, the cluster ions are typically confined in the ion trap for 10 ms before the laser excitation. With the buffer gas density of the order of $n_t \approx 10^{13}$ cm^{-3} as described earlier for He, more than 100 collisions occur between the trapped ion and the H_2 molecules. These stored cluster ions are therefore expected to thermalize with their surroundings before the spectroscopic measurements.

Figure 7 displays the infrared spectra of $H^+(H_2O)_6$ at 77–180 K in the free-OH stretching region. They are compared in parallel to the first spectrum (the topmost) acquired at room temperature without the buffer gas. The temperature of the cluster ions trapped under such collision-free conditions is roughly 200 K, as estimated from the measured metastable dissociation rates fitted to an evaporative ensemble model.[38,39] Notably, all of the spectra show 3 distinct features centered at $\nu_0 = 3740$, 3715, and 3650 cm^{-1}, corresponding respectively to the asymmetric, the 2-coordinated, and the symmetric free-OH stretches of the water molecules in either the first solvation shell or the second solvation shell of the H_3O^+ or $H_5O_2^+$ ion core.[18] The full widths at half-maximum (fwhm) of these three absorption bands are all larger than 15 cm^{-1}, but they decrease significantly when H_2 is introduced into the storage cell. An average reduction factor of 1.7 is found for the spectrum acquired at 200 K compared to that at 77 K. Table 2 lists the spectral assignment, vibrational frequencies, and bandwidths of the individual peaks observed at three different bath temperatures in comparison to those obtained at room temperature without H_2 buffer gas.

TABLE 2: Comparison of the Observed Band Centers and Widths (cm^{-1}) at Various Ion Trap Temperatures (K)[a]

	s-OH$_2$ stretch		f-OH stretch		a-OH$_2$ stretch	
temp.	ν_0	fwhm	ν_0	fwhm	ν_0	fwhm
77	3650.5	8.0	3713.0	15.6	3739.3	11.7
120	3650.2	8.8	3712.0	16.3	3738.8	13.7
180	3649.7	10.8	3711.1	19.4	3738.6	14.6
~200	3648.3	17.0	3710.5	25.0	3739.2	15.3

(without buffer gas)

[a] The notations s-OH$_2$ and a-OH$_2$ stand respectively for the symmetric and asymmetric stretches of H_2O acting as a single-proton acceptor, and the f-OH stands for the free-OH stretch of 2-coordinated H_2O acting as a single-proton donor and single-proton acceptor (cf. Figure 1).

Shown at the bottom of Figure 7 are the DFT-calculated stick diagrams of two isomers (**HW6I** and **HW6II**) for comparison with the experimental spectra. These two isomers are the lowest in energy among all stable structures of $H^+(H_2O)_6$ and are centered by the H_3O^+ and the $H_5O_2^+$ entity, respectively (cf. Figure 2). Identification of them has been successful in a corona-discharged supersonic expansion in our previous experiment.[18] Because the source condition used by this new spectrometer is similar to that of the room-temperature 8-pole ion trap apparatus used in ref 18, we expect that these two chainlike isomers exist in the present 22-pole ion trap mass spectrometer as well.

We note that in Figure 7 the shifts of the spectral band centers with temperature are not significant enough (<1 cm^{-1}) to lead to any conclusive remarks. In comparison, the cooling effect can be seen more readily in the change of the widths of the absorption bands. As listed in Table 2, the fwhm of the absorptions decreases roughly by factors of 1.2 and 1.1, respectively, as the bath temperature is lowered consecutively from 180 to 120 K and from 120 to 77 K. Overall, the fwhm decreases by a factor of roughly 1.3 across a temperature change range of $\Delta T = -113$ K. Such a bandwidth reduction is smaller than we expected because an fwhm of less than 10 cm^{-1} has already been observed for these bands at an estimated cluster temperature of ~140 K under collision-free conditions.[18] We attribute this unsatisfactory result to inefficient cooling of the internal rotations of the solvent water molecules attached to the H_3O^+ or $H_5O_2^+$ ion core.

The internal rotation within an ionic cluster was first observed by Price et al.[40] for $H^+(NH_3)_n$ generated by a supersonic expansion and stored in an empty octopole ion trap. From the rotation−vibration transitions resulting from a rotation of the NH$_3$ subgroups about its local C_3 axis, they estimated a **J** rotational temperature of ~20 K and a **K** rotational temperature of ~45 K for these jet-cooled cluster ions. We have previously also observed the subbands of the asymmetric free-OH stretch transitions due to the nearly free internal rotation of H_2O attached to the NH_4^+ core in $NH_4^+(H_2O)_n$.[41] These subbands have a characteristic spacing of 55 cm^{-1}, roughly twice the **A** rotational constant of H_2O along its C_2 axis, suggesting a **K** rotational temperature of ~50 K. Such free internal rotations clearly would play a significant role in band broadening when the cluster temperature is not sufficiently low. In this experiment, with the use of buffer gas, the rotational and vibrational temperatures are both thermalized to the bath temperature owing to the collisions. In a 77 K bath for example, the vibrational temperature of the cluster ions produced from the supersonic expansion is effectively lowered from ~200 to 77 K, but unfortunately, their rotational temperature is raised from ~50 to 77 K. In this aspect, it thus comes of little surprise that the bandwidths of these OH stretch transitions could be broadened to more than 10 cm^{-1} due to coupling of the high-frequency

vibrations with the thermally excited internal rotations, as observed experimentally.

Conclusions

We have shown that collisional cooling of protonated water clusters [$H^+(H_2O)_n$] and deprotonated water clusters [$OH^-(H_2O)_m$] can be achieved with chemically inert buffer gas (either He or H_2) in a temperature-variable 22-pole ion trap. Using this device has enabled us to conduct infrared spectroscopy as well as dehydration energy measurements under well defined conditions in the temperature range between 77 and 350 K for both positively and negatively charged cluster ions. In this work, we have determined the first dehydration energies of the water cluster ions from the dissociation activation energies measured in experiments and the internal energies provided by theoretical calculations. The results are in good agreement with literature values. For $H^+(H_2O)_n$, the cluster bond energy is determined to decrease smoothly from ~17 kcal mol^{-1} of $n = 4$ to ~9 kcal mol^{-1} of $n = 8$, and no distinct shell effects have been detected for the second solvation shell formation. In the spectroscopic measurements, we obtain vibrational predissociation spectra of $H^+(H_2O)_6$ in the free-OH stretch region at an equilibrium cluster temperature of 77 K. Significant reduction in the absorption bandwidths (up to a factor of 2) is observed when cooling the cluster ion from 200 to 77 K. It corroborates the suggestion that the combination of a temperature-variable 22-pole ion trap with infrared lasers is a promising approach for the study of structural transformation (induced either by laser excitation or by temperature change) of cluster ions.

The present work, together with previous experiments conducted for laser-induced reactions of molecular ions[42] in the Chemnitz group, demonstrates the versatility and utility of this unique trapping device. Future work of this collaboration includes in situ growth and fragmentation[43] as well as collision-induced isomerization and deuteration[44] of water cluster ions in the temperature-variable ion trap in a precisely controlled manner.

References and Notes

(1) Gerlich, D.; Horning, S. *Chem. Rev.* **1992**, *92*, 1509.
(2) Duncan, M. A. *Int. J. Mass Spectrom.* **2000**, *200*, 545.
(3) See, for example: Searcy, J. Q.; Fenn, J. B. *J. Chem. Phys.* **1974**, *61*, 5282.
(4) See, for example: Robertson, W. H.; Kelley, J. A.; Johnson, M. A. *Rev. Sci. Instrum.* **2000**, *71*, 4432.
(5) See, for example: Li, G.-Z.; Guan, S.; Marshall, A. G. *J. Am. Soc. Mass Spectrom.* **1997**, *8*, 793.
(6) See, for example: Schiffer, J. P.; Drewsen, M.; Hangst, J. S.; Hornekær, L. *Proc. Natl. Acad. Sci. U.S.A.* **2000**, *97*, 10697.
(7) Gerlich, D. *Adv. Chem. Phys.* **1992**, *82*, 1.
(8) Gerlich, D. *J. Chem. Soc., Faraday Soc.* **1993**, *89*, 2199.
(9) Gerlich, D. *Phys. Scripta* **1995**, *T59*, 256.
(10) Paul, W.; Lücke, B.; Schlemmer, S.; Gerlich, D. *Int. J. Mass Spectrom. Ion Processes* **1995**, *150*, 373. Paul, W.; Schlemmer, S.; Lücke, B.; Gerlich, D. *Chem. Phys.* **1996**, *209*, 265.
(11) Duley, W. W. *Astrophys. J.* **1996**, *471*, L57.
(12) Wayne, R. P. *Chemistry of Atmospheres*; Oxford University Press: Oxford, U.K., 1991.
(13) Fredericks, S. Y.; Jordan, K. D. *Mol. Phys.* **1997**, *92*, 445.
(14) Hunter, E. P. L.; Lias, S. G. *J. Phys. Chem. Ref. Data* **1998**, *27*, 413.

(15) Cunningham, A. J.; Payzant, J. D.; Kebarle, P. *J. Am. Chem. Soc.* **1972**, *94*, 7627. Lau, Y. K.; Ikuta, S.; Kebarle, P. *J. Am. Chem. Soc.* **1982**, *104*, 1462.

(16) Yeh, L. I.-C.; Okumura, M.; Myers, J. D.; Price, J. M.; Lee, Y. T. *J. Chem. Phys.* **1989**, *91*, 7319.

(17) Crofton, M. W.; Price, J. M.; Lee, Y. T. In *Clusters of Atoms and Molecules*; Haberland, H., Ed.; Springer-Verlag: Berlin, 1994; Vol. II, p 44. Price, J. M. Ph.D. Thesis, University of California at Berkeley, 1990.

(18) Jiang, J. C.; Wang, Y.-S.; Chang, H.-C.; Lin, S. H.; Lee, Y. T.; Niedner-Schatteburg, G.; Chang, H.-C. *J. Am. Chem. Soc.* **2000**, *122*, 1398.

(19) Meot-Ner, M.; Speller, C. V. *J. Phys. Chem.* **1986**, *90*, 6616.

(20) Magnera, T. F.; David, D. E.; Michl, J. *Chem. Phys. Lett.* **1991**, *182*, 363.

(21) Shi, Z.; Ford, J. V.; Wei, S.; Castleman, A. W. *J. Chem. Phys.* **1993**, *99*, 8009.

(22) Schindler, T.; Berg, Ch.; Niedner-Schatteburg, G.; Bondebey, V. E. *Chem. Phys. Lett.* **1996**, *250*, 301.

(23) Chaudhuri, C.; Wang, Y.-S.; Jiang, J. C.; Lee, Y. T.; Chang, H.-C.; Niedner-Schatteburg, G. *Mol. Phys.* **2001**, *99*, 1161.

(24) Tuckerman, M.; Lassonen, K.; Sprik, M.; Parrinello, M. *J. Phys. Chem.* **1995**, *99*, 5749. Tuckerman, M.; Lassonen, K.; Sprik, M.; Parrinello, M. *J. Chem. Phys.* **1995**, *103*, 150.

(25) Wales, D. J. *J. Chem. Phys.* **1999**, *110*, 10403. Wales, D. J. *J. Chem. Phys.* **1999**, *111*, 8429.

(26) Singer, S. J.; McDonald, S.; Ojamäe, L. *J. Chem. Phys.* **2000**, *112*, 710.

(27) Xantheas, S. S. *J. Am. Chem. Soc.* **1995**, *117*, 10373.

(28) Novoa, J. J.; Mota, F.; del Valle, C. P.; Planas, M. *J. Phys. Chem. A* **1997**, *101*, 7842.

(29) Lovejoy, E. R.; Bianco, R. *J. Phys. Chem. A* **2000**, *104*, 10280.

(30) Zemansky, M. W. *Heat and Thermodynamics*, 5th ed.; McGraw-Hill: New York, 1968; p 438.

(31) Jones, R. M.; Gerlich, D.; Anderson, S. L. *Rev. Sci. Instrum.* **1997**, *68*, 3357.

(32) Frisch, M. J.; Trucks, G. W.; Schlegel, H. B.; Scuseria, G. E.; Robb, M. A.; Cheeseman, J. R.; Zakrzewski, V. G.; Montgomery, J. A., Jr.; Stratmann, R. E.; Burant, J. C.; Dapprich, S.; Millam, J. M.; Daniels, A. D.; Kudin, K. N.; Strain, M. C.; Farkas, O.; Tomasi, J.; Barone, V.; Cossi, M.; Cammi, R.; Mennucci, B.; Pomelli, C.; Adamo, C.; Clifford, S.; Ochterski, J.; Petersson, G. A.; Ayala, P. Y.; Cui, Q.; Morokuma, K.; Malick, D. K.; Rabuck, A. D.; Raghavachari, K.; Foresman, J. B.; Cioslowski, J.; Ortiz, J. V.; Stefanov, B. B.; Liu, G.; Liashenko, A.; Piskorz, P.; Komaromi, I.; Gomperts, R.; Martin, R. L.; Fox, D. J.; Keith, T.; Al-Laham, M. A.; Peng, C. Y.; Nanayakkara, A.; Gonzalez, C.; Challacombe, M.; Gill, P. M. W.; Johnson, B. G.; Chen, W.; Wong, M. W.; Andres, J. L.; Head-Gordon, M.; Replogle, E. S.; Pople, J. A. *Gaussian 98*, revision A.5; Gaussian, Inc.: Pittsburgh, PA, 1998.

(33) Wang, Y.-S.; Jiang, J. C.; Cheng, C.-L.; Lin, S. H.; Lee, Y. T.; Chang, H.-C. *J. Chem. Phys.* **1997**, *107*, 9695. Chang, H.-C.; Wang, Y.-S.; Lee, Y. T.; Chang, H.-C. *Int. J. Mass Spectrom.* **1998**, *179/180*, 91.

(34) Troe, J. *J. Chem. Phys.* **1977**, *66*, 4745. Troe, J. *J. Chem. Phys.* **1977**, *66*, 4758.

(35) Lide, D. R. *CRC Handbook of Chemistry and Physics*, 76th ed.; CRC Press: Boca Raton, FL, 1995; pp 6−10.

(36) Keesee, R. G.; Castleman, A. W. *J. Phys. Chem. Ref. Data* **1986**, *15*, 1016.

(37) Ochterski, J. W. download of whitepaper from www.Gaussian.com, 2000.

(38) Klots, C. E. *J. Chem. Phys.* **1985**, *83*, 5854. Klots, C. E. *Z. Phys. D* **1991**, *20*, 105.

(39) Dunbar, R. C. *J. Phys. Chem.* **1994**, *98*, 8705.

(40) Price, J. M.; Crofton, M. W.; Lee, Y. T. *J. Chem. Phys.* **1989**, *91*, 2749. Price, J. M.; Crofton, M. W.; Lee, Y. T. *J. Phys. Chem.* **1991**, *95*, 2182.

(41) Wang, Y.-S.; Chang, H.-C.; Jiang, J. C.; Lin, S. H.; Lee, Y. T.; Chang, H.-C. *J. Am. Chem. Soc.* **1998**, *120*, 8777.

(42) Schlemmer, S.; Kuhn, T.; Lescop, E.; Gerlich, D. *Int. J. Mass Spectrom.* **1999**, *187*, 589. Schlemmer, S.; Lescop, E.; von Richthofen, J.; Gerlich, D.; Smith, M. A. *J. Chem. Phys.* **2002**, *117*, 2068.

(43) Schlemmer, S.; Luca, A.; Glosik, J.; Gerlich, D. *J. Chem. Phys.* **2002**, *116*, 4508.

(44) Yamaguchi, S.; Kudoh, S.; Okada, Y.; Orii, T.; Takeuchi, K. *Chem. Phys. Lett.* **2002**, *359*, 480.

Appendix B

Variable temperature ion trap studies of $CH_4^+ + H_2$, HD and D_2: negative temperature dependence and significant isotope effect

O. Asvany, I. Savić, S. Schlemmer, D. Gerlich

ELSEVIER

Variable temperature ion trap studies of $CH_4^+ + H_2$, HD and D_2: negative temperature dependence and significant isotope effect

O. Asvany, I. Savić, S. Schlemmer, D. Gerlich *

Department of Physics, Technische Universität Chemnitz, 09126 Chemnitz, Germany

Abstract

Reactions of methane cations, CH_4^+, with H_2, HD and D_2 have been studied in a variable temperature 22-pole ion trap from room temperature down to 15 K. The formation of CH_5^+ in collisions with H_2 is slow at 300 K, but it becomes faster by at least one order of magnitude when the temperature is lowered to 15 K. This behavior is tentatively explained with a longer complex lifetime at low temperatures. However, since tunneling is most probably not responsible for product formation, other dynamical or statistical restrictions must be responsible for the negative temperature dependence. In collisions of CH_4^+ with HD, the CH_5^+ product ion (68% at 15 K) prevails over CH_4D^+ (32%). Reaction of CH_4^+ with D_2 is found to be much slower than with H_2 or HD. The rate coefficient for converting CH_4^+ into CH_3D^+ by H–D exchange has been determined to be smaller than 10^{-12} cm^3/s, indicating that scrambling in the CH_6^+ complex is very unlikely.
© 2003 Published by Elsevier B.V.

Keywords: Laboratory astrochemistry; Reactive collisions; Deuteration; ISM: molecules; CH_4^+; CH_5^+; CH_4D^+

1. Introduction

Collisions at very low relative velocities and with cold reactants are of fundamental interest because they can be used as a very sensitive probe of the potential energy surfaces, especially if weak barriers or small endothermicities are involved or if dynamical constraints hinder the transition from reactants to products. In addition, experimental studies of ion molecule reactions performed at the low temperatures prevailing in dense interstellar clouds are of key importance for understanding the synthesis of molecular species in interstellar space. Rate coefficients are especially needed if they change significantly as a function of temperature, in contrast to the majority of the known reactions.

One of the best understood examples where the reactivity changes remarkably with temperature is the hydrogen abstraction $NH_3^+ + H_2 \rightarrow NH_4^+ + H$. This reaction has been measured by several groups and using complementary techniques, e.g., in a flowing afterglow

apparatus (FA) between 300 and 800 K [1], in a SIFT apparatus between 80 and 300 K [2], in a Penning trap at very low temperatures (11–20 K) [3], in a SIDT between 20 and 300 K [4], and finally in a 22-pole ion trap at 15 K [5]. In the early measurements starting from room temperature it was observed, that the rate coefficient falls with falling temperature. Later a minimum has been identified at about 150 K and, finally, a significant reincrease was found towards very low temperatures. Furthermore, measurements with isotopic variants of the ammonia ion reaction by Kim et al. [6], Adams and Smith [7] and Dunn and Barlow [8] showed a pronounced isotopic effect, i.e., the rate coefficient of the reaction of NH_3^+ with D_2 is lower than that with H_2 while the reaction of ND_3^+ with H_2 has a larger rate coefficient than $NH_3^+ + H_2$. Calculations by Herbst and co-workers [9], using a statistical phase space approach, confirmed the former hypothesis [3,4] that, at low temperatures, the mechanism of $NH_4^+ + H$ formation is dominated by the initial formation of a long-lived complex, from which tunneling through a small transition state barrier occurs. For high enough temperatures, on the other side, the reaction rate increases due to the

* Corresponding author. Fax: +49-371-531-3103.
E-mail address: gerlich@physik.tu-chemnitz.de (D. Gerlich).

increasing probability of classical passage over the transition state barrier.

Some related observations have been made for the isoelectronic reaction, the hydrogen abstraction

$$CH_4^+ + H_2 \rightarrow CH_5^+ + H \qquad (1)$$
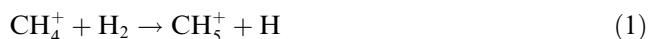
however, only at room temperature and above. This interaction of methane cations with hydrogen has been observed several decades ago in a mass spectrometer by Munson et al. [10]. An absolute rate coefficient was first measured by Kim et al. [6] in a 300 K Ion Cyclotron Resonance (ICR) apparatus. This result and also the measurements of Adams and Smith [11] performed in a room temperature Selected Ion Flow Tube (SIFT) showed that reaction (1) is very slow at room temperature despite the fact that the H atom transfer is slightly exothermic. Only every 50th collision leads to a CH_5^+ product indicating some hindrance along the reaction pathway, perhaps a potential barrier. The first dedicated energy-dependent investigations were performed by Federer et al. [12] who measured rate coefficients at energies between 40 and 120 meV, accelerating the ions in a Selected Ion Flow Drift Tube (SIFDT). They found that the rate coefficients decrease with increasing energy. The results presented in this paper, extend the measurements into the opposite direction. In accordance with the trend, the rate coefficients for the title reaction continue to increase with falling temperature. The value at interstellar temperatures is one order of magnitude larger than at room temperature. In contrast, the UMIST database for interstellar chemistry [13] contains a fixed value for reaction (1) which is claimed to be valid for a wide temperature range.

Federer et al. also studied the reverse of reaction (1), $CH_5^+ + H \rightarrow CH_4^+ + H_2$, by injecting H-atoms into the drift tube. In this case, it was observed that, at room temperature, destruction of CH_5^+ is almost 10 times faster than its formation, although the reaction is endothermic in this direction. The experimental findings have been taken as a hint that reaction (1) must be endoentropic, i.e., the free energy $\Delta G = \Delta H - T\Delta S$ must become negative above a certain value of T. This temperature has been estimated to be 150 K [12]. The question whether one is allowed to use simple thermodynamics for describing a bimolecular reaction will be raised in the discussion section. So far, the backward reaction has not been measured below 300 K.

More insight into the energetics of a near-thermoneutral reaction can be obtained by using isotope substitution due to significant shifts in zero-point energies. In addition the replacement of H by D can modify remarkably the statistical factors, governing the reaction [14]. Up to now only the combination $CH_4 + D_2$ has been reported in the literature by Inoue and Wexler [15] as well as Munson [10] who observed very low reaction rates. It must be noted, however, that their low values

may have partly been caused by the non-thermal experimental conditions prevailing in their machines. In the present contribution not only D_2 but also the astrochemically important HD has been used as target.

One interesting additional aspect of this work is that reaction (1) leads to CH_5^+, a so-called hypercoordinated carbocation (see [16] and references therein). Despite many spectroscopic efforts culminating in the high-resolution infrared spectrum of White et al. [17] the structure of this fluxional molecular ion is an object of an ongoing debate since the spectrum is still awaiting an assignment. One of the basic questions is, whether all five hydrogen atoms are equivalent or whether the three-center-two-electron bound favors a different structure, e.g., a separate H_2 sub-unit bound to a CH_3^+ ion. If there are different bounds, isotope labeling leads to different isomers which may be distinguished via chemical probing. Such an approach has been described in [18] where CH_4 and CD_4 gas has been used to form different isotopomers of $CH_xD_y^+$ and NH_3 has been used as a probing gas (see also [19]). From these experiments, which have been performed at temperatures above 300 K, rather speculative conclusions have been drawn. Unfortunately, the present work, dealing with cold $(CH_4 \cdot H_2)^+$ and $(CH_5 \cdot H)^+$ collision complexes, does not provides help to solve this puzzle; however, as briefly outlined in the conclusion, more can be expected from a dedicated research of forming CH_5^+ via radiative association of $CH_3^+ + H_2$ and isotopic variants or from probing CH_5^+ via scrambling collisions with D or HD, especially at low temperatures.

2. Experimental

2.1. Basics of experiment

The laboratory measurements have been performed in a variable temperature 22-pole ion trap machine. The basics of the trapping technique are summarized in [20], more details can be found in recent publications [21,22]. In brief, ions generated in a storage ion source, are mass selected and injected into a 22-pole ion trap mounted onto a closed cycle He refrigerator. Trapping of the ions in radial direction is achieved by applying two opposite phases of an rf generator (80 V, 17 MHz) to the 2×11 poles of the trap, while confinement in longitudinal direction and control of the ion storage time is done by pulsing the entrance and exit electrodes. The wide field-free region of the 22-pole trap makes experiments at low collision temperatures possible. Reactant and buffer gases are introduced by cooled tubes and are in thermal equilibrium with the cold walls surrounding the trap. The translational and internal degrees of freedom of the ions are coupled to this environment by inelastic collisions with continuously or pulsed introduced buffer gas

or via radiation. In the present configuration, the lowest temperature achieved was about 15 K, higher temperatures are attained with heater wires winded around the trap holder. Temperatures are measured at several points with carbon resistors. Stored ions react with target gas (here hydrogen) the number density of which is determined with an ion gauge which is routinely calibrated with respect to a spinning rotor gauge. After each trapping cycle, primary and product ions are extracted, analyzed by a second quadrupole mass filter and finally detected with high efficiency by a Daly-type detector.

2.2. Ion preparation and mass selection

The CH_4^+ ions are produced by electron bombardment of methane gas (Messer-Griesheim 5.5 purity) in an external rf storage ion source. Trapping the ions in the source makes it possible to operate at pressures below 10^{-5} mbar of methane. For pre-cooling the stored ions to the source temperature of about 350 K, helium gas is added to the source gas. Furthermore, electrons with low kinetic energies (<18 eV) are utilized to reduce internal excitation or fragmentation of the ions. After extracting the ions through a pulsed electrode, they are mass selected by a quadrupole operated either in the low-pass or in the mass-selective mode. The low-pass mode has the advantage of injecting ions with well defined very low kinetic energies into the 22-pole trap; however, at the expense of admitting also some lower mass ions to the trap. The mass-selective mode fully suppresses the unwanted ions but in this case with a broader kinetic energy distribution. As mentioned above, all ions are finally cooled to the desired low temperatures by a short intense He pulse ($\sim$10 ms) in the trap.

2.3. Target gas

The purity of the deuterium hydride (Cambridge Isotope Laboratories Inc.) is specified to be 97%, the major contamination being H_2 and D_2. This specification has been confirmed in situ by a detailed analysis based on the $Ar^+ + HD$ charge transfer reaction in the trap [23]. Ar^+ is known to react with HD mostly to ArH^+ and ArD^+, but about 10% of the reaction yields HD^+ by charge transfer. Assuming equal charge transfer probabilities for the various hydrogen isotopes, the H_2 impurity can be derived directly from a comparison of the H_2^+ and the HD^+ product signal. In this way, it was confirmed that the H_2-content in the bottle was less than 1%. Direct determination of the D_2 impurity is not so simple with this method, because the signal of interest (mass 4) coincides with other products from secondary reactions, for instance with H_2D^+ from a reaction of ArH^+ with HD. Nonetheless, it could be concluded that

D_2 has the same abundance as H_2, i.e., the total impurity is less than 2%.

Another chemical test of the isotopic purity of the HD target gas was based on the observation of products, formed via specific association reactions ([23]). For example, hydrocarbon ions which do not react with HD or which are already at the end of a deuteration sequence only can grow via such a process. For example, association of CD_3^+ with HD yields CHD_4^+ while a collision with H_2 and D_2 impurities produces $CH_2D_3^+$ and CD_5^+ ions, visible as "side-bands" of the central peak in the mass spectrum. Also this method has lead to an upper limit of 2% for the impurities, assuming equal association probabilities.

The H_2 and D_2 gases used in these experiments were purchased from Messer–Griesheim with specified purity of 6.0 and 2.7, respectively.

2.4. Measuring procedure

The measurement of rate coefficients for chemical reactions are performed in the trap in an iterative mode. First, a pulsed bunch of ions is injected with low kinetic energies into the 22-pole trap. The ions are then stored for times varying from microseconds to minutes, the main limitation being the residual gas components which deplete the number of primary ions due to parasitic reactions. In the present case, the unwanted residual gas components are mostly hydrogen and water. At
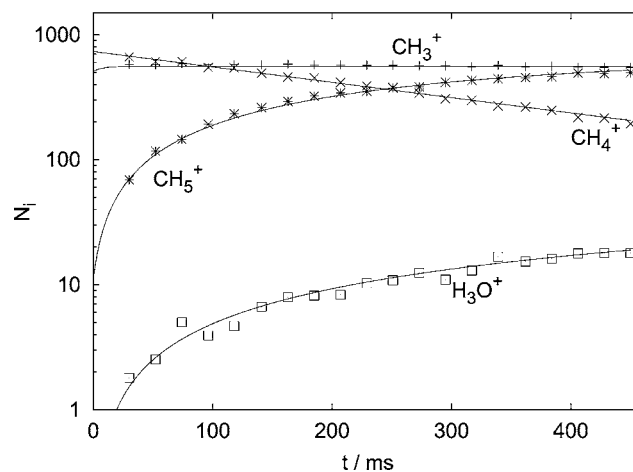
Fig. 1. The number of molecular ions, N_i, trapped and formed for each iteration, is plotted as a function of the storage time t. Twenty different times ranging from 30 to 450 ms were used. Every data point was measured 15 times to obtain better statistics. After injection, primary ions are relaxed to the ambient temperature by using an intense pulse of He buffer gas. In this example, a mixture of both CH_3^+ and CH_4^+ has been used. While the first ion remains almost unchanged, the second one reacts with hydrogen, $[H_2] = 7.4 \times 10^{10}$ cm^{-3}, to CH_5^+. At the temperature of this measurement (300 K), there are minor losses due to reactions with H_2O background gas leading to H_3O^+ products. The solid lines are solutions of an adequate rate equation system leading to a set of rate coefficients (see Table 2).

room temperature, for example, the water number density was in the range of $[H_2O] = 1 \times 10^7$ cm^{-3}. At cryogenic temperatures, this number is much lower, at least by 2 orders of magnitude.

Typically, only a few hundred parent ions are trapped per pulse in order to avoid saturation of the Daly detector. For improving the statistics and for determining the rates of the investigated reactions with good precision, the procedure *ion formation/trapping* and *reaction/ analysis* is repeated often (about 20 times) for typically 20 different storage times and for each of the masses of interest. This is further explained with the example of Fig. 1. In this 300 K experiment, about 700 CH_4^+ ions are injected per pulse into the trap filled with hydrogen at a number density of $[H_2] = 7.4 \times 10^{10}$ cm^{-3}. As the first mass filter was operated in the low-pass mode, in addition some 500 CH_3^+ ions were in the primary ion beam coming from the source. Also a few CH_2^+ were initially present; however, they quickly react to CH_3^+. These ions do not disturb this investigation, as they react extremely slow with H_2 at room temperature. The CH_4^+ ions are transformed via reaction (1) into CH_5^+. In addition, there are also a few H_3O^+ formed via proton transfer of stored ions to background water molecules.

The solid lines in Fig. 1 represent solutions of a set of coupled rate equations describing the formation and destruction of the corresponding ions. Initial conditions are the number of various ions at short storage times as well as the density of the neutral reactant gas and the background gas. The coupled differential equations are usually solved numerically with a set of assumed rate coefficients which are varied systematically until the agreement with the experimental data is satisfactory. The output of this procedure is a set of rate coefficients.

3. Results

3.1. Temperature dependence

With the methods outlined above and illustrated in Fig. 1, rate coefficients of reaction (1) have been determined for selected temperatures in the range from 15 to 300 K. Hydrogen number densities have been varied between 1×10^{10} and 1×10^{11} cm^{-3}. Typically, repetition periods between 500 ms and 1 s were chosen. The resulting rate coefficients are shown in Fig. 2 as a function of temperature. The errors for the rate coefficients are around 10% and are mainly due to uncertainties in determining the effective H_2 number density. The indicated errors in the measured temperatures are assumed to be 10 K for high temperatures and not more than 5 K in the low temperature range. Inspection of Fig. 2 reveals that the rate coefficient decreases by more than one order of magnitude from $(4.0 \pm 0.2) \times 10^{-10}$ cm^3/s at 15 K to $(3.3 \pm 0.2) \times 10^{-11}$ cm^3/s at room tem-
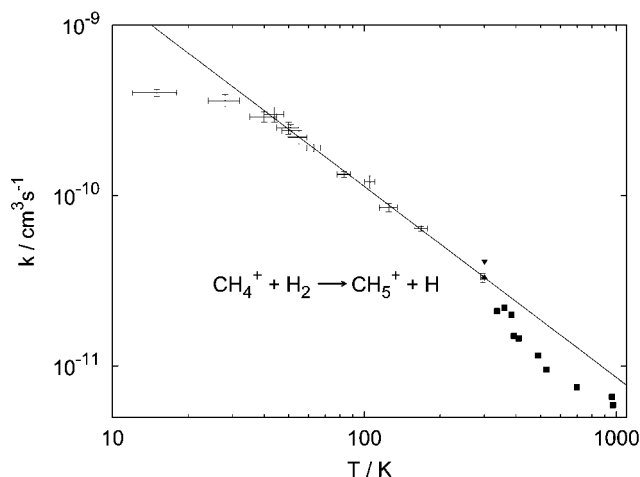

Fig. 2. Temperature-dependent rate coefficients for reaction (1). The results from this work (including error bars) cover the range from 15 to 300 K. These data have been fitted with $k(T) = \alpha(T/300)^\beta$ for $T > 50$ K, see also Table 1. The two additional points at 300 K are from [11] (▲) and [6] (▼). At higher energies results from a SIFDT experiment [12] are included (■). For details see text.

perature. The data have been fitted using the function $k = \alpha(T/300)^\beta \exp(-\gamma/T)$. This parameterization is commonly used for including experimental or theoretical results in reaction networks describing interstellar chemistry [13]. For the high temperature range, the parameter γ was set to zero while α and β were fitted (straight line in Fig. 2). For including the low temperature behavior, also γ was varied. The resulting best fit parameters are listed in Table 1.

At 300 K two earlier measured values are included as filled triangles in Fig. 2. The result of Adams and Smith [11] (upright triangle), $k = 3.3 \times 10^{-11}$ cm^3/s, is in excellent agreement with the present work. Kim et al. [6] have reported $k = 4.1 \times 10^{-11}$ cm^3/s. In addition, values from the SIFDT-measurements of Federer et al. [12] are shown in Fig. 2 as filled squares. For comparing these non-thermal results with the other ones, the mean kinetic energy of the drifting ions has been converted into an effective temperature T by using simply the relation $\langle E_{trans} \rangle = 3/2kT$. According to their data, the rate coefficient reaches a value of around 6.5×10^{-12} cm^3/s at an energy of 120 meV (corresponding to 960 K, see Fig. 2). Due to the well-known difficulties of comparing thermal rate coefficients with results from SIFDT ex-

Table 1
Temperature dependence of the rate coefficient, $k = \alpha(T/300)^\beta \exp(-\gamma/T)$

Reaction	α (10^{-11} cm^3/s)	β	γ (K)	Temperature range (K)
$CH_4^+ + H_2 \rightarrow CH_5^+ + H$	3.3	−1.12	0	50–300
	3.4	−1.35	23	15–300

The indicated temperature ranges were fitted.

periments, the deviation of the high temperature data from the low temperature fit should not be over-interpreted. In any case, however, these data demonstrate that the rate coefficient is still decreasing with increasing kinetic and internal energies, which are equivalent to temperatures of about 1000 K.

3.2. Formation of CH_4D^+ in collisions with HD

Rate coefficients with a negative temperature dependence have also been measured for reactions of CH_4^+ with HD and D_2 at temperatures between 300 and 15 K. Table 2 compiles the results for collisions with H_2, HD and D_2. Also for the deuterated reactants the rate coefficients drop by at least one order of magnitude between 15 and 300 K. To get a deeper insight into the underlying reaction dynamics, the two separated product channels for collisions with HD,

$$CH_4^+ + HD \rightarrow CH_4D^+ + H \qquad (2a)$$
$$\rightarrow CH_5^+ + D \qquad (2b)$$

Table 2
Rate coefficients (in units of 10^{-11} cm^3/s) and branching fraction for reactions with H_2, HD and D_2

T (K)	H_2	HD		D_2
	k	k	CH_5^+ fraction (%)	K
15	40 ± 2	45 ± 2	(68 ± 2)	12 ± 2
300	3.3 ± 0.2	2.2 ± 0.1	(58 ± 2)	1.1 ± 0.2
k_L	157	132	–	117

k_L denotes the Langevin rate coefficient for the corresponding target molecule.
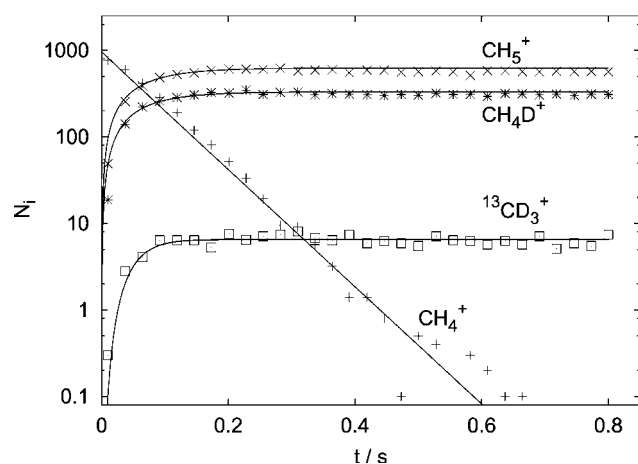

Fig. 3. CH_4^+ stored at $T = 15$ K in pure HD ([HD] = 3.5×10^{10} cm^{-3}). The rate coefficient derived form the decay of CH_4^+ is $k = (4.5 \pm 0.2) \times 10^{-10}$ cm^3/s, the branching fraction to form CH_5^+ is 68%. Also visible as a product is $^{13}CD_3^+$, originating from $^{13}CH_3^+$ parent ions overlapping with the primary injected beam of CH_4^+ (both mass 16). $^{13}CH_3^+$ is completely deuterated in three fast reactions with HD.

have been investigated at 15 and 300 K. One typical measurement performed at 15 K and at a number density of [HD] = 3.5×10^{10} cm^{-3} is shown in Fig. 3. In this experiment around 1000 primary CH_4^+-ions were injected into the trap and every storage step was repeated ten times. It can be seen that the number of CH_4^+ ions decays exponentially while CH_5^+ ions (mass 17) and CH_4D^+ ions (mass 18) are formed. The origin of the minor product $^{13}CD_3^+$ (mass 19) will be discussed below.

It is obvious that reaction (2b), i.e., formation of CH_5^+ dominates over reaction (2a) leading to the deuterated CH_4D^+. Interestingly the branching fraction of the formation of CH_5^+ increases from 0.58 at 300 K to 0.68 at 15 K. Special care has been taken for the branching measurements not to be influenced by small CH_2D^+-impurities injected with the CH_4^+ primary beam. These species are completely deuterated in two fast consecutive steps to CD_3^+ (mass 18) which are then indistinguishable from the CH_4D^+ products under investigation. These two species can be separated since association of CD_3^+ in collisions with HD is much faster than any further reaction of the CH_4D^+/CH_5^+ products of reaction (2). Radiative and ternary association of these CH_5^+-analogues are at least three orders of magnitude slower than those of CD_3^+, see [23] for details. The results for the branching fractions are included in Table 2.

An important experimental test for understanding the reaction mechanism is whether HD scrambling occurs in a collision with HD, i.e.,

$$CH_4^+ + HD \rightarrow CH_3D^+ + H_2 \qquad (3)$$
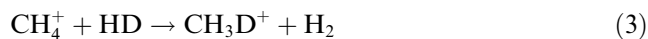
The CH_3D^+ product has the mass 17 and it is therefore indistinguishable from CH_5^+ from reaction (2b). One clear hint that reaction (3) is only a minor channel compared to reaction (2) is that the rate coefficients determined from the exponential decay of CH_4^+ are quite similar for collisions with H_2 and HD at 15 K (see Table 2). Since this attenuation rate coefficient also includes reaction (3) it can be deduced that the reactivity is not much enhanced by taking HD instead of H_2. Moreover, at 300 K the reaction rate with HD is even smaller than with H_2. Thus the presence of the additional reaction channel (3) does not seem to play a role.

Due to the mentioned mass overlap problem it is hard to determine an accurate value for the rate coefficient of reaction (3). However, a simulation of the subsequent reaction steps has been used to derive an upper limit. CH_3D^+ is a deuterated version of CH_4^+ and will therefore most likely be subject of hydrogen (deuterium) abstraction, similar to reaction (2). For this consecutive reaction the same rate coefficients have been assumed as for reaction (2) and the products are CH_4D^+ on mass 18 and $CH_3D_2^+$ on mass 19. CH_4D^+ from these subsequent reactions and from reaction (2)

Table 3
There is no experimental evidence for H–D scrambling in CH_4^+ + HD/D_2 collisions

Reaction	k (15 K)
$CH_4^+ + HD \rightarrow CH_3D^+ + H_2$	$<1 \times 10^{-12}$ cm³/s
$CH_4^+ + D_2 \rightarrow CH_3D^+ + HD$	$<1 \times 10^{-13}$ cm³/s

The given values for the rate coefficients are upper limits for k from the numerical solutions of the sets of coupled rate equations.

cannot be distinguished. A certain fraction of the mass 19 signal corresponds to $^{13}CD_3^+$ which stems from $^{13}CH_3^+$ (mass 16) entering the trap together with the CH_4^+ parent ions. Its contribution has been determined in independent measurements to be $(0.7 \pm 0.1)\%$ as can be seen in Fig. 3. In the simulation, the number of mass 19 products would increase significantly above this level when the rate coefficient of reaction (3) is assumed to exceed 1×10^{-12} cm³/s. Therefore one can take this value as an upper limit. Kim and co-workers give a similar upper limit for the exchange reaction of $CD_4^+ + H_2 \rightarrow CD_3H^+ + HD$ ([6]). For the H-atom exchange in the reaction of CH_4^+ with D_2 an even lower limit of 1×10^{-13} cm³/s has been derived in the present study, see Table 3. In the latter case, the experimental sensitivity to derive an upper limit is somewhat higher due to the smaller total reaction rate, as detailed in the following section.

Another indication that the four hydrogen atoms bound to the carbon do not exchange with the atoms from the target molecule comes from the $CH_4^+ + D_2$ collision system. If scrambling would play a role in the course of hydrogen addition, one would also expect $CH_3D_2^+$ products where the colliding D_2 is incorporated while a hydrogen atom from the CH_4^+ parent is removed. From a point of view of simple statistics this case should occur in 4 out of 6 cases. However, the signal on the corresponding mass is measured to be smaller than 1% (see [23]). Therefore it can be concluded that reaction (1) proceeds via addition of one hydrogen atom which is abstracted from the incident target molecule.

3.3. Differences in collisions with H_2, HD and D_2

As has been mentioned above and can be seen from Table 2, the rate coefficients for D-atom abstraction in collisions of CH_4^+ are strongly dependent on temperature between 15 and 300 K. The rate coefficient at room temperature has been determined before by Inoue and Wexler [15] to be 0.9×10^{-11} cm³/s. Note that their value might be somewhat low due to the higher kinetic energy of ions in ICR-experiments leading to non-thermal conditions. Utilizing the technique of resonance-heating, they also observed a falling rate coefficient with increasing energy.

As can be seen from the summary in Table 2, the total rate coefficients at $T = 300$ K decrease substantially with the level of deuteration of the neutral reactant. It drops by a factor of three when using D_2 instead of H_2. A similar drop is present at $T = 15$ K. However, at low temperatures the total rate coefficient with HD as a target is significantly larger than that for H_2. In contrast to these findings the Langevin rate coefficients for the three neutral reactants are not much different. Using simply the averaged polarizability, one obtains $k_L = 1.57 \times 10^{-9}$ cm³/s for collisions of methane cations with H_2, $k_L = 1.32 \times 10^{-9}$ cm³/s with HD, and $k_L = 1.17 \times 10^{-9}$ cm³/s with D_2, the small changes being due to the increasing reduced mass. The contribution of the quadrupole term of hydrogen as well as the ion-dipole interaction for HD as target has been neglected in this calculation. Nonetheless the dipole moment of HD, which is 8.51×10^{-4} debye [24] most probably plays a role in favoring reaction (2a) over (2b) (see below). In summary, other dynamical constraints have to be considered in order to explain the rather large differences in the total rate coefficients for H_2, HD and D_2.

4. Discussion

Several pieces of information concerning the hydrogen abstraction reaction of CH_4^+ have been collected in this work. First, at low temperatures reaction (1) is proceeding at a substantial fraction of the collision rate. Second, this reaction follows a strong negative temperature dependence up to at least 1000 K. Third, reaction (3), H–D exchange of CH_4^+ in collisions with HD, is very slow. Therefore it can be assumed that H–H scrambling is also very unlikely to occur. Fourth, the branching ratio of reaction (2) is in favor of the hydrogenated CH_5^+ product over the deuterated CH_4D^+ product. Fifth, hydrogen abstraction is slowed down when using HD or D_2 instead of H_2. In the following a qualitative picture of the potential energy surface (PES) is discussed and some remarks concerning reaction dynamics are made which may explain the experimental facts.

Reaction (1) is near thermoneutral. From the heats of formation of reactants and products at 0 K [13] an exothermicity of 19 kJ/mol is derived. In Federer et al. [12] a value of 5 kJ/mol has been used in their discussion. This is the first information the PES shown in Fig. 4 is based on. Since at 300 K, 98% of the $CH_4^+ + H_2$ decay back to the input channel, the transfer to the product channel must be significantly hindered, e.g., by a potential barrier, a dynamical bottle neck or by an extremely small phase space (endoentropic). It is surprising that, at 15 K, the path towards products is found in every fourth collision. As common in low-temperature collision processes the discussion is simpli-
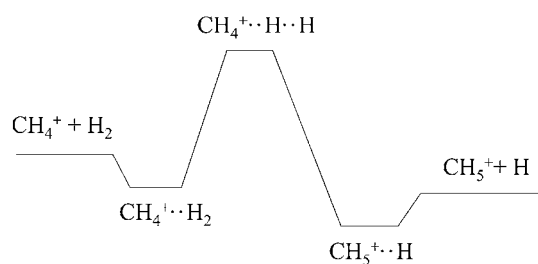
Fig. 4. Schematic illustration of the stationary points of the potential energy surface for the $CH_4^+ + H_2$ collision system. The absolute values which are not known, have been adopted from [9] for the isoelectronic $NH_3^+ + H_2$ system. Note that there is probably no barrier in the transition region. This is used here only symbolically for indicating the fact, that the transfer from the left to the right is hindered by some dynamical constraints.

fied if one makes the assumption that the abstraction reaction (1) proceeds in two well separated steps. First, an intermediate collision complex is formed which, at low enough temperatures, may be long-lived even if the H_2 molecule is only loosely attached to the CH_4^+ ion,

$$CH_4^+ + H_2 \rightarrow CH_4^+ \cdot H_2 \tag{1a}$$

An upper limit for the rate coefficient for this process, K_{1a}, is the Langevin rate coefficient k_L. No substantial barrier has to be overcome to reach this complex since the measured low temperature rate coefficient amounts to a considerable fraction of the collision limit, k_L. This complex is weakly bound since there does not exist a bound CH_6^+ molecule. Due to its fragile nature the complex usually redissociates quickly into the educts

$$CH_4^+ \cdot H_2 \rightarrow CH_4^+ + H_2 \tag{1b}$$

but there must be a way to proceed towards products,

$$CH_4^+ \cdot H_2 \rightarrow CH_5^+ + H \tag{1c}$$

Within this simple model, the dynamics of the $CH_4^+ + H_2$ reaction system (1) is determined predominantly by the two decay rates for process (1b) and (1c), K_{1b} and K_{1c}. As a consequence the rate coefficient for reaction (1) can be approximated by

$$k = k_L K_{1c}/(K_{1b} + K_{1c}). \tag{4}$$

According to the Langevin model the rate coefficient k_L at which the reactants can overcome the centrifugal barrier in the entrance channel to form the complex is temperature independent. Therefore the complex formation is thought to be of minor importance for the temperature dependence of reaction (1). The second important parameter in expression (4) is K_{1b}. The order of magnitude of the life time of the CH_6^+ complex, $\tau_{dis} = 1/K_{1b}$, may be about 1 ns at 15 K assuming that it is similar to that of the CH_6D^+ complex formed in $CH_5^+ + HD$ collisions. The latter complex is also bound only by van der Waals forces and its lifetime has been estimated from the rate of ternary association (see [23]).

Since it is rather safe to assume, within this simple model, that the lifetime of the complex increases monotonically with decreasing temperatures, K_{1b} drops accordingly. Statistical models usually predict a T^n dependence. The third and presently most uncertain parameter is the rate K_{1c}. If tunneling would be the determining process, this value would drop also significantly with decreasing temperature. This would lead to an obvious contradiction to the experimental observations. From the experimental results it can be concluded that $K_{1c} \sim 1/3 K_{1b}$ at 15 K and $K_{1c} \sim 0.02 K_{1b}$ at room temperature. This indicates that K_{1c} may be only weakly temperature-dependent.

As discussed above the lifetime of the complex is rather long compared to the time scale of any internal motion (vibration, rotation). This can be taken as an argument that the collision complex has enough time to redistribute the energy statistically among all states which are in accordance with its good quantum numbers. If this is really fulfilled, the rates K_{1b} and K_{1c} can be calculated from the relevant phase space volumina. In this context it becomes evident, that the question, whether a bimolecular reaction can be treated with simple thermodynamic quantities as presented in [12] and mentioned in Section 1, and whether it is allowed to say that reaction (1) is an endoentropic reaction must be obviously denied. The complete mixing of the phase space is a necessary condition, but a statistical theory which correctly describes the collision of two molecules, must account properly for all constants of the motion!

In the present case, especially with the unknown structure of the CH_5^+ product, it is not easy to get a reasonable estimate for the competing phase space volumina. However, it is presumed that also an exact statistical calculation will lead to a result deviating from the experimental observations. Most probably reaction (1) is influenced by additional dynamical constraints, hindering the access to some regions of the phase space. There may be degrees of freedom which are only weakly coupled, or there are additional hidden constants of the motion, restricting the reaction steps (1b) and (1c). One candidate is the total nuclear spin which plays an important role if identical atoms are involved as in the title reaction.

Despite the fact that the $NH_3^+ + H_2$ system and the $CH_4^+ + H_2$ are isoelectronic and that, at first side, the negative temperature dependence of the rate coefficients for both reaction systems may have a similar explanation, the dynamical reasons must be quite different. For the ammonia system, rate coefficients have been calculated as a function of temperature and compared to a variety of experimental results [1–4,6]. The theoretical treatments were based on the minimum energy pathway of Herbst et al. [9], which also has been used as illustration in Fig. 4. In these calculations good qualitative

agreement has been obtained and it has been found that tunneling is the dominant pathway at low temperatures.

With increasing temperatures the complex lifetime becomes shorter thus leading to a negative temperature dependence. In the $NH_3^+ + H_2$ case a minimum value for the rate coefficients has been found at a temperature of about 150 K followed by a positive temperature dependence at higher temperatures. In this temperature range, Fehsenfeld et al. have derived an effective barrier height of 0.09 eV (9 kJ/mol) from an Arrhenius plot. Taking tunneling into account, Herbst et al. [9] derived a larger value of (20 ± 2) kJ/mol. In view of these considerations one could argue that also $CH_4^+ + H_2$ may have a minimum in the rate coefficient at higher temperatures. However, it is apparent from Fig. 2 that this minimum must occur at temperatures exceeding 1000 K implying a barrier height much larger than for the ammonia system and subsequently even smaller reaction rate coefficients. In reality the rate coefficients are more than a factor of 100 larger thus ruling out tunneling in the present case.

A more subtle question to address is why significant isotope effects are observed when using deuterated hydrogen instead of H_2. When comparing the absolute values of the rate coefficients for H_2, HD and D_2 one has to take into account the branching ratios and the fact that, for example in reaction (2), the unbiased probability to pick an H atom from HD is only half the one for H_2 as a target in reaction (1). Accounting for this the rate coefficient for the formation of CH_5^+ is almost the same for HD and H_2 at 300 K. However, at 15 K this channel is faster by a factor of 1.5 when using HD instead of H_2. In a similar comparison the CH_4D^+ product channel is favored at both temperatures for HD as compared to D_2 as a target by a factor of about two. In general HD is reacting faster with respect to H_2 and D_2. Therefore, the heteronuclear nature of HD might be a root to understand the isotope effect.

As has been discussed in detail in state selected low temperature experiments on $CO^+ + CO$ [25] the rate of redissociation of a loosely bound complex depends strongly on the rotational state of the reactants. It is significantly slower for low lying rotational states than it is for high energy states. Therefore one could interpret the differences in collisions with H_2 and HD as the result of reactions with two species at different energies. In fact, at 15 K only the lowest rotational state, $j = 0$, is occupied in HD while the n-H_2 used in the experiment consists of 75% o-H_2 ($j = 1$) and 25% p-H_2 ($j = 0$). Thus using n-H_2 leads to a population of higher energy states in the complex. However, as described before, the H_2, HD and D_2 entities remain as intact molecules in the complex. Therefore it is supposed that orthopara conversion within the complex is

an unlikely process since it would require a nuclear spin flip. Another way of converting H_2 rotation into internal energy of the whole complex would be proton or H-atom scrambling between the ion and the neutral molecule. The exchange reaction (3) has been shown to be a very unlikely process. Also from the absence of $CH_3D_2^+$ products in $CH_4^+ + D_2$ collisions it may be concluded that reorganization of hydrogen atoms or molecules is not very probable, also at long complex life times. In summary there is no obvious route for o-H_2 to release its internal energy to the complex in order to decrease the lifetime. Dedicated experiments with p-H_2 should be performed to see whether the results are more consistent with those for HD or for n-H_2. From such experiments it might be possible to judge whether the physical picture of an increased temperature is correct.

A final question to discuss is the fact that CH_4^+ prefers to abstract the H atom from the HD target molecule instead of the D atom. As discussed in detail in [14], e.g., for $D_3^+ + H_2$ scrambling collisions, the simple statistical weight of the competing product channels determines often the outcome at elevated temperatures while, at low temperatures, the difference in zero-point energies restricts the formation of certain product channels. Based on such results, the energetically lower lying product channel $CH_4D^+ + H$ would dominate. If, however, scrambling is not occurring like for the title reaction, the branching ratio is determined by other mechanisms, may be just by the orientation of the HD during the approach of the ion. An example illustrating this is the isotopic branching ratio which has been calculated for the $O^+ + HD$ reaction using the rotationally adiabatic capture theory [26]. The authors find the branching ratio $[OH^+]/[OD^+]$ larger than unity, especially for non rotating HD. An explanation based on a simple classical picture is that the isotopic substitution separates the center of charge from the center of mass leading to an enlarged orientation probability of the H-atom facing the ion prior to reaction. At the moment this is the most likely explanation of the isotope effect observed in reaction (2), however, it also may be taken as a hint to other dynamic restrictions controlling reaction (1).

5. Conclusions

Our investigations with a 22-pole ion trap show that temperature dependent reaction rate measurements using different isotopic configurations give detailed insight into the dynamics of ion-molecule reactions. In the case of $CH_4^+ + H_2$, a picture different from common tunneling mechanism, had to be drawn to explain the negative temperature dependence of the rate coefficient. Detailed calculations are needed to explain the dynamical re-

strictions within the collision complex. The similarity of the isotope effect of the hydrogen abstraction for $CH_4^+ + HD$ and $O^+ + HD$ suggests that long-range HD orientation via the dipole may play a role. Thus the isotope effect may be partly related to the entrance channel while the negative temperature dependence is most probably affected by properties of the exit channel of this reaction.

It is hoped that these studies encourage ab initio calculations of the PES of the $CH_4^+ + H_2$ system and quantum chemical investigations, especially at low temperatures. Dedicated experiments to measure the energy dependence at higher collision energies may indicate an minimum in the rate coefficient like in the case of $NH_3^+ + H_2$. The most important next experimental step is, however, to study the reverse of reaction (1), especially in the threshold region which should be somewhere between 15 and 300 K. The combination of a temperature variable 22-pole ion trap with a beam of slow hydrogen atoms is close to completion and first results for $CH_5^+ + H$ and $CH_5^+ + D$ are expected soon.

Besides the efficiency of the various reaction paths leading to final product states in $CH_4^+ + H_2$ collisions, the question remains, whether all hydrogen atoms are equivalent in the formed protonated methane. It is rather sure that the dynamics of the reaction system discussed in this paper are to complicated to draw some related conclusions. An important experimental observation providing information on the structure of CH_5^+ is that this ion survives millions of collisions with HD without deuteration. Another may be better defined synthesis of CH_5^+ ions can be achieved via radiative or ternary association. In any case it is very challenging if not impossible to develop chemical probing methods for distinguishing different isomers of this floppy molecule. A more realistic approach with a 22-pole trap is probably to utilize the method of IR laser induced reactions [27] and to record infrared and far-infrared spectra of very cold CH_5^+ relaxed in p-H_2 or alternatively in n-H_2. Partial substitution of hydrogen with deuterium, may be also tritium can be used to break the exchange symmetry. Of course this also may lead to structural modifications due to changes in zero point energies.

References

[1] F.C. Fehsenfeld, W. Lindinger, A.L. Schmeltekopf, D.L. Albritton, E.E. Ferguson, J. Chem. Phys. 62 (1975) 2001.
[2] D. Smith, N.G. Adams, Mon. Not. Roy. Astr. Soc. 197 (1981) 377.
[3] J.A. Luine, G.H. Dunn, Astrophys. J. Lett. 299 (1985) L67.
[4] H. Böhringer, Chem. Phys. Lett. 122 (1985) 185.
[5] D. Gerlich, J. Chem. Soc., Faraday Trans. 89 (1993) 2199.
[6] J.K. Kim, L.P. Theard, W.T. Huntress Jr., J. Chem. Phys. 62 (1975) 45.
[7] N.G. Adams, D. Smith, Int. J. Mass Spectrom. Ion Proc. 61 (1984) 133.
[8] S.E. Barlow, G.H. Dunn, Int. J. Mass Spectrom. Ion Proc. 80 (1987) 227.
[9] E. Herbst, D.J. DeFrees, D. Talbi, F. Pauzat, W. Koch, A.D. McLean, J. Chem. Phys. 94 (1991) 7842.
[10] M.S.B. Munson, F.H. Field, J.L. Franklin, J. Am. Chem. Soc. 85 (1963) 3584.
[11] N.G. Adams, D. Smith, Chem. Phys. Lett. 47 (1977) 383.
[12] W. Federer, H. Villinger, P. Tosi, D. Bassi, E. Fergusson, W. Lindinger, in: G.H.F. Diercksen et al. (Eds.), Molecular Astrophysics – State of the Art and Future Directions, Reidel, Boston, 1985, p. 649.
[13] Y.H. Le Teuff, T.J. Millar, A.J. Marwick, Astron. Astrophys. Suppl. Ser. 146 (2000) 157.
[14] D. Gerlich, E. Herbst, E. Roueff, Planet. Space Sci. 50 (2002) 1275.
[15] M. Inoue, S. Wexler, Am. Chem. Soc. 91 (1969) 5730.
[16] D. Marx, M. Pironello, Science 284 (1999) 59.
[17] E.T. White, J. Tang, T. Oka, Science 284 (1999) 135.
[18] A.J.R. Heck, L.J. de Kroning, N.M.M. Nibbering, J. Am. Soc. Mass Spectrom. 2 (1991) 453.
[19] G.M. Kramer, Science 286 (1999) 1051a.
[20] D. Gerlich, Adv. Chem. Phys. LXXXII (1992) 1.
[21] D. Gerlich, S. Schlemmer, Planet. Space Sci. 50 (2002) 1287.
[22] D. Gerlich, Phys. Scri. T59 (1995) 256.
[23] O. Asvany, Ph.D. thesis, University of Technology, Chemnitz, 2003.
[24] W.R. Thorson, J.H. Choi, S.K. Knudson, Phys. Rev. A 31 (1985) 22.
[25] D. Gerlich, T. Rox, Z. Phys. D 13 (1989) 259.
[26] Ch.E. Dateo, D. Clary, J. Chem. Soc., Faraday Trans. 2 (85) (1989) 1685.
[27] S. Schlemmer, E. Lescop, J.V. Richthofen, D. Gerlich, M. Smith, J. Chem. Phys. 117 (2002) 2068.

Appendix C

Deuteration of CH_n^+ (n=3-5) in collisions with HD measured in a low temperature ion trap

O. Asvany, S. Schlemmer, D. Gerlich

Deuteration of CH_n^+ (n=3-5) in collisions with HD measured in a low temperature ion trap

O. Asvany, S. Schlemmer, and D. Gerlich

Department of Physics, Technische Universität Chemnitz, 09126 Chemnitz, Germany

Abstract

Deuteration of small hydrocarbon ions CH_n^+ via H − D exchange (n = 3 - 5) has been studied in a 22-pole ion trap at a nominal temperature of 15 K. Sequential deuteration from CH_3^+ to CD_3^+ is very fast if one uses pure HD as target gas. Rate coefficients have been measured to be 1.65×10^{-9} $cm^3 s^{-1}$, 1.59×10^{-9} $cm^3 s^{-1}$, and 1.5×10^{-9} $cm^3 s^{-1}$. If, however, CH_3^+ is relaxed in p-H_2 containing traces of HD, the rate coefficient for isotope enrichment is significantly smaller, $(4\pm2) \times 10^{-10}$ $cm^3 s^{-1}$. This important result is most probably due to symmetry selection rules influencing this reaction. The ions CH_4^+ and CH_5^+ are not observed, within the experimental uncertainties, to exchange H-atoms for D-atoms at all. Upper limits for the rate coefficients for forming CH_3D^+ and CH_4D^+ are 1×10^{-12} $cm^3 s^{-1}$ and 5×10^{-18} $cm^3 s^{-1}$, respectively. Hydrogen or deuterium abstraction in collisions of CH_4^+ with HD occurs with a sum rate coefficient of 4.5×10^{-10} $cm^3 s^{-1}$. Surprisingly, the more exoenergetic and statistically favored product CH_4D^+ is formed only in 1/3 of the reactive collisions, while CH_5^+ dominates with 2/3. The results are discussed on the basis of the formation of long lived collision intermediates, open and closed shell ions, and barriers along the reaction path. All experimental data clearly indicate that conservation of total nuclear spin plays an important role in these low temperature chemical reactions involving identical nuclei. Implications of this laboratory work to isotopic fractionation in astrophysical environments are discussed.

1. Introduction

In the last two decades about twenty singly, some doubly and even triply deuterated molecules have been detected in cold interstellar clouds (Millar 2002). Recent observations include fully deuterated ammonia (Lis *et al.* 2002), triply deuterated methanol (Parise *et al.* 2004), and D_2H^+ (Vastel *et al.* 2004). It is well-known and reasonably well-understood that the measured abundance ratios of the singly deuterated molecules to their non-deuterated counterparts are significantly larger than the D/H cosmic ratio, sometimes up to a factor 10^4. The D/H ratio has been determined to be around 1×10^{-5}, e.g., by measuring the $J = 0 \leftarrow 1$ rotational line of HD. A recent example is the observation by Wright and coworkers (1999) towards the Orion Bar. Deuterium fractionation is strongly related to the physical conditions of the interstellar medium, namely low temperatures ($T = 10$ to 100 K) and low-densities ($[H_2] \sim 10^3 \, cm^{-3}$ to $10^6 \, cm^{-3}$). The reason is that most deuterium exchange reactions are exothermic due to the difference in zero point vibrational energies of reactants and products. In molecular clouds most of the deuterium is contained in the form of HD. Therefore it is assumed that deuterium fractionation is first initiated by simple ion-molecule collisions involving HD followed by D atom or deuteron transfer to more complex molecules provided that there are no significant barriers on the reaction pathway. Up to date only three initial gas phase reactions are included in the models, the reactions of H_3^+, CH_3^+ and $C_2H_2^+$ with HD. For more details see Millar (2002); Millar *et al.* (1989); Roberts *et al.* (2002), Maluendes *et al.* (1992), or Gerlich & Schlemmer (2002).

Deuteration can be used as a very sensitive probe for the physical conditions existing in specific interstellar regions and for the chemistry occurring there. It can give hints to the temperature of the cloud, the densities of atoms, electrons and concentrations of specific molecules, and, as emphasized in this work, to the fractional abundance of o-H_2. These insights into the prevailing conditions depend on our theoretical and experimental knowledge of many elementary processes. Modern model calculations (Roberts *et al.* 2002, Millar 2002) take into account both gas phase as well as gas - grain processes; however, rather few reliable input data are available, such as rate coefficients from low temperature experiments or accurate quantum chemical calculations. Even with the sophisticated methods of quantum chemistry available today, barrier heights and other details of the potential energy surface often cannot be predicted with the required accuracy. Therefore low temperature experimental work is necessary to study the related processes. Investigations of ion-molecule reactions have been conducted with various techniques in the last decades, mainly at room temperature or at higher energies and under non-thermal conditions. In a selected ion flow tube (SIFT), Adams and Smith examined many reactions down to 80 K (Adams & Smith 1977, Smith 1992). In the eighties first trapping experiments have been developed in which chemical processes could be studied at temperatures of a few K and at low densities prevailing in dense interstellar clouds (Barlow & Dunn 1987, Gerlich & Käfer 1989, Gerlich 1995). The need for low temperature experiments is especially evident for reactions which show a different behavior at low temperatures in comparison to room temperature. One prominent example is the chain of H-atom abstraction reactions starting with N^+ in a bath of H_2 and leading finally to NH_4^+, which, via dissociative recombination with an electron, is assumed to be a major source of interstellar NH_3 (Herbst *et al.* 1991, Gerlich 1993). Also for simple systems such as $CH_4^+ + H_2$ a negative temperature dependence has been observed recently (Asvany *et al.* 2004).

As mentioned above, there are only three molecular ions believed to contribute significantly to the transfer of deuterium from HD to more complex species: H_3^+, CH_3^+, and $C_2H_2^+$. Besides elemental and molecular abundances, the main reason for this limited number is that many exothermic exchange reactions have transition state barriers inhibiting the reaction to proceed at low temperatures, one example being the reaction of HCO^+ with HD (Smith *et al.* 2002). Therefore a major aim of theoretical treatments of the problem involves the prediction of barrier heights in order to classify the deuterium exchange reactions. The nature of the barriers has been discussed semi-quantitatively by Henchman *et al.* (1988). According to their model the ion AH^+ and the HD form an entrance channel complex $AH^+\cdot\cdot HD$ in which the reactants remain distinct. Via a transition state, H and D can be exchanged or a strongly bound complex can be formed where mixing of the chemically equivalent atoms occurs. Due to the exoergicity of the exchange process the complex prefers to decompose into $AD^+ + H_2$, as can be predicted from a simplified phase space theory just counting asymptotic states of the products.

A classification of transition state barriers was proposed by Henchman *et al.* (1988) based on reactant ions with "filled" and "unfilled" valence shells. In the first case the entrance channel complex is only weakly bound and the energy of the transition state is much higher than the entrance channel. Therefore H - D exchange does not occur at low collision energies. In the second case the "unfilled" valence shell ion can form a strongly bound complex with a transition state which is way down in the valley of the attractive potential energy surface. In this situation H - D exchange can become a rapid process. Maluendes *et al.* (1992) replaced the somewhat misleading distinction between "filled" and "unfilled" valence shell ions by the more precise characterization based on a large and small HOMO - LUMO gap. For example they report for the $CH_3^+ + HD$ collision system, based on detailed *ab initio* calculations, that formation of CH_2D^+ is 3.4 kJ/mol (405 K) exothermic and that scrambling can occur very efficiently in the strongly bound (-198 kJ/mol) collision complex which is characterized by a double well potential with a completely negligible barrier laying -192 kJ/mol below the reactants energy. Based on a simple statistical argument they predict that the overall efficiency for H - D exchange must approach unity at low temperatures. According to these guidelines, ions like H_3^+ or CH_3^+ and its isotopomers which are known to have strong chemical binding with hydrogen molecules, will undergo deuteration, while ions such as CH_5^+ can form only a weakly bound $CH_5^+\cdot\cdot HD$ complex and are therefore not expected to become deuterated in collisions with HD.

It is an open question whether this simple reaction model holds for all astrophysically relevant systems or whether more details of the potential energy surface and dynamical calculations are needed in order to explain dynamical restrictions or for locating reaction paths avoiding barriers. Fundamental questions are related to the role of tunneling or to the j-dependent capture cross section caused by the anisotropy of the ion-molecular hydrogen interaction potential. A special dynamical effect of deuteration may concern the $CH_5^+ + HD$ system studied here. According to recent theoretical work (e.g. Marx & Parinello 1999) the structure of CH_5^+ is sometimes resembling to a CH_3^+ and a distinct H_2 entity. Due to this fluctuating nature one may speculate that it could be possible to exchange the incoming HD molecule for the complete H_2 while the HOMO-LUMO gap rule excludes the exchange of atoms.

Besides the details of the potential energy surfaces, symmetry selection rules closely correlated with the separate conservation of the total nuclear spin play a central role in the process of deuteration as discussed for example for $H_3^+ + HD$ by Gerlich *et al.* (2002). Recently it was pointed out (Gerlich 2004) that the well-documented basic ideas

on symmetry selection rules in chemical reactions (Quack 1977) have not yet been implemented in a consistent way into statistical models describing the influence of the ortho and para forms of the reactants in H - D scrambling. A well-documented example is the process of ternary and radiative association in $CH_3^+ + H_2$ collisions. It was attempted by Bates (1987, 1991) to develop a theoretical model which explicitly treats the different nuclear spin configurations, for comparing results performed under different experimental conditions (Barlow & Dunn 1987, Gerlich & Kaefer 1989) and for making predictions for interstellar environments. The detailed experimental results obtained at 10 K (Gerlich 1994 and 1995) did not show the increase for para hydrogen as predicted by the model of Bates indicating that it does not account properly for the restrictions imposed by the exchange symmetry.

In addition to the just mentioned studies, the $CH_3^+ + H_2$ system has been the focus of many other experimental investigations. Isotope exchange and association reactions of CH_3^+ and its deuterated analogues with H_2, HD, and D_2 have been studied in a variable temperature SIFT apparatus by Smith *et al.* (1982a). From forward and backward reaction rates measured at 295 K, 205 K, and 80 K, enthalpy changes have been determined. In particular the rate coefficients for CH_2D^+ formation in $CH_3^+ + HD$ collisions have shown a negative temperature dependence. Extrapolation to interstellar cloud temperatures has indicated that the collisional limiting value should be reached. Due to the fact that the backward reaction $CH_2D^+ + H_2$ is rather endothermic and must be therefore slow it has been concluded that CH_2D^+ plays an important role in the synthesis of deuterated molecules in interstellar space (Smith *et al.* 1982b).

Low temperature trap experiments, performed with hydrogen containing traces of HD, always show contributions from isotope enrichment (Gerlich 1995). Unfortunately, the analysis of such data is complicated by the fact that several product channels, interfering masses and back reactions of deuterated species in collisions with hydrogen (especially o-H_2) complicate the evaluation of such data. Some related results were presented by Gerlich & Schlemmer (2002). Among others it was reported that the rate coefficient for isotope exchange in $CH_3^+ + HD$ is significantly smaller than the collision limit, if the ions are relaxed in p - H_2. Since this is in contrast to the theoretical predictions mentioned above, H - D exchange reactions of CH_n^+ (n = 3 - 5) have been reinvestigated in our laboratory. The experiments were carried out with pure HD in the trap in order to avoid complications with competing forward and backward reactions.

2. Experimental

The laboratory measurements have been performed in an ion trapping apparatus, which has been developed for investigating ion-molecule collisions at conditions representative of interstellar clouds. The ion guiding and trapping technique has been thoroughly reviewed by Gerlich (1992) while detailed descriptions of the temperature variable radio-frequency 22-pole ion trap has been given by Gerlich & Horning (1992) and by Gerlich (1995). This central element of the apparatus is shown schematically in Fig. 1. The trap consists of 22 stainless steel rods of 1 mm diameter circumscribing a circle of 1 cm diameter and connected alternatively to the two phases of an rf power supply. Typical rf frequencies and amplitudes are $\Omega/2\pi = 17$ MHz and $V_0 = 20$ V, respectively. Radial confinement of the ion cloud is achieved by the very steep effective potential, created by the multipole rf field, whereas trapping in the axial direction is achieved by repulsive DC voltages applied to the entrance and exit gate electrodes. This arrangement is completely enclosed by copper walls (not shown in Fig. 1), which are mounted onto a closed cycle He refrigerator that can be cooled down to a nominal temperature of 10 K.

Reactant and buffer gases can be admitted to the 22-pole trap by cooled tubes. The ion cloud injected into the trap adapts to the trap temperature by collisions with the buffer gas leaked in either in a continuous mode or in short (~ms) intense pulses.

The investigated ions are generated by electron bombardment, mass selected in a quadrupole mass filter and then injected into the 22-pole ion trap filled with the reactant gas. After a certain trapping time, the trap content is extracted by an electric pulse applied to the exit electrode, analyzed with a second quadrupole mass spectrometer, and detected with near unit efficiency by an ion counting detector (Daly-detector). For determining the changes of the ion composition due to reactions, the sequence (i) ion formation, (ii) injection, (iii) relaxation and reaction, and (iv) analysis is repeated many times for each product mass and typically for twenty different storage times. More details of the method and typical applications in interstellar gas phase chemistry, in cluster growth, or in state specific ion-molecule reactions can be found in recent publications (Schlemmer *et al.* 1999; Gerlich *et al.* 2002; Smith *et al.* 2002; Asvany 2004).

For the preparation of ionic hydrocarbons CH_n^+ (n=3-5) methane gas (Messer-Griesheim, purity 5.5) was used at a pressure of about 10^{-5} mbar in an external rf storage ion source. The ions CH_4^+ and CH_3^+ are directly generated by electron bombardment while CH_5^+ is created in the source by the subsequent reaction $CH_4^+ + CH_4 \rightarrow CH_5^+ + CH_3$. To avoid internal excitation of the ions, the electron energy is kept as low as possible, typically 18 eV. Helium gas can be added to the source to thermalize the ions to the source temperature of ~ 350 K. In the case of CH_3^+ and CH_5^+, hydrogen has been used as an additional buffer gas in the source, as the reactions of CH_n^+ (n=1-5) with H_2 are known to stop at these two species and further association processes are unlikely at the high source temperature. In this way, D - or ^{13}C - containing hydrocarbon ions with $m = 15$ u or $m = 17$ u, e.g., CHD^+ or $^{13}CH_4^+$, are quenched by chemical reactions.

After extraction of the primary ions from the source through a pulsed electrode, the ions are selected in a first rf quadrupole operated either at high frequencies and low dc differences, i.e., in the low band-pass mode, or in the standard high mass resolution mode. In the first mode all ions with a mass smaller than a certain cutoff value are injected "smoothly" into the trap. This mode is used if very slow ions with a narrow energy distribution have to be injected into the trap and if the presence of lower mass ions does not disturb the reaction kinetics. The other mode (upper corner of the stability triangle) is used if it is necessary to inject exclusively ions of a particular mass into the 22-pole ion trap, of course at the expenses of a wider energy spread. For example, the mass-selective mode was necessary to search for minor traces in determining the upper limit of deuteration of CH_5^+ with HD. After injection of the ions into the trap through the pulsed entrance electrode, they are cooled down to the nominal temperature by using a short He pulse of typically a few ms and of high density ($n_{max} \sim 10^{15}$ cm^{-3}).

The target gas HD has been purchased from Cambridge Isotope Laboratories Inc. who specify the purity of the deuterium hydride to be 97 %, the rest mainly being H_2 and D_2. We confirmed this specification by a detailed *in situ* analysis using the $Ar^+ + HD$ reaction in the trap. More details about these tests have been reported by Asvany *et al.* (2004) and Asvany (2004).
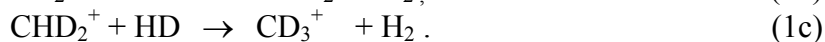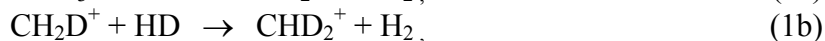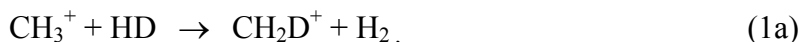
A wide range of storage times (< ms to > 100 s) and densities (< 10^8 cm^{-3} to 10^{15} cm^{-3}) of the neutral reaction partner can be used in trapping experiments thus allowing for a large dynamic range in the determination of rate coefficients. The high sensitivity of the 22-pole trapping apparatus is very important for the determination of very small rate

coefficients such as observed for the reaction between CH_5^+ and HD. This sensitivity is achieved by optimizing the trapping time, the target gas number density and number of stored ions (typically 1000). Using the maximum values and accounting for the noise of the detector (typically one count per second), rate coefficients as small as $k = 1 \times 10^{-20}$ cm^3s^{-1} can be determined. Depending on the reaction system investigated, this sensitivity is reduced by reaction channels leading to interfering product masses.

3. Results

3.1 Sequential H-D exchange in CH_3^+

The following sequential reactions have been measured at a nominal temperature of 15 K:

$$CH_3^+ + HD \rightarrow CH_2D^+ + H_2 , \qquad (1a)$$
$$CH_2D^+ + HD \rightarrow CHD_2^+ + H_2 , \qquad (1b)$$
$$CHD_2^+ + HD \rightarrow CD_3^+ + H_2 . \qquad (1c)$$

All three reactions are exothermic due to differences in zero-point vibrational energy. For example the exoergicity of reaction (1a) has been determined to be 370 K (Smith *et al.* 1982a) or 405 K (Maluendes *et al.* 1992). A typical measurement of the sequential deuteration of CH_3^+ is presented in Fig. 2. On average about 500 CH_3^+ ions were injected per pulse into the trap filled with HD at a number density of 1.8×10^{10} cm^{-3}. Inspection of Fig. 2 reveals a mono-exponential decay of the primary ions via reaction (1a) over four orders of magnitude. In the nearly pure HD environment, deuteration is so efficient that, within 0.3 s, the subsequent reactions (1b) and (1c) convert more than 99% of all ions into fully deuterated CD_3^+. Additional careful studies at longer reaction times revealed that the remaining number of CHD_2^+ ions is at least a factor 1000 smaller than the CD_3^+ ions with no indication for an onset of an equilibrium between these two product ions. In addition no residual CH_3^+ or CH_2D^+ could be detected within the sensitivity of the instrument. This implies that the hydrogenation reactions with HD are at least a factor of thousand slower than the deuteration reactions.

The lines in Fig. 2 are numerical solutions to a set of appropriate rate equations yielding the three rate coefficients for reactions (1a-c) which are summarized in Table 1. Details of the fitting procedure of the data are reported by Asvany (2004). As can be seen from Table 1, the first deuteration step is 1.04 times faster than the second one, and the second one is 1.06 times faster than the last one. Note that the rate coefficients for reactions (1a-c) are slightly larger than $k_L = 1.32 \times 10^{-9}$ cm^3s^{-1} where k_L is the capture rate coefficient predicted by the Langevin model just using the polarizability of HD. Such a behavior has also been observed for the abstraction reaction $CH_2^+ + HD$ (Asvany 2004). The deviation of almost 20 % is larger than the estimated experimental uncertainties (± 10 %) which are mainly due to the calibration of the pressure of the reactant gas and the determination of the actual trap temperature. The reliability of the measured number density has been cross checked using the calibration reaction $Ar^+ + HD$ for which the 300 K literature value is 8.6×10^{-10} cm^3s^{-1} (Ervin & Armentrout 1985). Other reaction rates measured for different ions with hydrogen and its isotopomers as reactant are also in good accordance with published rate coefficients. As discussed in more detail below, one of the reasons for the measured larger rate coefficients is the long range attraction with HD.

3.2 Reaction of CH_4^+ with HD

The slightly exothermic reaction of CH_4^+ with hydrogen and especially its temperature dependence is subject of a separate paper (Asvany *et al.* 2004), so we summarize here only the most important results for deuteration. Of importance are the deuteration channel via H - D exchange,

$$CH_4^+ + HD \quad \rightarrow \quad CH_3D^+ + H_2 \,, \tag{2a}$$
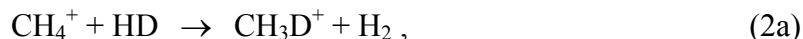
and the two abstraction reaction channels,

$$\rightarrow \quad CH_4D^+ + H \tag{2b}$$
$$\rightarrow \quad CH_5^+ \quad + D \,. \tag{2c}$$

Fig. 3 shows the time evolution of N_i, the number of ions of type i, after initial injection of CH_4^+ in a pure HD environment. The number density was $[HD] = 5.0 \times 10^{10}\,cm^{-3}$. It is evident, that the abstraction reactions (2b) and (2c) prevail. i.e., CH_4^+ ($m = 16$ u) is converted to CH_5^+ ($m = 17$ u) and CH_4D^+ ($m = 18$ u). At the temperature of this measurement, the three reactions (2a-c) proceed with a sum rate coefficient of $k = (4.5 \pm 0.2) \times 10^{-10}\,cm^3 s^{-1}$. The dominant product is CH_5^+ with a branching fraction of 68 %. Both abstraction reactions show the same strong negative temperature dependence as has been reported for the interaction with H_2 (Asvany *et al.* 2004).
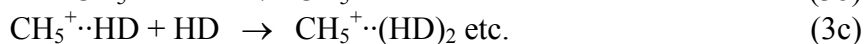
The problem in determining a reliable rate coefficient for reaction (2a) is that the product CH_3D^+ appears at the same mass as the main reaction product, CH_5^+. Therefore it was necessary to apply a more complicated analysis based on the careful evaluation of a variety of subsequent reactions. Especially important is that CH_3D^+ product ions formed via reaction (2a), would also abstract an H or a D atom in subsequent collisions with HD, leading to CH_4D^+ ($m = 18$ u) or $CH_3D_2^+$ ($m = 19$ u). As can be seen in Fig. 3, ions with $m = 19$ u are detected indeed; however, this minor product channel is assigned to be $^{13}CD_3^+$. One proof is the time dependence of this channel which grows very similarly to the main products for t > 0.05 s. The slight difference at the beginning is due to the initial $^{13}CH_3^+ + HD$ processes. From this and other tests it is concluded that the $m = 19$ u ions are predominantly produced from $^{13}CH_3^+$ via fast subsequent deuteration reactions with HD, in analogy to reactions (1a-c). Since these primary ions appear on the same mass as $^{12}CH_4^+$, they cannot be eliminated by the first mass filter. Using chemical quenching in the ion source, the fraction could be reduced to below 0.5 % of the primary ions. Assuming that the secondary abstraction reactions of CH_3D^+ proceed with the same rate as those of the CH_4^+ ion and accounting for other uncertainties, an upper limit of the rate coefficient, $k < 1 \times 10^{-12}\,cm^3 s^{-1}$, has been determined for reaction (2a) (see Table 1).

3.3 Collisions of CH_5^+ with HD

Finally, we present experimental results for collisions of protonated methane, CH_5^+, with HD. In extensive measurements no hint has been obtained that the exchange reaction

$$CH_5^+ + HD \quad \rightarrow \quad CH_4D^+ + H_2 \tag{3a}$$
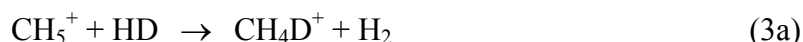
takes place at low temperatures. As can be seen from Fig. 4, initially injected CH_5^+ ions disappear slowly due to radiative and ternary association, i.e., via

$$CH_5^+ + HD \quad \rightarrow \quad CH_5^+ \cdot\cdot HD \tag{3b}$$
$$CH_5^+ \cdot\cdot HD + HD \quad \rightarrow \quad CH_5^+ \cdot\cdot (HD)_2 \text{ etc.} \tag{3c}$$

A rather high HD number density of $[HD] = 1.7 \times 10^{13}$ cm^{-3} has been used in the example shown in Fig. 4. In addition the storage time was extended up to 4 s for further increasing the sensitivity. In order to concentrate on the dominant association processes, and to find a limit for the deuteration reaction (3a), some less important trace ions such as $m = 19$ u, 21 u, and 24 u have been omitted in the plot but not in the evaluation. Inspection shows that CH_5^+ is growing in the HD bath according to reactions (3b) and (3c). At the high number density used in this experiment, association is dominated by three-body processes. The effective rate coefficients for reactions (3b) and (3c), i.e., the product $k^* = k_3[HD]$, are determined from comparisons with numerical simulations to be both $k^* = 5.8 \times 10^{-15}$ cm^{3}s^{-1} (see fit in Fig. 4). Measurements at different HD number densities yield for the association reaction (3b) both the radiative and the ternary rate coefficients, $k_r = 2 \times 10^{-16}$ cm^{-3}s^{-1} and $k_3 = 2.9 \times 10^{-28}$ cm^{-6}s^{-1}, respectively. Further details about the association processes of CH_n^+ + HD and H_2 (n=3, 5) have been discussed by Asvany (2004).

To determine the upper experimental limit of the rate coefficient for reaction (3a), dedicated measurements with long trapping time, high HD number density and a rather large number of CH_5^+ ions have been conducted. As can be seen in Fig. 4, there is a minor amount of CH_4D^+ ions present in the trap. This fraction is most probably originating from CH_3D^+ or $^{13}CH_4^+$ injected with the primary beam ($m = 17$ u). These ions react very fast to CH_4D^+ in a step similar to reaction (2c). The CH_3D^+ ions in the primary beam are generated in the ion source due to some back-streaming of HD from the trap. In Fig. 4, there is no increase of an CH_4D^+-signal which could be attributed to the deuteration step (3a). In total, the CH_4D^+ ions rather disappear due to secondary reactions, namely association similar to reaction (3b). Assuming equal association rates for CH_4D^+ and CH_5^+ leads to the simulation (solid line) for the CH_4D^+ contribution shown in Fig. 4. Taking the experimentally determined standard deviation of the decay rate of CH_4D^+ into account, one obtains an upper limit for the rate coefficient for deuteration of CH_5^+, reaction (3a), $k < 5 \times 10^{-18}$ cm^{3}s^{-1}. This value is included in Table 1 as upper limit for this reaction.

4. Discussion

The systematic experimental study on the deuteration of CH_n^+ (n = 3-5) ions in collisions with HD reveals fast (CH_3^+) and slow (CH_4^+ and CH_5^+) deuteration processes which, at first glance, can be predicted using the simple rule given by Henchman *et al.* (1988). In particular the slow reactions (2a) and (3a) are in agreement with the expectations from the model as they give a yes or no answer when the rate coefficient is as small as found. This is not so for the fast reaction. Especially the differences between the results obtained with pure HD and the previous measurements summarized by Gerlich & Schlemmer (2002) need some thoughts beyond the level of the model.

4.1 CH_3^+ + HD

The effective sequential deuteration of CH_3^+ in HD found in this study can be described by assuming that a strongly bound collision complex is formed (e.g. 198 kJ/mol without zero point energy as reported by Maluendes *et al.* (1992)). This complex is a hypercoordinated carbocation, a molecule which has been subject of many experimental and theoretical investigations (see for example Sefcik, Henis & Gaspar 1974; Komornicki & Dixon 1987; Müller *et al.* 1997; Marx & Parrinello 1999; or White *et al.* 1999) since its first mass spectrometric detection in 1952. Most of these investigations show that there are only negligibly small barriers to the scrambling movements of H- or D-atoms. Re-

cent theoretical calculations confirm the near equivalence of the H-atoms, obtaining a barrier height of only ~3.4 kJ/mol (Müller *et al.* 1997) for the C_{2v}-transition between two minima of C_s symmetry. Since this molecule is already very floppy in its ground state, it is not easy to envision that dynamical effect can restrict the H-D scrambling, one exception may be complexes with large total orbital angular momenta.

Using a simple statistical counting model, one expects from a decay of the CH_4D^+ collision complex a 40 % chance to get $CH_3^+ + HD$ products and a 60 % chance to get a deuterated ion, $CH_2D^+ + H_2$. In the experiment deuteration is even more efficient than this simple counting of outcomes suggests. Maluendes *et al.* (1992) have proposed another simple model for deuteration reactions with HD by treating separately the entrance and the exit channel, which can be reached via a transition state. Starting from the transition state, such a system can either deuterate (probability: x < 1) or fall back into the entrance complex (probability: 1-x). However, in the latter case due to the low collision energy and the large phase space being available for the entrance complex, the system has only a small chance to decompose back into reactants. Therefore it reaches the transition state over and over again until finally the deuterated ion is formed. In fact, the presently measured rate coefficients for pure HD turn out to be 10 – 20 % larger than the Langevin limiting value. HD possesses a dipole moment, an anisotropic polarizability and, most importantly, a permanent quadrupole moment all contributing in addition to the long range ion-induced dipole interaction. Quantitatively, the dipole moment of HD (8.51×10^{-4} debye, see Thorson *et al.* (1985)) is too small to be of importance, while the quadrupole moment is known to influence the capture cross section, especially if hydrogen is in its rotational ground state. Of importance for the long range interaction and for orienting the HD is also the fact that the center of mass and center of charge is separated in HD. A detailed statistical calculation has to account for all this.

As already indicated above rate coefficients for reaction (1a) have also been determined by analyzing data from trapping experiments, performed with H_2, containing only traces of HD in its natural abundance, $[HD]/[H_2] = 3 \times 10^{-4}$ (Gerlich & Schlemmer 2002, Gerlich 1995). These experimental data which have been obtained with the same apparatus as the new results, have been critically reevaluated and are included in Table 1. Most surprising is the result that relaxation of CH_3^+ in p-H_2 reduces the H-D exchange efficiency by a factor 4 while the corresponding experiment with n-H_2 leads to a result in agreement with the rate coefficient measured with pure HD. The rather large errors are a consequence of the complicated reaction scheme which involves p-H_2, o-H_2 and HD as reaction partners and a variety of competing reactions and inelastic collisions. In the reevaluation, deuteration of CH_5^+ has been completely switched off in accordance with the results of the present study. It also was tested, that a faster backward process (reverse of reaction (1a)) could not lead to the necessary increase of the rate coefficient for the forward reaction. In addition a variety of possible experimental artifacts have been discussed and excluded as potential cause for the observed differences such as depletion of HD by condensation in the para hydrogen generator or any type of segregation of H_2 and HD in the trap itself.

The difference between the present and the previous rate coefficients for reaction (1a) given in Table 1, must be a consequence of the relaxation of the stored CH_3^+ ions in the ambient p-H_2. For example, a well-understood result from 10 K trapping experiments (Gerlich 1995) is the dependence of the lifetime of $CH_3^+ \cdot H_2$ collision complexes on the ratio of the ortho to para hydrogen prevailing in the trap. In the case of nearly pure p-H_2, the mean complex lifetime is 386 ns, much longer than in the case of n-H_2, 123 ns. In analogy one would also expect that the $CH_3^+ \cdot HD$ complexes live longer in the para-

hydrogen environment which would lead, in contrast to the experiment, to more scrambling. Also from a point of view of energetics, there are no obvious reasons for restricting the H-D exchange. Reaction (1a) is so exothermic (370 K), that many product states can be excited. Remain the specific populations of the para and ortho form of CH_3^+. Inspection of the low lying rotational states (Crofton *et al.* 1988) reveals that there are, for pure p-CH_3^+, at maximum two states accessible at 15 K. Note that the rotational ground state of p-CH_3^+ is forbidden by symmetry. In contrast, relaxation of CH_3^+ in n-H_2 can lead to higher rotational states of n-CH_3^+. If there is no He buffer gas present, also the process of energy pooling explained by Gerlich *et al.* (2002) for H_3^+ may play a role. Nonetheless it is very unlikely that these small changes in internal energy of the reactant ions are the reason for the difference in reactivity.

In summary it is speculated that the restrictions imposed by the exchange symmetry and the conservation of total nuclear spin reduce the H - D exchange efficiency in the para-environment. Only a complete statistical calculation accounting properly for all symmetry selection rules may solve the problem as emphasized recently by Gerlich (2004). In order to stimulate such theoretical activities, more systematic experimental tests are planned based on a systematic variation of well-defined amounts of HD and o-H_2 added to the p-H_2 target gas or on separating relaxation and reaction by using a pulsed HD gas inlet. In addition, laser induced reactions (Schlemmer et al. 1999, 2002) shall be used to probe *in the trap* the stationary population of the ortho and para forms of CH_3^+ and, potentially, determine state-specific rate coefficients.

4.2 CH_4^+ and CH_5^+ + HD

The results for the other two systems, studied in this work, seem to be easier to understand. Obviously the $CH_4^+ \cdot HD$ collision complex decays rather quickly into the exothermic channels (2b,c) leaving no chances for H-D exchange. Surprising is, however, that channel (2c) dominates. Also this may be caused by symmetry selection rules. More information on this system can be found in Asvany *et al.* (2004).

The upper limit of the H - D exchange rate coefficient determined for low temperature collisions of CH_5^+ with HD indicates that the approaching HD cannot penetrate into the "closed shell" of the CH_5^+ sphere. At maximum one out of 10^8 collisions may lead to deuteration although collision complexes are formed with life times of a few ns corresponding to thousands of vibrational periods, as derived from ternary association (Asvany 2004). This complex must be considered as a cluster ion, where the HD molecule is bound only by a rather weak van der Waals forces to the central CH_5^+ ion core. Apparently the inner and outer H-atoms in this system are not at all equivalent and scrambling probably would require the breaking of the outer HD-bond. The barrier for this process is apparently too high to occur. The other possible reaction mechanism mentioned briefly in the introduction would involve the replacement of an H_2 unit by HD which was suspected to be possible due to the fluxional nature of CH_5^+. This can be ruled out by the present experiment. It may even be that the presence of the HD in the entrance channel complex leads to a slight structural rearrangement of the CH_5^+ such that exchange becomes even more restricted. Infrared spectroscopy of $CH_5^+ \cdot (H_2)_n$ by Boo *et al.* (1995) and calculations have indicated that the presence of solvating H_2 leads to a more rigid structure of the CH_5^+ core. This leads to the interesting question, whether there is any chance that the stable $CH_5^+ \cdot HD$ cluster ion isomerizes spontaneously to the energetically favored $CH_4D^+ \cdot H_2$ structure. Spectroscopy on stored ions or chemical probing could reveal such processes and help to find reaction paths which would need minutes instead of ns.

5. Interstellar implications

Fractionation of deuterium in interstellar clouds is a complex affair. There are a variety of secondary exchange reactions, all of which compete with many other thermal and non-thermal processes such as radiative association, grain-surface reactions, mantle evaporation, dissociative recombination (Millar *et al.* 1989, Roberts & Millar 2000a, 2000b; Millar 2002). It was mentioned in the introduction that a crucial point is the use of the proper temperature dependence of the rate coefficients. A recent example is the unexpected discovery of a large rate coefficient for hydrogen abstraction in $CH_4^+ + H_2$ collisions at 15 K. The results from the present study clearly show that, in addition, it is a must to study the influence of the ortho and para-forms of the involved molecules both on inelastic collisions (energy pooling) and on H - D or D - H scrambling processes. It can be foreseen that, finally, state specific rate coefficients are required for understanding in detailed the interactions of hydrogen and deuterium containing molecules with HD. The central role of conserving the total nuclear spin is best illustrated by the inefficiency of ortho - para transitions in scrambling $H^+ + H_2$ collisions (Gerlich 1989); however, we are still not yet able to fully understand the more complex reactions presented here.

A variety of important conclusions can be drawn from the present results. There are presently no consequences concerning the role of CH_5^+ since this ion has been known by chemists and modelers to be inert toward D-atom exchange in collisions with HD at room temperature. In accordance with theoretical considerations (Maluendes *et al.* 1992) the present work confirms that this also holds at the low temperatures prevailing in the interstellar medium. If deuterated CH_5^+ would be observed at all it may have been formed via radiative association of deuterated CH_3^+ or H_2. Also formation of $CH_5^+ \cdot HD$ via radiative association (Asvany 2004) is possible although probably too slow ($k_r = 2 \times 10^{-16} \, cm^3 s^{-1}$) since CH_5^+ is efficiently destroyed via dissociative recombination with electrons leading to CH_4 and CH_3 as described by Smith (1992). An interesting related project which is ongoing in this laboratory is the low temperature outcome of $CH_5^+ + H$ or D collisions. The question whether scrambling or CH_4^+ formation prevails, is still open.

Important for interstellar and circumstellar chemistry are the experimental findings for the methane cation, CH_4^+, for which only data measured by Adams & Smith (1977) at room temperature have been available up to now. Our measurements (Asvany *et al.* 2004) show that the reaction of CH_4^+ with HD and H_2 has a strong negative temperature dependence with rate coefficients at least one order of magnitude higher at 10 K than at room temperature. Inclusion of this new data in models (Le Teuff *et al.* 2000) will certainly have an impact on future model calculations of interstellar gas-phase chemistry.

Deuteration of CH_3^+ has been found to be rather fast and this ion will probably keep, together with H_3^+ and $C_2H_2^+$, its central role in passing the interstellar deuterium, available as HD, to more complex molecules via gas phase reactions (Millar 2002, Gerlich & Schlemmer 2002). Due to their higher exothermicity, the deuterated hydrocarbon ions are of special importance for higher temperature interstellar clouds (e.g. Orion, $T = 70$ K, Millar *et al.* (1989)). In order to get the models more realistic, the experimentally determined rate coefficients have to be included, of course in addition to the gas-grain interaction. For the recently measured reaction rate coefficients for forming and destroying H_2D^+ (Gerlich *et al.* 2002) this already has been done by Roberts *et al.* (2002). Remains the question which value one should take for reaction (1a). The result obtained with pure HD is a factor 1.3 higher than used by Millar *et al.* (1989). Nonethe-

less it is not recommended to use this new value since it is rather certain that the rotational population of the CH_3^+ ions in interstellar space is different from the present 15 K experiment using He as cooling gas. It is also questionable whether thermalization in p-H_2 really leads to an ion ensemble which is representative for dense interstellar clouds. If one assumes that cold p-CH_3^+ ions dominate in dense interstellar clouds the much smaller rate coefficient given in Table 1 should be used in chemical model calculations.

Acknowledgments

References

Adams, N.G., & Smith, D. 1977, Chem. Phys. Lett., **47**, 383

Asvany, O., Savić, I., Schlemmer, S., & Gerlich, D. 2004, Chem. Phys., **298**, 97

Asvany, O., PhD thesis, 2004, University of Technology, Chemnitz, to be published

Barlow, S.E., & Dunn, G.H. 1987, Int. J. Mass Spectrom. Ion Proc., **80**, 227

Bates, D.R. 1987, ApJ, **312**, 363

Bates, D.R. 1991, ApJ, **375**, 833

Boo, D.W. , Liu, Z.F. , Suits, A.G., Tse, J.S., & Lee, Y.T. 1995, Science, **269**, 57

Crofton, M.W., Jagod, M.-F., Rehfuss, B.D., Kreiner, W.A. & Oka, T., 1988, J. Chem. Phys., **88**, 666

Ervin, K.M., & Armentrout, P.B. 1985, J. Chem. Phys., **83**, 166

Gerlich, D., Kaefer, G. 1989, ApJ. 347, 849

Gerlich, D. 1990, J. Chem. Phys. **92,** 2377

Gerlich, D. 1992, Adv. in Chem. Phys. LXXXII, 1

Gerlich, D., Horning, S. 1992, Chemical Reviews 92, 1509

Gerlich, D. 1993, J. Chem. Soc. Faraday Trans. 89, 2199

Gerlich, D. 1994 in "Molecules and Grains in Space" ed. by I. Nenner, AIP Press, New York, 489

Gerlich, D. 1995, Physica Scripta, **T59**, 256

Gerlich, D., Herbst, E., & Roueff E. 2002, PSS, **50,** 1275

Gerlich, D., & Schlemmer, S. 2002, PSS, **50,** 1287

Gerlich, D. 2004, in "Symposium on Atomic, Cluster and Surface Physics", edited by G. Capozza and P. Casavecchia, IL-2

Henchman, M., Paulson, J.F., Smith, D., Adams, N.G., & Lindinger, W. 1988, in Rate coefficients in Astrochemistry, ed. T.J. Millar & D.A. Williams, 201

Herbst, E., DeFrees, D.J., Talbi, D., Pauzat, F., Koch, W., & McLean, A.D. 1991, J. Chem. Phys., **94**, 7842

Komornicki, A., & Dixon, D.A. 1987, J. Chem. Phys., **86**, 5625

Lis, D.C., Roueff, E., Gerin, M., Phillips, T.G., Coudert, L.H., van der Tak, F.F.S., & Schilke, P. 2002, ApJ, **571**, L55

Maluendes, S.A., McLean, A.D., & Herbst, E. 1992, ApJ, **397**, 477

Marx, D., & Parrinello, M. 1999, Science, **284**, 59

Marx, D., & Parrinello, M. 1999a, Science, **286**, 1051

Millar, T. J. 2002, PSS, **50**, 1189

Millar, T.J., Bennett, A., & Herbst, E. 1989, ApJ, **340**, 906

Müller, H., Kutzelnigg, W., Noga, J., & Klopper, W. 1997, J. Chem. Phys., **106**, 1863

Quack, M. 1977, Mol. Phys., **34**, 477

Parise, B. Castets, A., Herbst, E., & Caux, E. 2004, A&A, **416**, 159

Roberts, H., & Millar, T.J. 2000a, A&A, **361**, 388

Roberts, H., & Millar, T.J. 2000b, A&A, **364**, 780

Roberts, H., Herbst, E., & Millar, T.J. 2002, MNRAS, **336**, 283

Schlemmer, S., Kuhn, T., Lescop, E., & Gerlich, D. 1999, Int. J. Mass Spectrom. Ion Proc., **185**, 589

Schlemmer, S. Lescop, E., von Richthofen, J., Gerlich, D. & Smith, M. 2002, J. Chem. Phys. **117**, 2068

Sefcik, M.D., Henis, J.M.S., & Gaspar, P.P. 1974, J. Chem. Phys., **61**, 4321

Smith, D., Adams, N.G., & Alge, E. 1982a, J. Chem. Phys., **77**, 1261

Smith, D., Adams, N.G., & Alge, E. 1982b, ApJ, **263**, 123

Smith, D. 1992, Chem. Rev., **92**, 1473

Smith, M. A., Schlemmer, S., Richthofen, J. v., and Gerlich, D. 2002, ApJ Letters, **578**, 87

Le Teuff, Y.H., Millar, T.J., & Marwick, A.J. 2000, A&AS, **146**, 157

Thorson, W.R., Choi, J.H., & Knudson, S.K. 1985, Phys. Rew. A, **31**, 22

Vastel, C., Phillips, T.G., & Yoshida, H. 2004, ApJ, **606**, L127

White, E.T., Tang, J., & Oka, T. 1999, Science, **284**, 135

Wright, C.M., Van Dishoeck, E.F., Cox, P, Sidher, S.D., & Kessler, M.F. 1999, ApJ, **515**, L29

Tables

Table 1. Rate coefficients for various deuteration reactions at $T = 15$ K, for details see text.

| Reaction	k / cm^3 s^{-1}	Remarks
$CH_3^+ + HD \rightarrow CH_2D^+ + H_2$	$(1.65 \pm 0.10) \times 10^{-9}$	ions 350 K source target: pure HD
n - $CH_3^+ + HD \rightarrow CH_2D^+ + H_2$	$(1.5 \pm 0.8) \times 10^{-9}$	relaxation of CH_3^+ in n-H_2
p - $CH_3^+ + HD \rightarrow CH_2D^+ + H_2$	$(0.4 \pm 0.2) \times 10^{-9}$	relaxation of CH_3^+ in p-H_2
$CH_2D^+ + HD \rightarrow CHD_2^+ + H_2$	$(1.59 \pm 0.10) \times 10^{-9}$	pure HD
$CHD_2^+ + HD \rightarrow CD_3^+ + H_2$	$(1.50 \pm 0.10) \times 10^{-9}$	pure HD
$CH_4^+ + HD \rightarrow CH_3D^+ + H_2$	$< 1 \times 10^{-12}$	Deuteration
$CH_4^+ + HD \rightarrow CH_4D^+ + H$ 32 % $\rightarrow CH_5^+ + D$ 68 %	$(4.5 \pm 0.2) \times 10^{-10}$	D-abstraction H-abstraction
$CH_5^+ + HD \rightarrow CH_4D^+ + H_2$	$< 5 \times 10^{-18}$	Deuteration
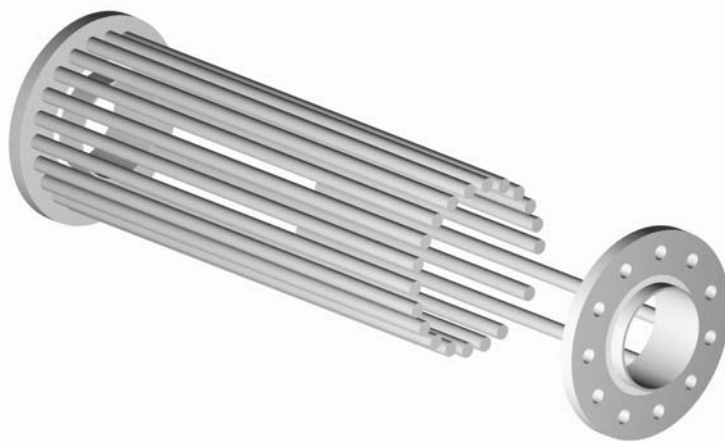
Fig. 1. Schematic drawing of the 22-pole ion trap consisting of 22 stainless steel rods, each 1 mm in diameter and 36 mm long, circumscribing a circle of 10 mm diameter. As indicated, 11 rods fit into holes of the left ring, 11 into the right one. These two electrodes are connected to the two ends of an rf coil providing the two phases of the rf. Inside of these holders, there is on each side an electrode, operated with pulsed dc voltages. They are used for filling the trap with primary ions and for extracting the remaining primaries and products towards the detector. The structure is surrounded by a copper box (not shown) which can be cooled to 15 K via a cold head.
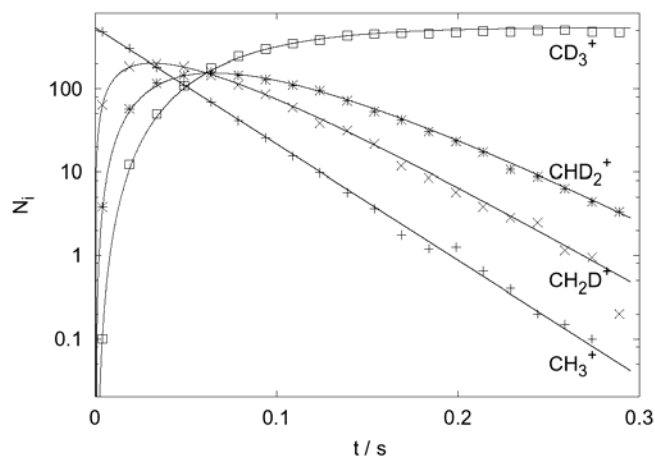

Fig. 2. The change of the number of different ions, $N_i(t)$, extracted from the trap per iteration after a certain storage time t, shows the sequential deuteration of CH_3^+. The nominal temperature was $T = 15\,K$ and pure HD with a number density of $[HD] = 1.8 \times 10^{10}\,cm^{-3}$ was used as reactant gas. After 0.3 s, nearly all ions are converted into CD_3^+. The lines are numerical solutions of a suitable rate equation system fitted to the data. The resulting rate coefficients are listed in Table 1.
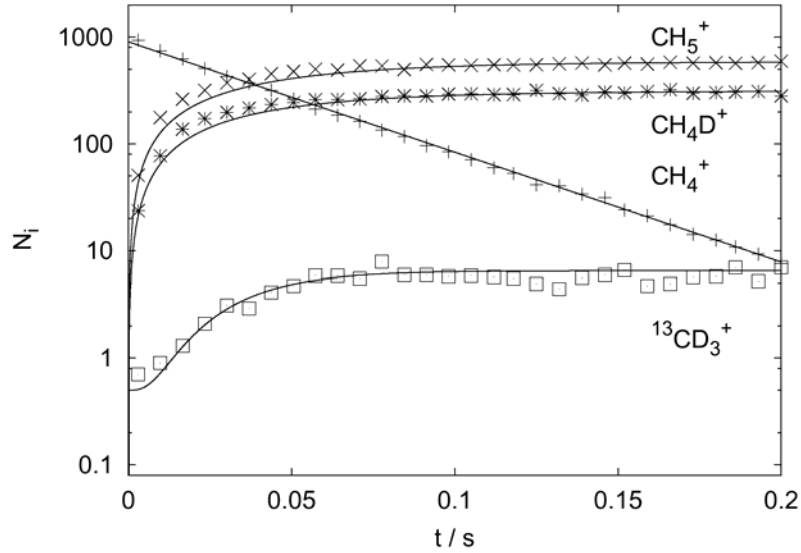
Fig. 3. CH_4^+ stored at $T = 15$ K and $[HD] = 5 \times 10^{10}$ cm^{-3}. As can be seen from the $N_i(t)$, H-atom abstraction is with 68% the dominant channel leading to the formation of CH_5^+. Only 32% of the reactive collisions yield the deuterated product CH_4D^+. The total rate coefficient at this temperature is 4.5×10^{-10} cm^{3}s^{-1}. The $^{13}CD_3^+$-signal comes from sequential deuteration of $^{13}CH_3^+$-impurities contained in the injected $^{12}CH_4^+$ beam ($m = 16$ u).
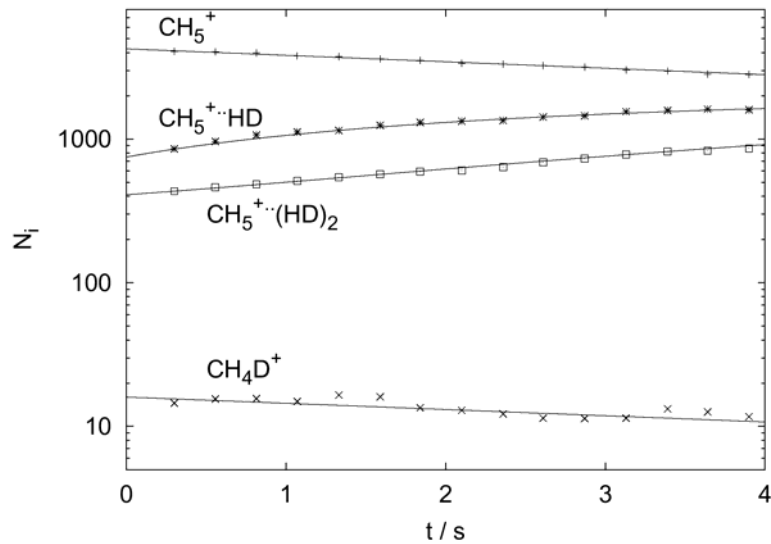
Fig. 4. CH_5^+ stored at $T = 15$ K and $[HD] = 1.72 \times 10^{13}$ cm^{-3}. Two subsequent association steps to $CH_5^+ \cdot \cdot (HD)$ and $CH_5^+ \cdot \cdot (HD)_2$ can be observed. The CH_4D^+ (or also $^{13}CH_5^+$) signal stems merely from injected CH_3D^+-impurities (or $^{13}CH_4^+$). The contribution to form ions with $m = 18$ u via deuteration of CH_5^+ (reaction (3a)) is less than 5×10^{-18} cm^{3}s^{-1}. Some other minor impurities stored in the trap have been omitted in this figure for simplicity.

Bibliography

[ada77] N.G. Adams, D. Smith: *Reactions of Hydrocarbon Ions with Hydrogen and Methane at 300K*, Chem. Phys. Lett., **47**, 383, (1977)

[asm03] K.R. Asmis, N.L. Pivonka, G. Santambrogio, M. Brümmer, C. Kaposta, D.M. Neumark, L. Wöste: *Gas-Phase Infrared Spectrum of the Protonated Water Dimer*, Science, **299**, 1365, (2003)

[ber03] E.A. Bergin: *Molecules and the Process of Star Formation,* ECRA Vol. 5, Ed. C. Boutron, (2003)

[boo95] D.W. Boo, Z.F. Liu, A.G. Suits, J.S. Tse, Y.T. Lee: *Dynamics of Carbonium Ions solvated by Molecular Hydrogen: $CH_5^+(H_2)_n$ (n=1,2,3)*, Science, **269**, 57, (1995)

[boo95a] D.W. Boo, Y.T. Lee: *Infrared specctroscopy of the molecular hydrogen solvated carbonium ions, $CH_5^+(H_2)_n$ (n=1-6)*, J. Chem. Phys., **103**, 520, (1995)

[cha01] C. Chaudhuri, Y.S. Wang, J.C. Jiang, Y.T. Lee, H.C. Chang, G. Niedner-Schatteburg: *Infrared spectra and isomeric structures of hydroxide ion-water clusters $OH^-(H_2O)_{1-5}$: a comparison with $H_3O^+(H_2O)_{1-5}$*, Molecular Physics, **99**, 1161, (2001)

[cun72] A.J. Cunningham, J.D. Payzant, P. Kebarle: *A Kinetic Study of the Proton Hydrate $H^+(H_2O)_n$ Equilibria in the Gas Phase*, J. Am. Chem. Soc., **94**, 7627, (1972)

[cur01] J. Curtis, K.D. Froyd, E.R. Lovejoy: *Cluster Ion Thermal Decomposition (I): Experimental Kinetics Study and ab Initio Calculations for $HSO_4^-(H_2SO_4)_x(HNO_3)_y$*, J. Phys. Chem. A, **105**, 10867 , (2001)

[daw76] P.H. Dawson ed.: *Quadrupole Mass Spectrometry,* Elsevier, Amsterdam (1976)

[dis99] E.F. van Dishoeck, M.R. Hogerheijde: *Models and Observations of the Chemistry near young stellar Objects,* Review chapter in: The origin of stars and planetary systems, 97, (1999)

[dal60] N.R. Daly: *Scintillation Type Mass Spectrometer Ion Detector*, Rev. Sci. Instr., **31**, 3, (1960)

[dul96] W.W. Duley: *Molecular Clusters in Interstellar Clouds*, Astrophys. J., **471**, L57, (1996)

[dun91] R.C. Dunbar: *Kinetics of low-intensity infrared laser photodissociation. The thermal model and application of the Tolman theorem*, J. Phys. Chem., **95**, 2537, (1991)

[dun94] R.C. Dunbar: *Kinetics of Thermal Unimolecular Dissociation by Ambient Infrared Radiation*, J. Phys. Chem., **98**, 8705, (1994)

[ger92] D. Gerlich: *Inhomogeneous RF fields: A versatile Tool for the Study of processes with Slow Ions*, in: State-Selected and State-to-State Ion-Molecule Reaction Dynamics, **LXXXII**, 1, (1992)

[ger92a] D. Gerlich, S. Horning: *Experimental Investigations of Radiative Association Processes as Related to Interstellar Chemistry*, Chem. Rev., **92**, 1509, (1992)

[ger93] D. Gerlich: *Experimental Investigations of Ion-Molecule Reactions Relevant to Interstellar Chemistry*, J. Chem. Soc., Faraday Trans., **89**, 2199, (1993)

[ger02a] D. Gerlich, E. Herbst, E. Roueff: $H_3^+ + HD \leftrightarrow H_2D^+ + H_2$: *Low-temperature laboratory measurements and interstellar implications*, Planetary and Space Science, **50**, 1275, (2002)

[ger02b] D. Gerlich, S. Schlemmer: *Deuterium fractionation in gas phase reactions measured in the laboratory*, Planetary and Space Science, **50**, 1287, (2002)

[gns96] G. Niedner-Schatteburg: *Struktur und Reaktivität ionischer Metall und Molekülcluster mittels Fourier-Transform-Ionen-Cyclotron-Resonanz-Massenspektrometrie*, Habilitationsschrift TU München, (1996)

[hau97] E. Haufler: *Niederenergetische Elektronen- und Protonen-Transfer Prozesse, Experimente zur Stoßdynamik in Hochfrequenz-Ionenführungsfeldern*, Dissertation TU Chemnitz, (1997)

[her65] G. Herzberg: *Molecular Spectra and Molecular Structure I. Spectra of Diatomic Molecules*, Van Nostrad, (1965)

[hol96] J.M. Hollas: *Modern Spectroscopy*, Wiley (1996)

[hun98] E.P.L. Hunter, S.G. Lias: *Evaluated Gas Phase Basicities and Proton Affinities of Molecules: An Update*, J. Phys. Chem. Ref. Data, **27**, 413, (1998)

[jia00] J.C. Jiang, Y.S. Wang, H.C. Cheng, S.H. Lin, Y.T. Lee, G. Niedner-Schatteburg, H.C. Chang: *Infrared Spectra of $H^+(H_2O)_{5-8}$ Clusters: Evidence for Symmetric Proton Hydration*, J. Am. Chem. Soc., **122**, 1398, (2000)

[jia01] The given vibrational frequencies were calculated by Dr.J.C. Jiang at IAMS (Taipei) using the Gaussian98 package at the B3LYP/6-31+G* level

[jon97] R.M. Jones, D. Gerlich, S.L. Anderson: *Simple radio-frequency power source for ion guides and ion traps*, Rev. Sci. Instr., **68**, 9, (1997)

[jon00] R.M. Jones, S.L. Anderson: *Simplified radio-frequency generator for driving ion guides, traps and other capacitive loads*, Rev. Sci. Instr., **71**, 4225, (2000)

[kae89] G. Kaefer: *Stoßkomplexe in der Umgebung der Dissoziationsgrenze: Experimentelle Untersuchungen in einem temperaturvariablen Hf-Ionenspeicher,* Dissertation Uni Freiburg, (1989)

[kai02] R.I. Kaiser: *Experimental Investigation on the Formation of Carbon-Bearing Molecules in the Interstellar Medium via Neutral-Neutral Reactions,* Chem. Rev., **102**, 1309, (2002)

[kim74] J.K. Kim, L.P. Theard, W.T. Huntress Jr.: *ICR studies of some hydrogen abstraction reactions: $X^+ + H_2 \rightarrow XH^+ + H^*$,* J. Chem. Phys., **62**, 45, (1974)

[kom87] A. Komornicki, D.A. Dixon: *Structure, vibrational spectrum, and energetics of the CH_5^+ ion. A theoretical investigation,* J. Chem. Phys., **86**, 5625, (1987)

[laf98] J.M Laffetrty, Ed.: *Foundations of Vacuum Science and Technology,* Wiley, (1998)

[lau82] Y.K. Lau, S. Ikuta, P. Kebarle: *Thermodynamics and Kinetics of the Gas-Phase Reactions $H_3O^+(H_2O)_{n-1} + H_2O = H_3O^+(H_2O)_n$,* J. Am. Chem. Soc., **104**, 1462, (1982)

[les00] E. Lescope: *Laserinduzierte Prozesse im System $C_2H_2^+ + H_2$,* Dissertation TU Chemnitz, (2000)

[lev87] R.D.Levine, R.B. Bernstein: *Molecular Reaction Dynamics and Chemical Reactivity,* Oxford University Press, (1987)

[lid95] D.R. Lide, Ed.: *Handbook of Chemistry and Physics,* 76th edition, CRC Press (1995)

[lis02] D.C. Lis, E. Roueff, M. Gerin, T.G. Phillips, L.H. Coudert, F.F.S. van der Tak, P. Schilke: *Detection of triply deuterated Ammonia in the Barnard 1 Cloud,* Astrophys. J., **571**, L55, (2002)

[lov00] E.R. Lovejoy, R. Bianco: *Temperature Dependence of Cluster Ion Decomposition in a Quadrupole Ion Trap,* J. Phys. Chem. A, **104**, 10280, (2000)

[lov01] E.R. Lovejoy, J. Curtis: *Cluster Ion Thermal Decomposition (II): Master Equation Modeling in the Low-Pressure Limit and Fall-Off Regions. Bond Energies for $HSO_4^-(H_2SO_4)_x(HNO_3)_y$,* J. Phys. Chem. A, **105**, 10874, (2001)

[luc01] A. Luca: *Neuartige Speicherexperimente zur Untersuchung der Bildung atomarer und molekularer Strukturen,* Dissertation TU Chemnitz, (2001)

[lui85] J.A. Luine, G.H. Dunn: *Ion-Molecule Reaction Probabilities Near 10K,* Astrophys. J., **299**, L67, (1985)

[mag91] T.F. Magnera, Donald E. David, J. Michl: *The first twenty-eight gas-phase proton hydration energies,* Chem. Phys. Lett., **182**, 363, (1991)

[mar98] A.G. Marshall, C.L. Hendrickson, G.S. Jackson: *Fourier Transform Ion Cyclotron Resonance Mass Spectrometry: A Primer*, Mass Spectrometry Rewievs, **17**, 1, (1998)

[mar99] D. Marx, M. Parrinello: *CH_5^+: The Cheshire Cat Smiles*, Science, **284**, 59, (1999)

[meo86] M. Meot-Ner, C.V. Speller: *Filling of Solvent Shells about Ions. 1. Thermochemical Criteria and the Effects of Isomeric Clusters*, J. Phys. Chem., **90**, 6616, (1986)

[mil89] T.J. Millar, A. Bennett, E. Herbst: *Deuterium fractionation in dense interstellar clouds*, Astrophys. J., **340**, 906, (1989)

[mil02] T.J. Millar: *Modeling deuterium fractionation in interstellar clouds*, Planetary and Space Science, **50**, 1189, (2002)

[mks90] Manual spinning rotor gauge SRG2 from company MKS

[mul97] H. Müller, W. Kutzelnigg, J. Noga, W. Klopper: *CH_5^+: The story goes on. An explicitly correlated coupled-cluster study*, J. Chem. Phys., **106**, 1863, (1997)

[och00] J.W. Ochterski: *Thermochemistry in Gaussian,* download of whitepaper from www.gaussian.com, (2000)

[oku86] M. Okumura, L.I. Yeh, J.D. Myers, Y.T. Lee: *Infrared spectra of the cluster ions $H_7O_3^+ \cdot H_2$ and $H_9O_4^+ \cdot H_2$*, J. Chem. Phys., **85**, 2328, (1986)

[ola94] G. Olah: *My Search for Carbocations and Their Role in Chemistry,* www.nobel.se/chemistry/laureates/1994/

[par04] B. Parise, A. Castets, E. Herbst, E. Caux, C. Ceccarelli, I. Mukhopadhyay, A. Thielens: *First detection of triply-deuterated methanol*, Astron. Astrophys., **416**, 159, (2004)

[pau90] W. Paul: *Electromagnetic traps for charged and neutral particles*, Rev. of Modern Physics, **62**, 531, (1990)

[pau95] W. Paul, B. Lüecke, S.Schlemmer, D. Gerlich: *On the dynamics of the reaction of positive hydrogen cluster ions (H_5^+ to H_23^+) with para and normal hydrogen at 10K*, Int.J. Mass Spectrom. Ion Proc., **150**, 373, (1995)

[pau96] W. Paul: *Reaktionsdynamik schwach gebundener ionischer Cluster,* Dissertation, TU Chemnitz, (1996)

[pfe00] Manual for turbo pump TMU 400M company Pfeiffer

[pir97] V. Pirronello, C. Liu, L. Shen, G. Vidali: *Laboratory Synthesis of Molecular Hydrogen on Surfaces of Astrophysical Interest*, Astrophys. J., **475**, L69, (1997)

[ric02] J. v. Richthofen: *Untersuchungen zu dem Ionensystem HCO^+/HOC^+,* Dissertation TU Chemnitz, (2002)

[rob02] personal communication by email with Michael Robey, CIL Inc., USA

[ros02] J.E. Roser, G. Manicò, V. Pirronello, G. Vidali: *Formation of Molecular Hydrogen on Amorphous Water Ice: Influence of Morphology and Ultraviolet Exposure*, Astrophys. J., **581**, 276, (2002)

[row84] B.R. Rowe, G. Dupeyrat, J.B. Marquette, P. Gaucherel: *Study of the reactions $N_2^+ + 2N_2 \rightarrow N_4^+ + N_2$ and $O_2^+ + 2O_2 \rightarrow O_4^+ + O_2$ from 20 to 160 K by the CRESU technique*, J. Chem. Phys., **80**, 4915, (1984)

[sch77] H.A. Schwarz: *Gas phase infrared spectra of oxonium hydrate ions from 2 to 5 μ*, J. Chem. Phys., **67**, 5525, (1977)

[sch96] T. Schindler, Ch. Berg, G. Niedner-Schatteburg, V.E.Bondebey: *Protonated water clusters and their black body radiation induced fragmentation*, Chem. Phys. Letters, **250**, 301, (1996)

[sch02] S. Schlemmer, E. Lescop, J. v. Richthofen, D. Gerlich: *Laser Induced Reactions in a 22-Pole Trap: $C_2H_2 + h\nu_3 + H_2 \rightarrow C_2H_3^+ + H$*, J. Chem. Phys., **117**, 2068, (2002)

[sea74] J.Q. Searcy, J.B. Fenn: *Clustering of water on hydrated protons in a supersonic free jet expansion*, J. Chem. Phys., **61**, 5282, (1974)

[sef74] M.D. Sefcik, J.M.S. Henis, P.P. Gaspar: *The methanium ion, CH_5^+. Evidence for the structure of a nonclassical ion from reaction studies by ion cyclotron resonance spectroscopy*, J. Chem. Phys., **61**, 4321, (1974)

[shi93] Z. Shi, J.V. Ford, S. Wei, A.W. Castleman: *Water clusters: Contribution of binding energy and entropy to stability*, J. Chem. Phys., **99**, 8009, (1993)

[sig99] R. Signorell, F. Merkt: *First rotationally resolved spectrum of CH_4^+*, J. Chem. Phys., **110**, 2309, (1999)

[sig00] R. Signorell, M. Sommavilla: *CH_4^+: a fluxional ion?*, J. Electron Spectroscopy, **108**, 169, (2000)

[sor94] A. Sorgenfrei: *Ion-Molekül-Reaktionen kleiner Kohlenwasserstoffe in einem gekühltem Ionen-Speicher*, Dissertation Uni Freiburg, (1994)

[smi79] D. Smith, N.G. Adams: *Recent Advances in Flow Tubes: Measurement of Ion-Molecule Rate Coefficients and Product Distribution*, in: Gas Phase Ion Chemistry, Vol.1, Ed. M.T. Bowers, 1, Academic Press, New York, (1979)

[smi82] D. Smith, N.G. Adams, E. Alge: *Isotope exchange and collisional association in the reaction of CH_3^+ and its deuterated analogs with H_2, HD, and D_2*, J. Chem.Phys., **77**, 1261, (1982)

[smi92] D. Smith: *The Ion Chemistry of Interstellar Clouds*, Chem. Rev., **92**, 1473, (1992)

[teu00] Y.H. Le Teuff, T.J. Millar, A.J. Marwick: *The UMIST database for astrochemistry*, Astron. Astrophys. Suppl. Ser., **146**, 157, (2000)

[tol20] R.C. Tolman: *Statistical Mechanics Applied To Chemical Kinetics*, J. Am. Chem. Soc., **42**, 2506, (1920)

[tun11] Tünnes, Schäl: *Dat Kölsche Dreigestirn,* Kölle (1911)

[wan97] Y.S. Wang, J.C. Jiang, C.L. Cheng, S.H. Lin, Y.T. Lee, H.C. Chang: *Identifying 2- and 3-coordinated H_2O in ion-water clusters by vibrational pre-dissociation spectroscopy and ab initio calculations*, J. Chem. Phys., **107**, 9695, (1997)

[wan01] Y.S. Wang: *Infrared Spectroscopic Studies of Cluster Ions in Radio-Frequency Ion Traps,* Dissertation NTU Taipei, Taiwan, (2001)

[whi99] E.T. White, J. Tang, T. Oka: *CH_5^+: The Infrared Spectrum Observed*, Science, **284**, 135, (1999)

[wut97] M.Wutz, H. Adam, W. Walcher: *Handbuch Vakuumtechnik,* Vieweg, (1997)

[yeh89] L.I. Yeh, M. Okumura, J.D. Myers, J.M. Price, Y.T. Lee: *Vibrational spectroscopy of the hydrated hydronium cluster ions $H_3O^+ (H_2O)_n$ (n=1,2,3)*, J. Chem. Phys., **91**, 7319, (1989)

List of Publications

N. Balucani, O. Asvany, A.H.H. Chang, S.H. Lin, Y.T. Lee, R.I. Kaiser, H.F. Bettinger, P.v.R. Schleyer, H.F. Schaefer III: *Crossed-beam reaction of cyano radicals with hydrocarbon molecules I: Chemical dynamics of cyanobenzene (C_6H_5CN; X^1 A_1) and perdeutero cyanobenzene (C_6D_5CN; X^1 A_1) formation from reaction of $CN(X^2$ Σ^+) with benzene, $C_6H_6(X^1$ A_{1g}), and d_6-benzene, $C_6D_6(X^1$ A_{1g})*, J. Chem. Phys., **111**, 7457-7471, (1999)

N. Balucani, O. Asvany, A.H.H. Chang, S.H. Lin, Y.T. Lee, R.I. Kaiser, H.F. Bettinger, P.v.R. Schleyer, H.F. Schaefer III: *Crossed-beam reaction of cyano radicals with hydrocarbon molecules II: Chemical dynamics of 1,1-cyanomethylallene ($CNCH_3CCCH_2$; X^1 A') formation from reaction of $CN(X^2$ Σ^+) with dimethylacetylene, CH_3CCCH_3 (X^1 A_1)*, J. Chem. Phys., **111**, 7472-7479, (1999)

R.I. Kaiser, J.W. Ting, L.C.L. Huang, N. Balucani, O. Asvany, Y.T. Lee, H. Chan, D. Stranges, D. Gee: *A versatile source to produce high intensity, pulsed supersonic radical beams for crossed beams experiments - the cyano radical, $CN(X^2$ Σ^+), as a case study*, Rev. Sci.Instr., **70**, 4185-4191, (1999)

R.I. Kaiser, O. Asvany, Y.T. Lee, H.F. Bettinger, P.v.R. Schleyer, H.F. Schaefer III: *Crossed beam reaction of phenyl radicals with unsaturated hydrocarbon molecules I: Chemical dynamics of phenylmethylacetylene ($C_6H_5CCCH_3$; X^1 A_1) formation from reaction of $C_6H_5(X^2$ A_1) with methylacetylene, CH_3CCH (X^1 A_1)*, J. Chem. Phys, **112**, 4994-5001, (2000)

R.I. Kaiser, O. Asvany, Y.T. Lee: *Crossed molecular beams investigation of elementary chemical reactions relevant to polycyclic aromatic hydrocarbons (PAHs) in outflow of carbon stars and hydrocarbon rich planetary atmospheres*, Planetary and Space Science, **48**, 483-492, (2000)

N. Balucani, O. Asvany, Y. Osamura, L.C.L. Huang, Y.T. Lee, R.I. Kaiser: *Laboratory investigation the formation of unsaturated nitriles in Titan's atmosphere*, Planetary and Space Science, **48**, 447-462, (2000)

R.I. Kaiser, N. Balucani, O. Asvany, Y.T. Lee in: Astrochemistry: From molecular Clouds to Planetary systems, Y.C. Minh, E.F. van Dishoeck (eds.), *Crossed molecular beam experiments of radical- neutral reactions relevant to the formation of hydrogen deficient molecules in extraterrestrial environments*, IAU Series **197**, 251-264, (2000)

N. Balucani, O. Asvany, A.H.H. Chang, S.H. Lin, Y.T. Lee, R.I. Kaiser, Y. Osamura: *Crossed beam reaction of cyano radicals with hydrocarbon molecules III: Chemical dynamics of vinylcyanide (C_2H_3CN; X^1 A') formation from reaction of $CN(X^2$ Σ^+) with ethylene, $C_2H_4(X^1$ A_g)*, J. Chem. Phys, **113**, 8643-8655, (2000)

L.C.L. Huang, O. Asvany, A.H.H. Chang, N. Balucani, S.H. Lin, Y.T. Lee, R.I. Kaiser, Y. Osamura: *Crossed beam reaction of cyano radicals with hydrocarbon molecules IV: Chemi-*

cal dynamics of cyanoacetylene (HCCCN; $X^1 \Sigma^+$) formation from reaction of CN($X^2 \Sigma^+$) with acetylene, $C_2H_2(X^1 \Sigma_g^+)$, J. Chem. Phys., **113**, 8656-8666, (2000)

N. Balucani, O. Asvany, Y. T. Lee, R.I. Kaiser, N. Galland, Y. Hannachi: *Observation of Borirene from Crossed Beam Reaction of Boron Atoms with Ethylene,* J. Am. Chem. Soc., **122**, 11234-11235, (2000)

N. Balucani, O. Asvany, L.C.L. Huang, Y.T. Lee, R.I. Kaiser, Y. Osamura, H.F. Bettinger, P.v.R. Schleyer, H.F. Schaefer III: *Formation of Nitriles in the Interstellar Medium via reaction of cyano radicals, CN($X^2 \Sigma^+$), with unsaturated hydrocarbons,* Ap.J., **545**, 892-906, (2000)

R.I. Kaiser, C.C. Chiong, O. Asvany, Y.T. Lee, F. Stahl, P.v.R. Schleyer, H.F. Schaefer: *Chemical dynamics of d1-methyldiacetylene (CH_3CCCCD; $X^1 A_1$) and d1-ethynylallene ($H_2CCCH(C_2D)$; $X^1 A'$) formation from reaction of $C_2D(X^2 \Sigma^+)$ with methylacetylene $CH_3CCH(X^1 A_1')$,* J. Chem. Phys., **114**, 3488-3496, (2001)

C.C. Chiong, O. Asvany, N. Balucani, Y.T. Lee, R.I. Kaiser: *Nucleation of hydrogen deficient carbon clusters in circumstellar envelopes of carbon stars,* World Scientific Press, Proceedings of the 8th Asia- Pacific Physics Conference, APPC 2000, 167-169, (2001)

N. Balucani, O. Asvany, Y.T. Lee, R.I. Kaiser, N. Galland, M.T. Rayez, Y. Hannachi: *First gas phase detection of the closed shell boron species HBCC($X^1 \Sigma$) - A combined crossed beam and ab initio study of the reaction of B(^2P) with $C_2H_2(^1\Sigma_g^+)$,* J. Comp. Chem. (special issue in honor of Prof. Schleyers 70th birthday), **22**, 1359-1365, (2001)

N. Ballucani, O. Asvany, R.I. Kaiser, Y. Osamura: *Formation of three C_4H_3N isomers from the reaction of CN($X^2 \Sigma^+$) with allene, H_2CCCH_2 ($X^1 A_1$) and methylacetylene $CH_3CCH(X^1 A_1)$: A combined crossed beam and ab initio study,* J. Phys. Chem. A, **106**, 4301-4311, (2002)

Y.-S. Wang, C.-H. Tsai, Y.T. Lee, and H.-C. Chang, J. C. Jiang, O. Asvany, S. Schlemmer, D. Gerlich: *Investigations of protonated and deprotonated water clusters using a low-temperature 22-pole ion trap,* J. Phys. Chem. A, **107**, 4217-4225, (2003)

O. Asvany, I. Savić, S. Schlemmer, D. Gerlich: *Variable temperature ion trap studies of $CH_4^+ + H_2$, HD and D_2: negative temperature dependence and significant isotope effect,* Chem. Phys., **298**, 97-105, (2004)

O. Asvany, S. Schlemmer, D. Gerlich: *Deuteration of CH_n^+ (n=3-5) in collisions with HD measured in a low temperature ion trap,* submitted to Astrophys. J.

Conference Contributions

O. Asvany, Y.T. Lee, R.I. Kaiser: *A crossed molecular beams study on the reaction of $C_2D(^2\Sigma^+)$ radicals with acetylene, C_2H_2, and methylacetylene, CH_3CCH: A versatile pathway to form (substituted) diacetylenes in Titans atmosphere*, Talk, 31st Annual Meeting of the Division for Planetary Sciences AAS, Padova October 1999, Italy

O. Asvany, N. Balucani, A. Mebel, Y.T. Lee, R.I. Kaiser: *Crossed molecular beam reactions of C_2 clusters with unsaturated hydrocarbons*, Poster, 8th Asian Chemical Congress, Taipei November 1999, Taiwan

O. Asvany, S. Schlemmer, D. Gerlich, Y.-S. Wang, J.C. Jiang, C.-H. Tsai, Y.T. Lee, and H.-C. Chang: *Temperature dependence of decomposition of protonated water clusters in a 22-pole in trap*, Poster, TMR Astrophysical Chemistry Final Network Meeting, Perugia April 2002, Italy

O. Asvany, S. Schlemmer, D. Gerlich: *Reactions with HD in a low temperature 22-pole ion trap*, Poster, FGLA symposium, Großbothen September 2002, Germany

O. Asvany, S. Schlemmer, D. Gerlich: *Investigation of protonated water clusters in a variable tempereature 22-pole ion trap*, Poster, 67. DPG-Frühjahrstagung, Hannover March 2003, Germany

O. Asvany, S. Schlemmer, D. Gerlich: *Reactions with HD in a low temperature 22-pole ion trap*, Poster, Workshop on Solid State Astrochemistry of Star Forming Regions, Leiden April 2003, Netherlands

O. Asvany, I. Savić, S. Schlemmer, and D. Gerlich: *Collisions of $CH_4^+ + H_2$, HD and D_2 at low temperatures: Negative temperature dependence and anomalous isotope effect*, Poster, XX International Symposium on Molecular Beams, Lissabon June 2003, Portugal

Selbstständigkeitserklärung

Ich versichere, dass ich die vorliegende Arbeit selbstständig und nur unter Verwendung der angegebenen Literatur und Hilfsmittel angefertigt habe. Ich erkläre, nicht bereits früher oder gleichzeitig bei anderen Hochschulen oder an dieser Universität ein Promotionsverfahren beantragt zu haben. Ich erkläre, obige Angaben wahrheitsgemäß gemacht zu haben und erkenne die Promotionsordnung der Fakultät für Naturwissenschaften der Technischen Universität Chemnitz von 10. Oktober 2001 an.

Oskar Asvany

Curriculum Vitae

Personal:

name:	Oskar Asvany
birth time and place:	12 September 1971, Lund (Sweden)
citizenship:	German

Education:

school:	1977-1981	Grundschule Mechernich, Germany
	1981-1990	'Gymnasium am Turmhof', Mechernich, Germany
university:	1990-1997	studies of physics at the university of Bonn, Germany
	1993-1994	studies of physics at the university of Lund, Sweden
	July 1997	Diploma thesis: 'Strahllagemessung in Elektronenbeschleunigern zur Korrektur der Gleichgewichtsbahn und ihre Anwendung zur Minimierung der vertikalen Strahlemittanz'
traineeships:	1998	engineering department of company 'Orbis S.A.I.C.', Buenos Aires, Argentina
PhD studies:	1999-2000	Crossed molecular beam studies in the group of R.I. Kaiser at IAMS, Taipei, Taiwan
	2000-2001	Ion trap studies of $H^+(H_2O)_n$ in the group of H.C. Chang at IAMS, Taipei, Taiwan
	2001-2003	Ion trap studies of CH_n^+ in the group of D. Gerlich, Chemnitz, Germany

Thanks to all the people who helped me during the last 4 years:

in Chemnitz:

Prof. Dr. Dieter Gerlich for the supervision of this research work

Special thanks to PD Dr. Stephan Schlemmer for his excellent supervision and the friendly atmosphere

All the Chemnitz group members, namely Silko Barth, Gheorghe Borodi, Dr. Ivo Čermák, Silvio Decker, Michael Grimm, Dr. Alfonz Luca, Igor Savić and Dr. Stefan Wellert for the nice Saxonian atmosphere and help

For technical support our engineer-ladies Doreen Kunte and Adelheid Steinrücken and last, but not least, for the excellent administrative support VZD Annett Kurasch

in Taipei:

Dr. Ralf Ingo Kaiser for his introduction into the field of crossed beams

All the people in the laboratory of Prof. Dr. Huan Chen Chang for their help, especially Dr. Yi-Sheng Wang for his ceaseless patience

我誠摯地感謝所有在張煥正教授研究室同仁們的助，
特別是王亦生博士所付出的無限耐心.